Supporting Information

Stable Helicene Radicals: Synthesis, Structure, Physical Properties, and Photocatalysis

Aslam C. Shaikh,[a] Md Mubarak Hossain,[a] Jules Moutet,[a] José M. Veleta,[a] Jan Bloch,[b] Andrei V. Astashkin,[a] and Thomas L. Gianetti*[a]

[a]Department of Chemistry and Biochemistry, University of Arizona, Tucson, AZ, United States.

[b]Department of Chemistry and Applied Biosciences, ETH Zürich, Zürich, Switzerland

*Email: tgianetti@email.arizona.edu

Table of Contents

I. General information

Unless otherwise stated, the syntheses of radicals were carried out in oven-dried vials or reaction vessels loaded with magnetic stirring bars inside an N_2 filled glove box. Dried solvents and liquid reagents were transferred by oven-dried or hypodermic syringes. Experiments were monitored by analytical thin layer chromatography (TLC), on pre-coated silica gel plates. After elution, plates were revealed under UV light with 254 nm wavelength. Melting points are uncorrected and recorded using digital Buchi Melting Point Apparatus B-540. ^{1}H and ^{13}C NMR spectra and were recorded on Bruker AVII 400/500, spectrometers in deuterated solvents using TMS as internal standard, or the solvent residue signals as secondary standards, and the chemical shifts are shown in δ scales. Multiplicities of the ^{1}H NMR signals are denoted by s (singlet), d (doublet), dd (doublet of doublet), dt (doublet of triplet), t (triplet), quin (quintet), m (multiplet), br.s (broad singlet)… etc. HRMS (ESI) were performed via LTQ Orbitrap Velos ETD mass-spectrometer (ThermoFisher Scientific, Bremen, Germany). Single-crystal X-ray diffraction data were collected on either a Bruker Kappa APEX II CCD diffractometer using Mo K_α radiation (λ = 0.71073Å) radiation, or a Bruker AXS single-crystal system equipped with a Excillum METALJET liquid gallium X-ray source, kappa goniometer, Oxford 800 series cryostream set to 100 K, and Photon III detector. Image collection, data reduction, and scaling were performed with Bruker AXS APEX3 software. Compounds were drawn using ChemDraw and the assignments of NMR spectra were done on MestReNova. All the chemicals and solvents were purchased from Sigma Aldrich, Fisher Scientific, or VWR and used without further purification. Organic solvents used were dried by using a solvent purification system. The electrolyte tetrabutylammonium hexafluorophosphate (TBAF-PF_6) was recrystallized from ethanol three times prior to use. Compound **1** was prepared according to Laursen report.[1]

[1] B. W. Laursen, F. C. Krebs, M. F. Nielsen, K. Bechgaard, J. B. Christensen, and N. Harrit *J. Am. Chem. Soc*. 1998, **120**, 12255-12263

II. General synthetic procedure

II.1 Typical procedures for synthesis of 2-H$^+$, 2-NO$_2^+$, and 3$^+$ - 5$^+$

Note: Compound **4**$^+$ was prepared according to previous report.[1]

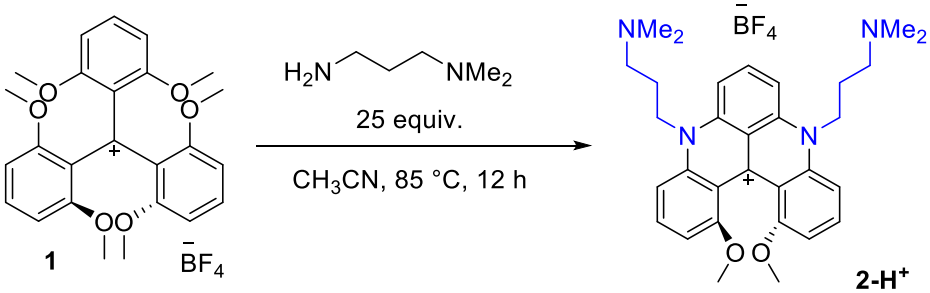

Racemic-5,9-bis(3-(dimethylamino)propyl)-1,13-dimethoxy-5,9-dihydro-13b*H*-quinolino[2,3,4-*kl*]acridin-13b-ylium tetrafluoroborate salt (2-H$^+$): *N,N*-dimethylpropane-1,3-diamine (6.28 ml, 49.46 mmol, 25 equiv) was added to a solution of tris(2,6 dimethoxyphenyl)carbenium tetrafluoroborate (1.00 g, 1.99 mmol, 1.0 equiv) in anhydrous acetonitrile (15 ml). The reaction mixture was heated at 85 °C for 12 hours then allowed to cool to room temperature. The crude product precipitated upon addition of Et_2O (~100 ml). The precipitate was filtered and washed several times with Et_2O, dried and collected. Selective precipitation by addition of Et_2O to a solution of crude product in CH_3CN afforded the dimethoxyquinacridinium tetrafluoroborate salts (1.12 g, 96%).

Grey solid; Melting point: 218-220 °C; R_f= 0.12 (SiO_2, CH_2Cl_2:MeOH (80:20));

^{1}H NMR (400 MHz, Acetonitrile-d_3) δ = 8.12 (t, *J* = 8.5 Hz, 1H), 7.88 (dd, *J* = 8.9, 8.0 Hz, 2H), 7.56 (dd, *J* = 15.9, 8.7 Hz, 4H), 6.90 (d, *J* = 8.0 Hz, 2H), 4.71 (ddd, *J* = 15.6, 9.9, 5.9 Hz, 2H), 4.50 (ddd, *J* = 15.5, 9.7, 5.9 Hz, 2H), 3.72 (s, 6H), 2.50 (t, *J* = 6.4 Hz, 4H), 2.28 (s, 12H), 2.12 (m, 4H).

^{13}C NMR (125 MHz, Acetonitrile-d_3) δ = 160.58, 143.43, 143.10, 139.90, 137.92, 137.33, 120.25, 113.86, 108.49, 105.86, 103.90, 57.16, 56.46, 48.99, 45.90, 25.14.

^{19}F NMR (376 MHz, Acetonitrile-d_3) δ = -152.71, -152.66.

HRMS(ESI): *m/z* = Calcd for $C_{31}H_{39}N_4O_2^+$ $[M]^+$ 499.3068, found 499.3056.

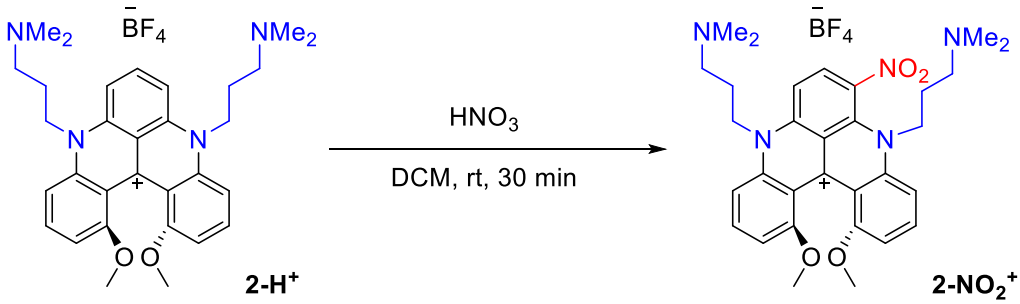

Racemic-5,9-bis(3-(dimethylamino)propyl)-1,13-dimethoxy-6-nitro-5,9-dihydro-13bH-quinolino[2,3,4-kl]acridin-13b-ylium tetrafluoroborate salt (2-NO_2^+): To a solution of **2-H^+** (500 mg) in CH_2Cl_2 (10 mL) was added aqueous HNO_3 (67%, 3 mL). After 30 min of stirring at 25 °C, the reaction mixture was quenched by addition of aqueous NaOH (1.0 M, 40 mL) and then extracted with CH_2Cl_2 (3 x 10 mL). Aqueous HBF_4 (1.0 M, 10 mL) was added to the combined organic layers, washed with NaOH (1.0 M, 20 mL) again, dried over Na_2SO_4, and evaporated under vacuum. The solid was precipitated using CH_2Cl_2 and Et_2O solvent mixture. After filtration a dark red solid was obtained (490 mg, 90 %). Layering with CH_2Cl_2 and *n*-hexanes yielded dark red crystals.

Melting point: 170-172 °C; R_f= 0.12 (SiO_2, CH_2Cl_2:MeOH (80:20));

^{1}H NMR (400 MHz, Methylene Chloride-d_2) δ = 8.79 (d, *J* = 9.6 Hz, 1H), 8.12 (t, *J* = 8.5 Hz, 1H), 7.99 (t, *J* = 8.4 Hz, 1H), 7.91 (d, *J* = 9.6 Hz, 1H), 7.81 (d, *J* = 8.9 Hz, 1H), 7.52 (d, *J* = 8.7 Hz, 1H), 7.10 (d, *J* = 8.1 Hz, 1H), 7.01 (d, *J* = 8.2 Hz, 1H), 4.99 (m, 2H), 4.88 (m, 1H), 3.84 (s, 3H), 3.79 (s, 3H), 3.73 (m, 1H), 2.54 (t, *J* = 5.9 Hz, 2H), 2.32 (s, 6H), 2.26 (br.s, 2H), 1.95 (m, 1H), 1.81 (m, 1H), 1.69 (m, 2H), 1.52 (s, 6H).

^{13}C NMR (100 MHz, Methylene Chloride-d_2) δ = 159.88, 159.58, 141.75, 141.73, 141.27, 141.21, 139.22, 137.75, 136.55, 134.17, 132.03, 120.49, 116.57, 113.95, 109.90, 108.42, 106.69, 105.42, 104.99, 56.35, 56.32, 56.29, 55.35, 54.38, 54.11, 53.84, 53.57, 53.30, 45.73, 44.97, 26.32, 25.88.

^{19}F NMR (376 MHz, Methylene Chloride-d_2) δ = -152.48, -152.53.

HRMS(ESI): *m/z*=Calcd for $C_{31}H_{38}N_5O_4^+$ $[M]^+$ 544.2918, found 544.2911.

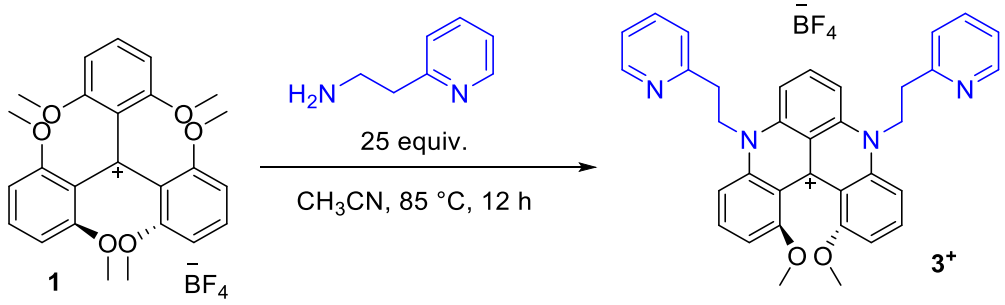

Racemic-1,13-dimethoxy-5,9-bis(2-(pyridin-2-yl)ethyl)-5,9-dihydro-13b*H*-quinolino [2,3,4-*kl*]acridin-13b-ylium tetrafluoroborate salt (3^+): *2-(pyridin-2-yl)ethan-1-amine* (5.97 ml, 49.75 mmol, 25 equiv) was added to a solution of tris(2,6 dimethoxyphenyl)carbenium tetrafluoroborate (1.00 g, 1.99 mmol, 1.0 equiv) in anhydrous acetonitrile (15 ml). The reaction mixture was heated at 85 °C for 12 hours then allowed to cool to room temperature. The crude product precipitated upon addition of Et_2O (~100 ml). The precipitate was filtered and washed several times with Et_2O, dried and collected. Selective precipitation by addition of Et_2O to a solution of crude product in CH_2Cl_2 afforded the dimethoxyquinacridinium tetrafluoroborate salts (1.15 g, 92%).

Grey solid; Melting point: 228-230 °C; R_f= 0.5 (SiO_2, CH_2Cl_2:MeOH (90:10));

^{1}H NMR (400 MHz, Acetonitrile-d_3) δ = 8.56 (s, 2H), 8.21 (t, *J* = 8.5 Hz, 1H), 7.90 (t, *J* = 8.5 Hz, 2H), 7.77 (d, *J* = 8.5 Hz, 2H), 7.73 – 7.57 (m, 4H), 7.34 (d, *J* = 7.7 Hz, 2H), 7.24 (t, *J* = 6.4 Hz, 2H), 6.93 (d, *J* = 8.0 Hz, 2H), 5.14 (ddd, *J* = 15.7, 9.5, 6.4 Hz, 2H), 5.02 – 4.80 (m, 2H), 3.74 (s, 6H), 3.49 (q, *J* = 5.9 Hz, 4H).

^{13}C NMR (100 MHz, Acetonitrile-d_3) δ = 160.59, 158.44, 150.49, 143.10, 138.07, 137.81, 137.48, 124.72, 123.13, 113.98, 108.47, 106.09, 104.04, 56.49, 50.18, 34.83.

^{19}F NMR (376 MHz, Acetonitrile-d_3) δ = -151.82 (dd, *J* = 12.5, 7.3 Hz).

HRMS(ESI): *m/z*=Calcd for $C_{35}H_{31}N_4O_2^+$ $[M]^+$ 539.2442, found 539.2425

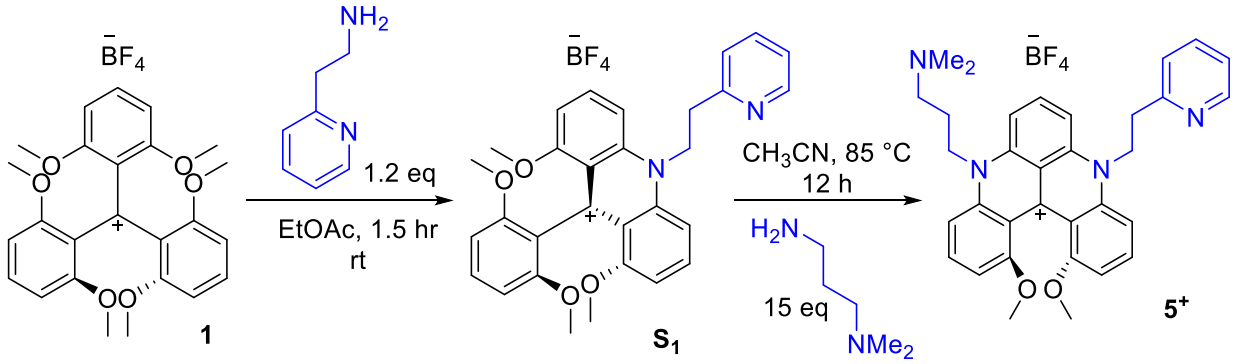

Racemic-5-(3-(dimethylamino)propyl)-1,13-dimethoxy-9-(2-(pyridin-2-yl)ethyl)-5,9-dihydro-13b*H*-quinolino[2,3,4-*kl*]acridin-13b-ylium tetrafluoroborate salt (5^+): 2-(pyridin-2-yl)ethan-1-amine (0.292 mg, 2.3 mmol, 1.2 equiv) was added to a solution of tris(2,6 dimethoxyphenyl)carbenium tetrafluoroborate (1.00 g, 1.99 mmol, 1.0 equiv) in anhydrous EtOAc (25 ml). The reaction mixture was stirred at room temperature for 1.5 hours. The crude product precipitated upon addition of hexane (~100 ml). The precipitate was filtered and washed several times with hexane and collected. Selective precipitation by addition of hexane to a solution of crude product in CH_2Cl_2 afforded the 9-(2,6-dimethoxyphenyl)-1,8-dimethoxy-10-(2-(pyridin-2-yl)ethyl)-9,10-dihydroacridin-9-ylium tetrafluoroborate salts (**S1**, 1.07 g, 95%).[2] The first step product (1.0 gm, 1.76 mmol, 1.0 equiv) was dissolved in anhydrous CH_3CN (15ml) and N,N-dimethylpropane-1,3-diamine (3.3 ml, 26.40 mmol, 15 equiv) was added. The reaction mixture was heated at 85 °C for 12 hours and then allowed to cool to room temperature. The crude product precipitated upon addition of Et_2O (~100 ml). The precipitate was filtered and washed several times with Et_2O and collected. Selective precipitation by addition of diethyl ether to a solution of crude product in CH3CN afforded the dimethoxyquinacridinium tetrafluoroborate salts (0.94 g, 88%).

Grey solid; Melting point: 218-220 °C; R_f= 0.30 (SiO_2, CH_2Cl_2:MeOH (80:20));

^{1}H NMR (400 MHz, Chloroform-*d*) δ = 8.67 – 8.51 (m, 1H), 8.24 (t, *J* = 8.5 Hz, 1H), 7.91 (ddd, *J* = 8.9, 8.0, 6.9 Hz, 2H), 7.76 (d, *J* = 8.5 Hz, 1H), 7.69 (td, *J* = 7.7, 1.9 Hz, 1H), 7.63 (t, *J* = 8.6 Hz, 2H), 7.53 (d, *J* = 8.9 Hz, 1H), 7.44 (d, *J* = 7.7 Hz, 1H), 7.22 (ddd, *J* = 7.6, 4.8, 1.1 Hz, 1H), 6.86 (dd, *J* = 8.0, 2.1 Hz, 2H), 5.12 (ddd, *J* = 15.8, 9.7, 6.7 Hz, 1H), 4.90 (ddd, *J* = 15.5, 9.7, 6.5 Hz, 1H), 4.81 (ddd, *J* = 15.5, 9.8, 6.0 Hz, 1H), 4.62 (ddd, *J* = 15.4, 9.8, 5.9 Hz,

[2] L. Mei, J. M. Veleta, J. Bloch, H. J. Goodman, D. Pierce-Navarro, A. Villalobos, T. L. Gianetti, *Dalton Trans.* **2020**, doi.org/ 10.1039/D0DT00419G.

1H), 3.77 (s, 3H), 3.76 (s, 3H), 3.53 (td, *J* = 6.2, 3.0 Hz, 2H), 2.58 (t, *J* = 6.3 Hz, 2H), 2.35 (s, 6H), 2.28 – 2.10 (m, 1H).

13C NMR (100 MHz, Chloroform-*d*) δ = 159.78, 156.98, 149.82, 142.94, 142.20, 142.14, 138.97, 138.82, 137.73, 137.58, 137,32, 137.17, 124.18, 122.48, 119.23, 113.34, 107.47, 107.40, 105.17, 105.07, 103.22, 103.11, 56.44, 55.83, 45.78, 34.39, 24.82.

^{19}F NMR (376 MHz, Chloroform-*d*)) δ = -151.90 (d, *J* = 20.3 Hz).

HRMS(ESI): *m/z*=Calcd for $C_{33}H_{35}N_4O_2^+$ $[M]^+$ 519.2755, found 519.2743.

II.2 Typical Procedure for synthesis of radicals

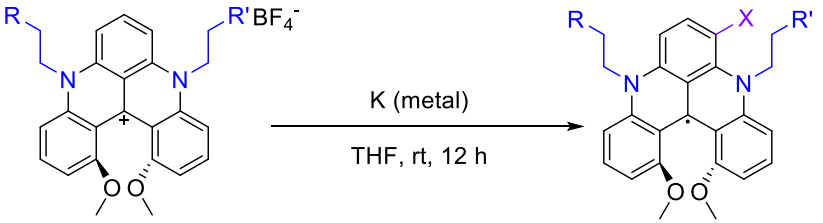

2-H , R=R'= -CH_2NMe_2, X = H, 82%,
2-NO_2 , R=R'= -CH_2NMe_2, X= NO_2, 80%,
3 , R=R'= -pyridyl, X = H, 80%,
4 , R=R'= -CH_3, X = H, 75%,
5 , R = -CH_2NMe_2, R' = -pyridyl, X = H, 86%

The potassium metal (1.1 equiv) was added to the stirred solution of dimethoxyquinacridinium tetrafluoroborate salts (200 mg, 1 equiv) in anhydrous THF (10 ml). The reaction mixture was stirred at rt for 12 hours and then reaction mixture was filtered and evaporated under vacuum pump. The crude product was triturated 2 times in 5 mL of Et_2O then extract with toluene and filtrated again. The filtrate was recrystallized from toluene and hexane layering to afford the radical **2•-5•**.

Paramagnetic NMR spectrums were obtained in C_6D_6 and the spectra are visible in what follows (Figures S14-15). Due to the important paramagnetic character paramagnetic character demonstrated by these species, the complete H attribution could not be completed.

HRMS(ESI) data for radicals:

2-H• : *m/z* = Calcd for $C_{31}H_{39}N_4O_2$: 499.3068, found 499.3068.

2-NO_2• : *m/z* = Calcd for $C_{31}H_{38}N_5O_4$: 544.2918, found 519.2893.

3• : *m/z* = Calcd for $C_{33}H_{35}N_4O_2$: 519.2755, found 519.2743.

4• : *m/z* = Calcd for $C_{35}H_{31}N_4O_4$: 539.2442, found 539.2443.

5• : *m/z* = Calcd for $C_{33}H_{35}N_4O_2$: 519.2755, found 519.2743.

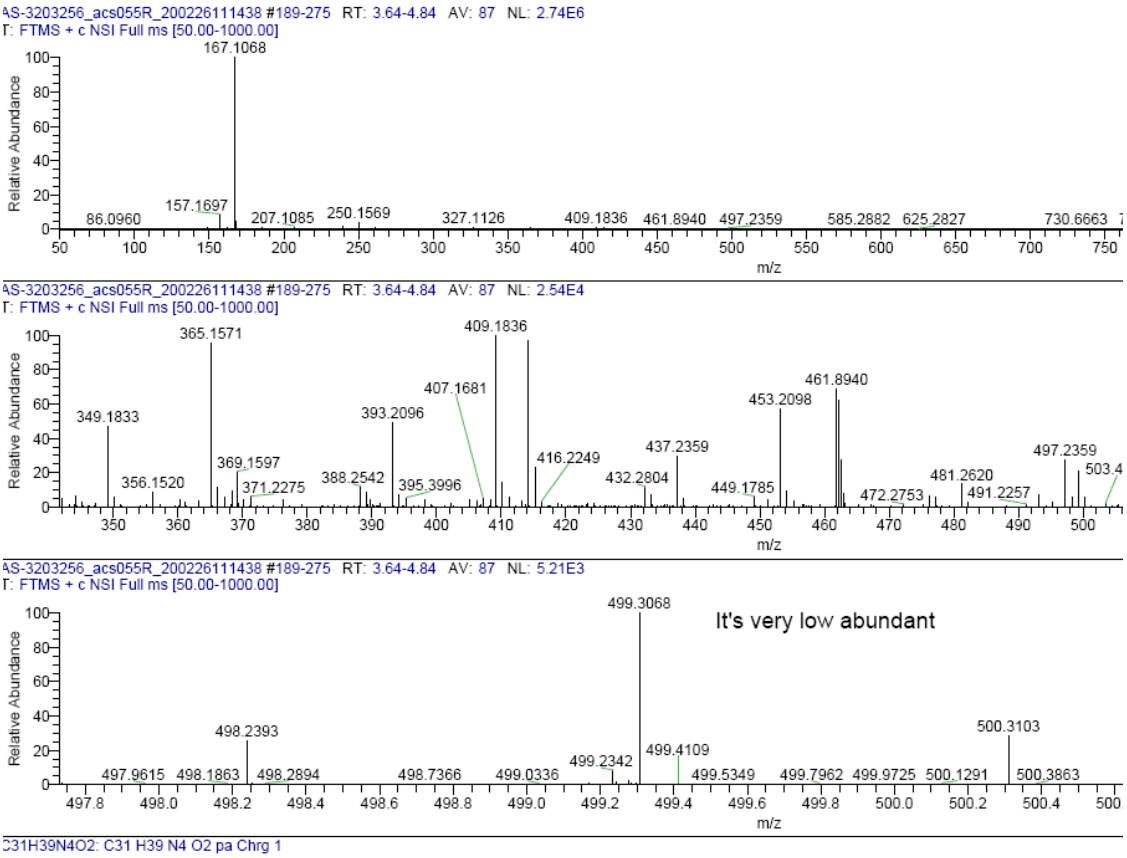

Figure S1. HRMS (ESI) spectra of **2-H**•

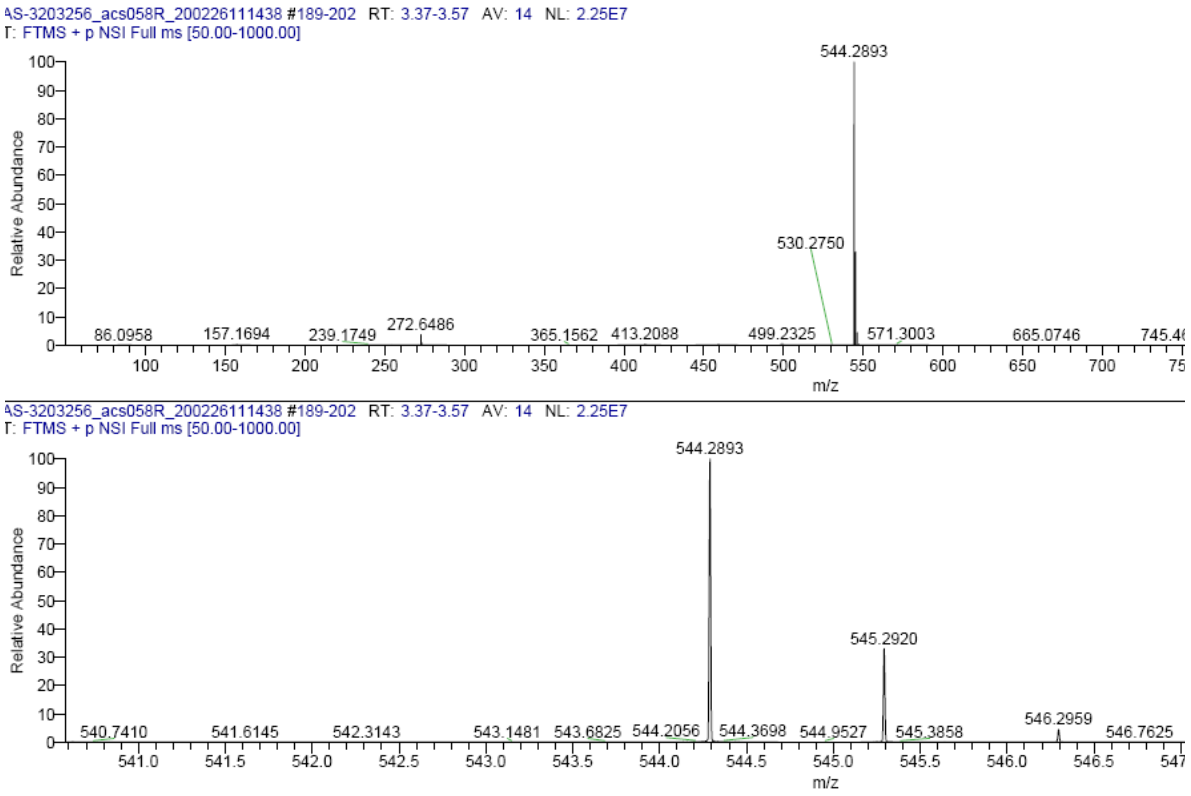

Figure S2. HRMS (ESI) spectra of **2-NO_2**•

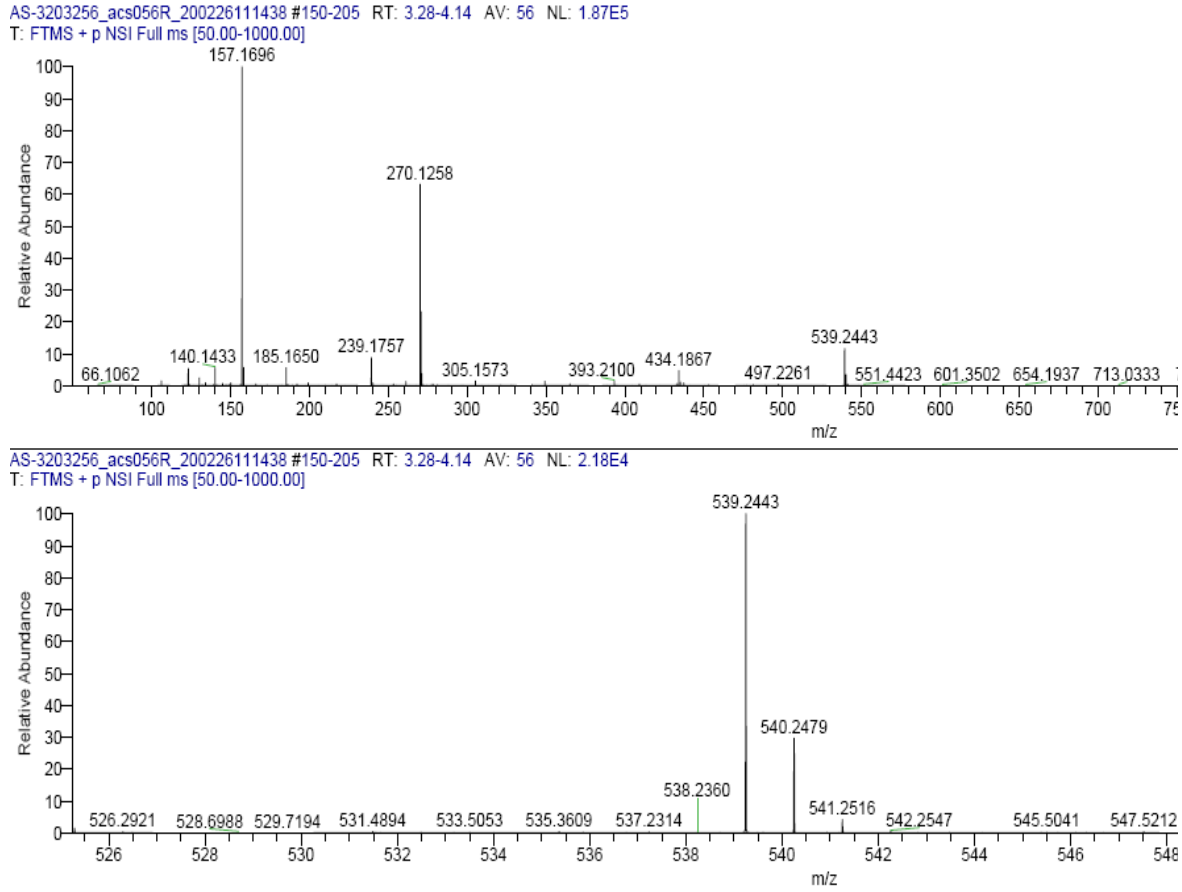

Figure S3. HRMS (ESI) spectrum of **3˙**

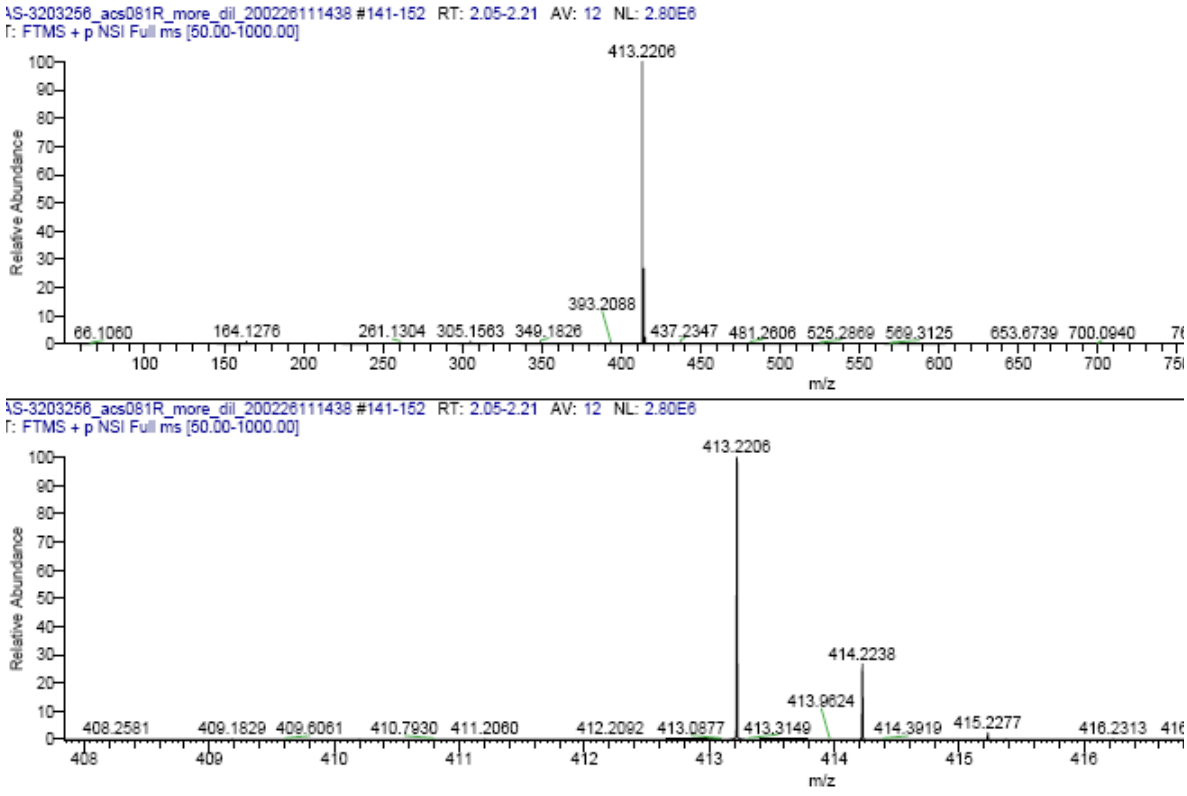

Figure S4. HRMS (ESI) spectra of **4˙**

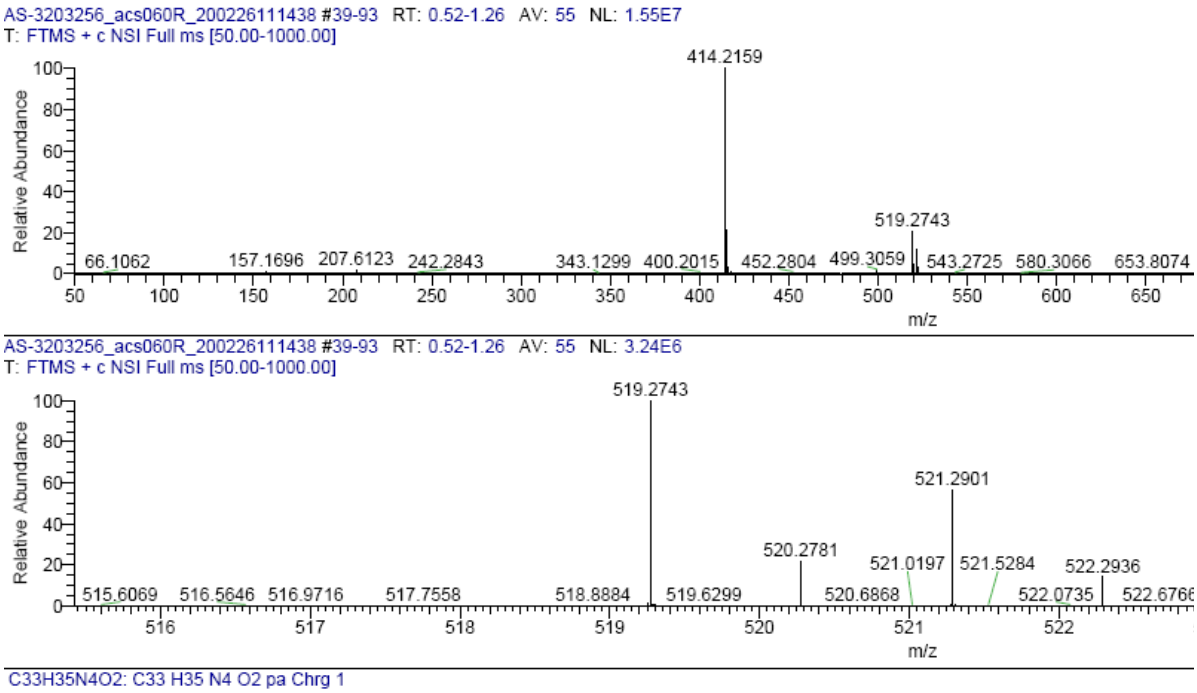

Figure S5. HRMS (ESI) spectraof **5**•

III. NMR Spectroscopy data

III.1 NMR spectra of carbenium 2-H⁺

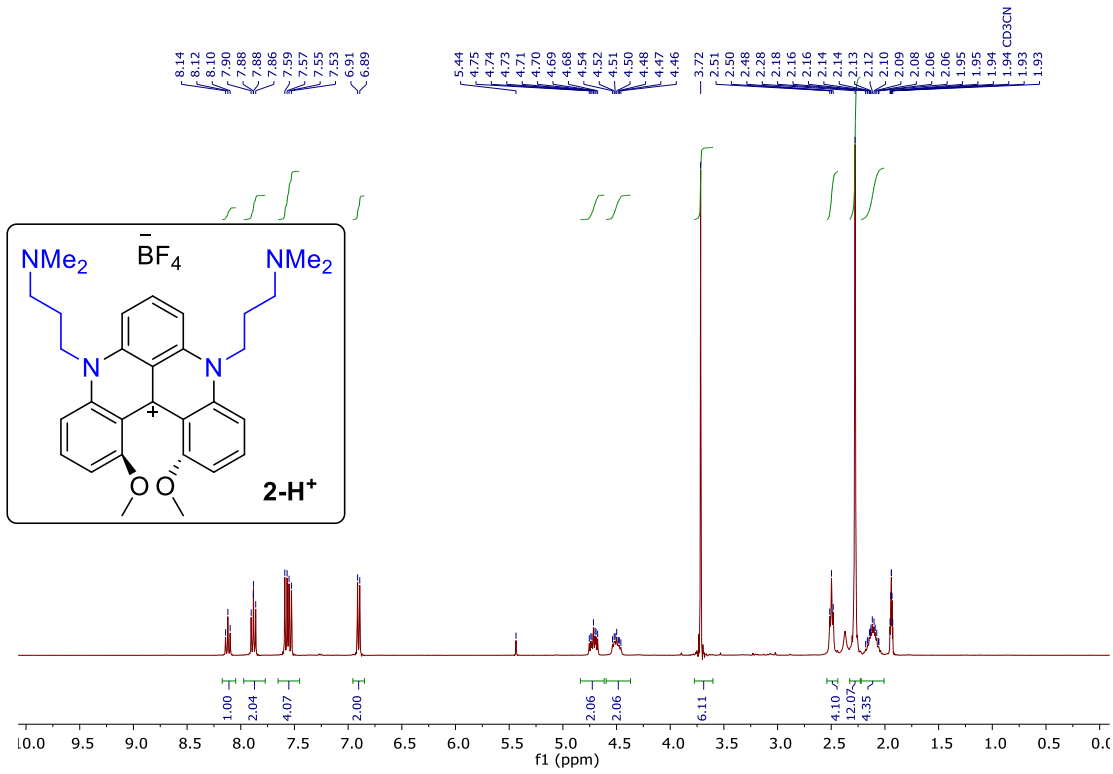

Figure S6. ^{1}H NMR spectrum of **2**$^{+}$ in CD_3CN

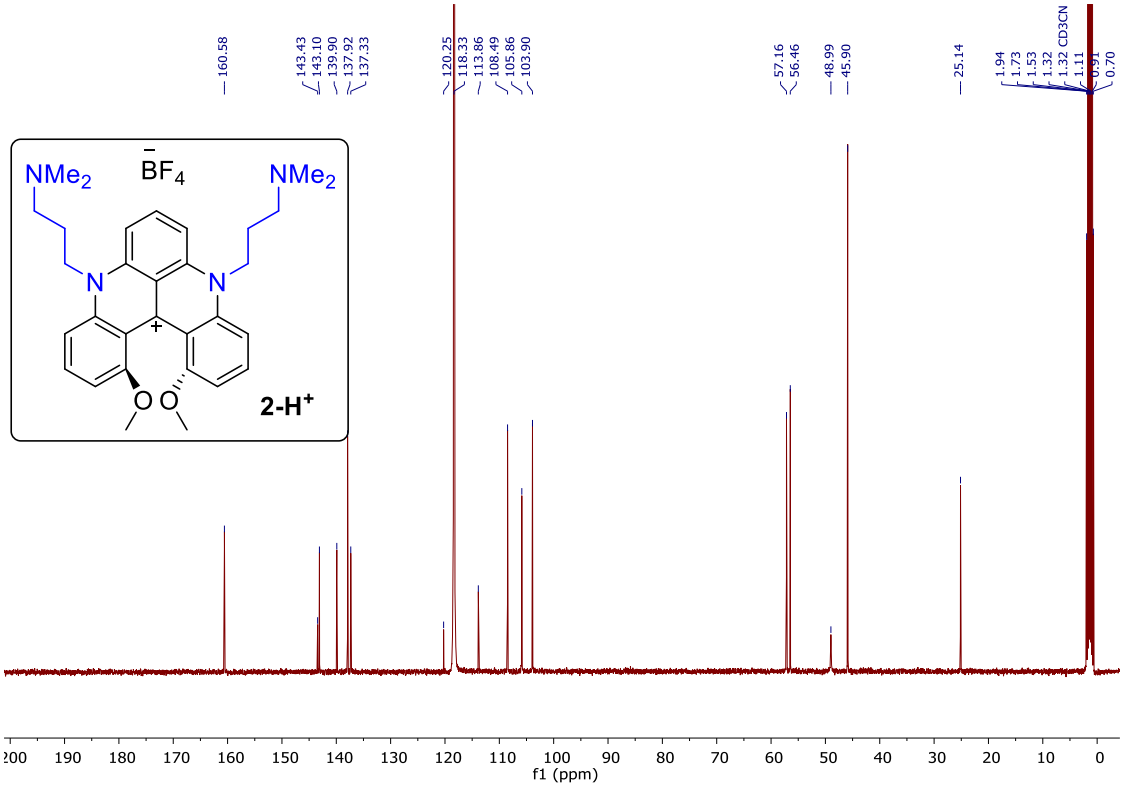

Figure S7. ^{13}C NMR spectrum of **2-H**$^{+}$ in CD_3CN

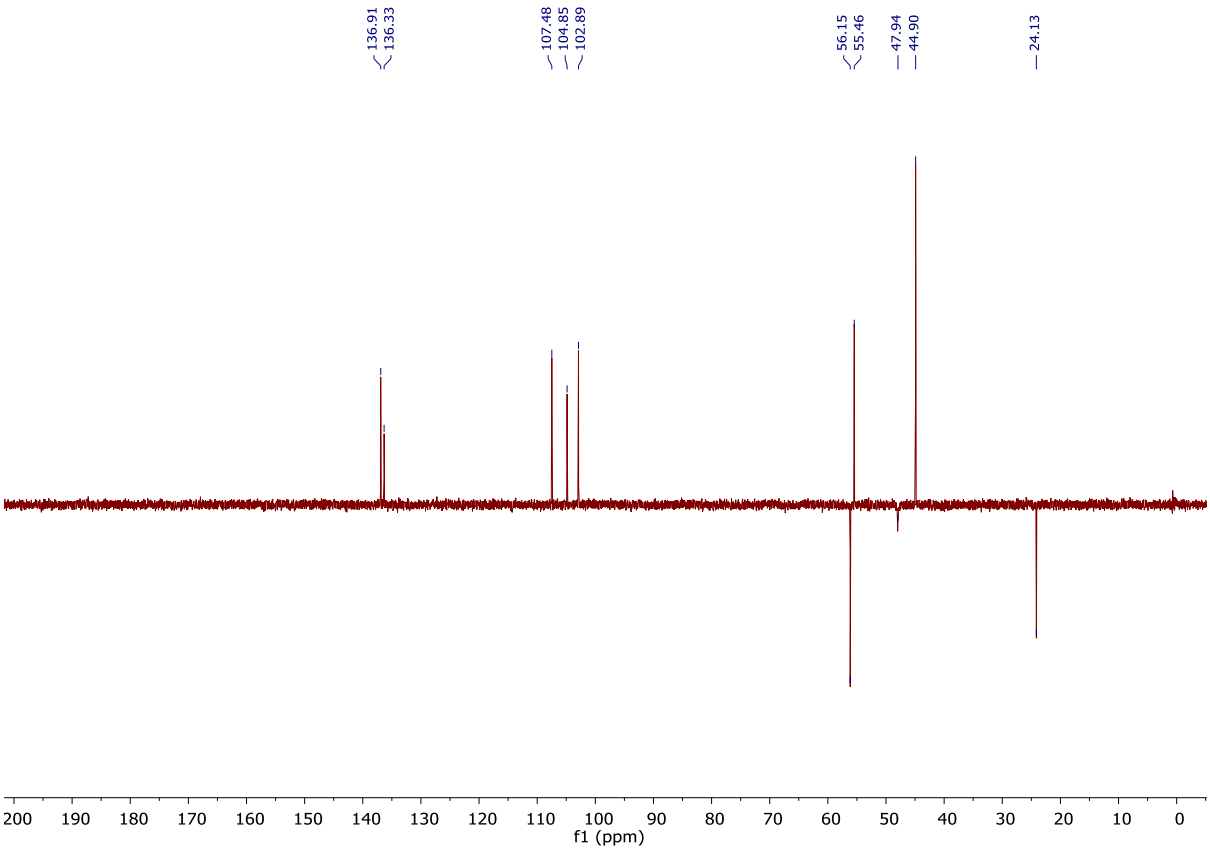

Figure S8. ^{13}C DEPT-135 NMR spectrum of **2-H**$^{+}$ in CD_3CN

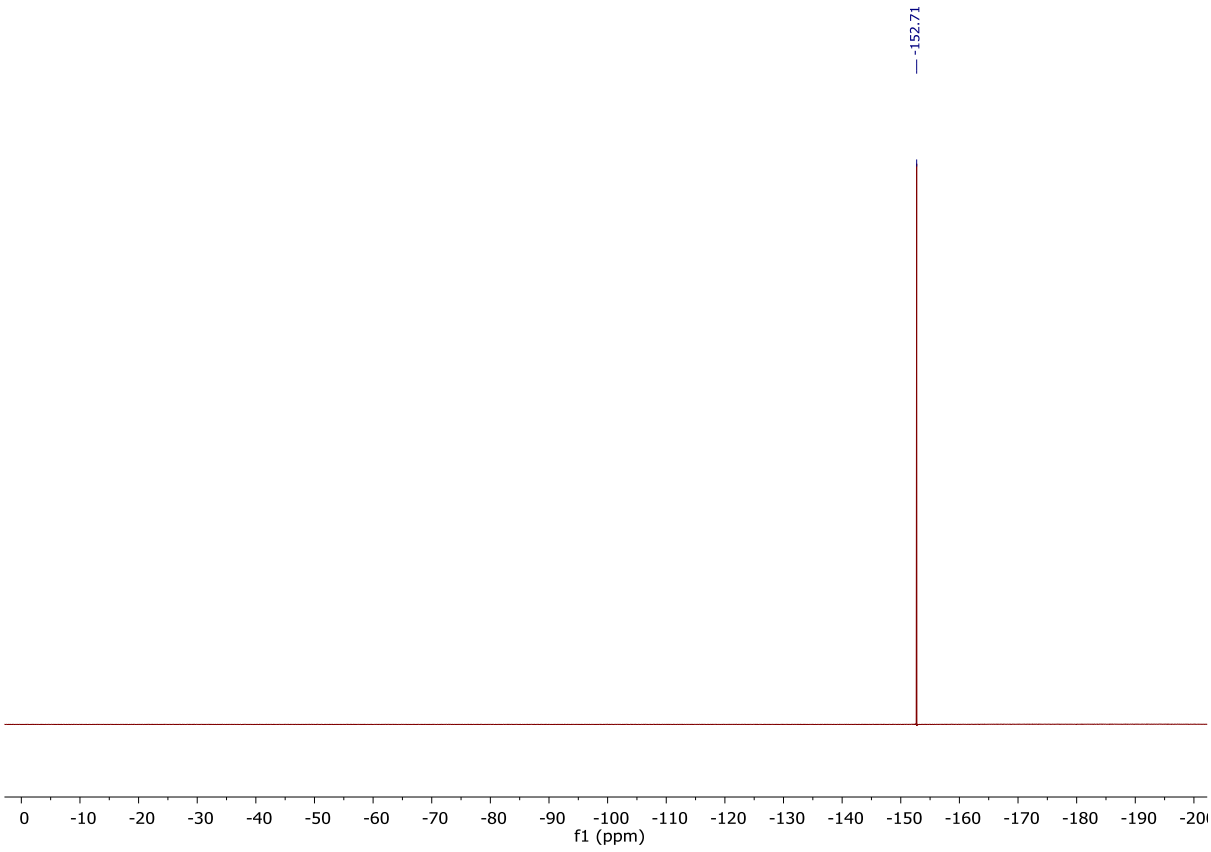

Figure S9. ^{19}F NMR spectrum of **2-H**$^{+}$ in CD_3CN

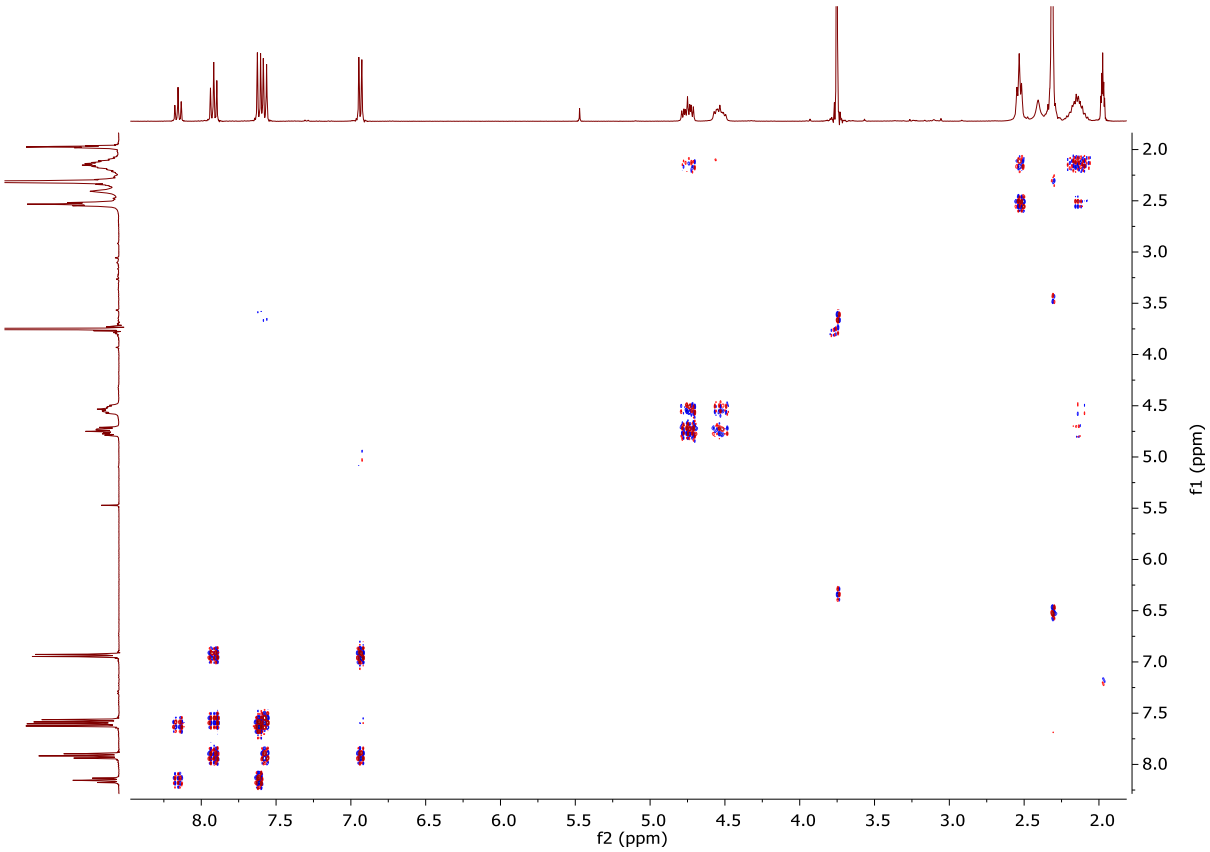

Figure S10. ^{1}H-^{1}H COSY spectrum of **2-H**$^{+}$ in CD_3CN

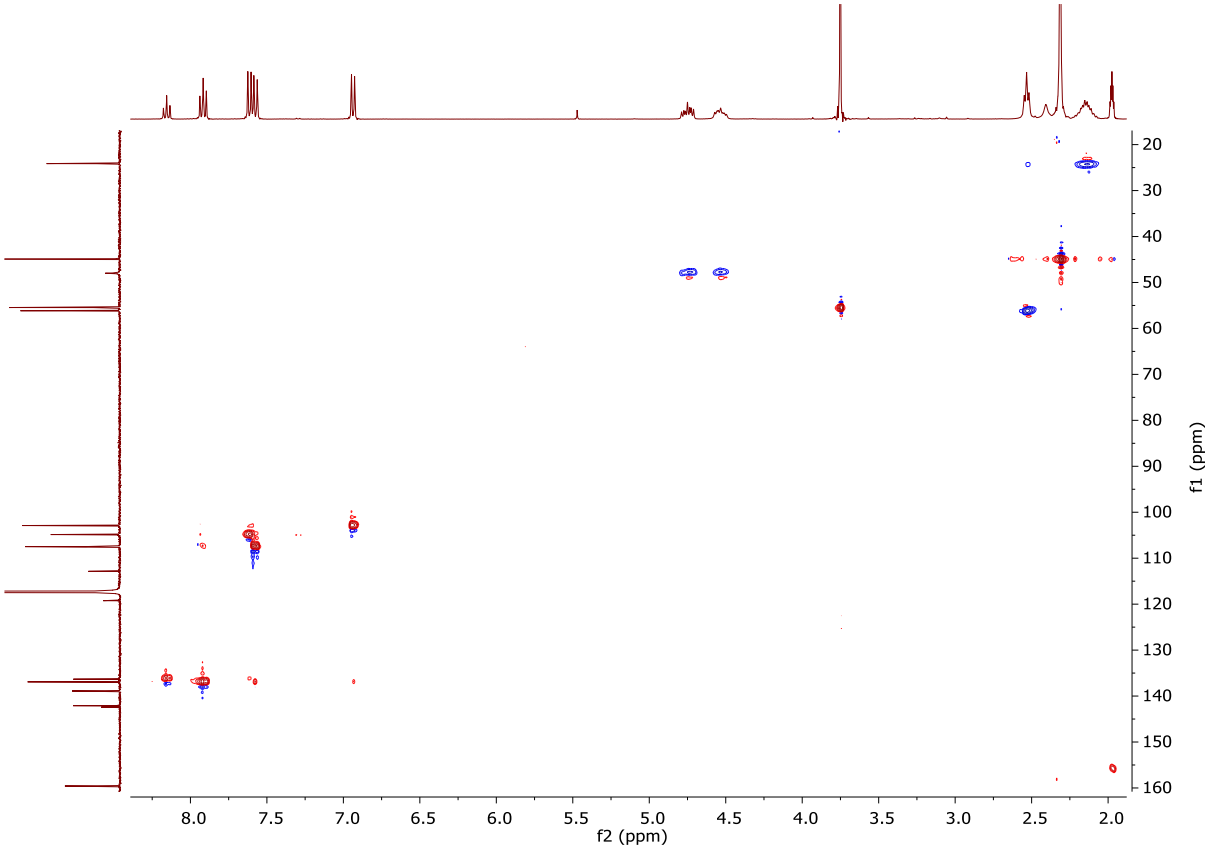

Figure S11. ^{1}H-^{13}C HMBC spectrum of **2-H**$^{+}$ in CD_3CN

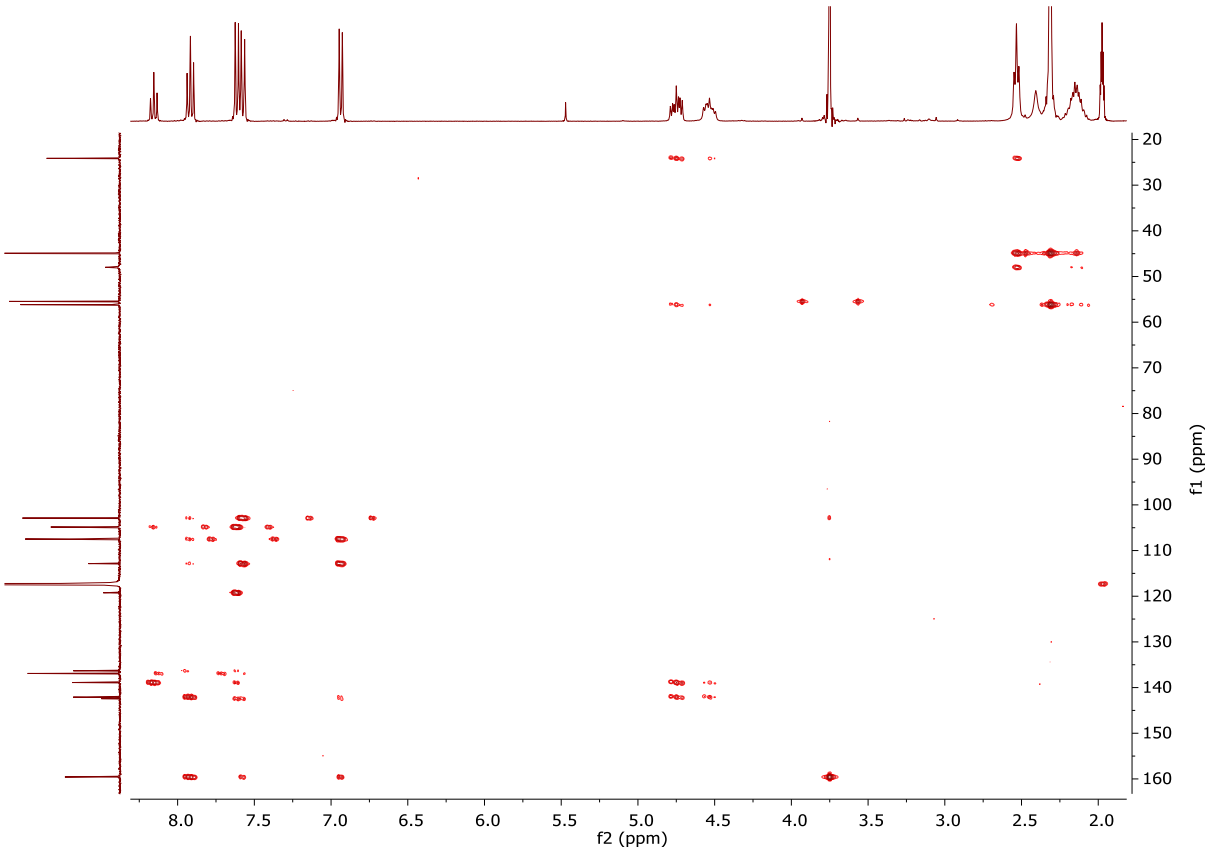

Figure S12. ^{1}H-^{13}C HSQC spectrum of **2-H**$^{+}$ in CD_3CN

III.2 NMR spectra of carbenium 2-NO_2^+

The carbenium **2-NO_2^+** has an unresolved ^{1}H NMR spectrum in CD_2Cl_2 at room temperature. Variable temperature (VT) ^{1}H NMR spectroscopy analysis of **2-NO_2^+** was conducted to resolve the broad signals observed. The sample was prepared in a non-coordinating deuterated dichloromethane and studied over a temperature range of 333 – 193 K (see Figures S13-S14). At room temperature (293 K), ^{1}H NMR spectrum shows that the aromatic protons are poorly resolved, and the amino arms are in a rapid exchange suggested by the broad signal at 4.94 ppm. Decreasing the temperature to 193 K results in a sharp and well-defined proton signals (See Figure S15). The presence of the NO_2 group result in a low symmetry molecule as exemplified by the aromatic region, the two signals for OMe groups (at 3.77 and 3.73 ppm), two signals for NMe2 groups (2.32 and 1.40 ppm). The assignment of the six methylenic protons of the -*n*Pr-NMe_2 arms was successfully carried out using low-temperature ^{1}H-^{1}H COSY NMR sequence (see Figure S17). As observed in **2-H^+**, the two methylene groups alpha to helicenium scaffold are diasterotopic with the CH_2 near the NO_2 group resonating at 4.95/3.55 ppm (H_A/$H_{A'}$) and the other resonating at 4.86/4.68 ppm. However, instead of four additional freely rotating methylene groups (-CH_2(**CH_2)$_2$**NMe_2), we observed another set of diasterotopic methylenic protons at 1.92/1.75 ppm (H_B/$H_{B'}$). The presence of diastereostopic H_B/$H_{B'}$ protons along with the large chemical shift difference between the NMe_2 groups suggest an interaction between the nitrogen-lone pair of one -*n*Pr-NMe_2 arm and the C^+ carbocation center (Scheme S1). This interaction is further supported by the presence of a resolved ^{1}H NMR spectrum at room temperature for the reported **4-NO_2^+** compound containing -^{n}Pr arms instead of -*n*Pr-NMe_2.[3]

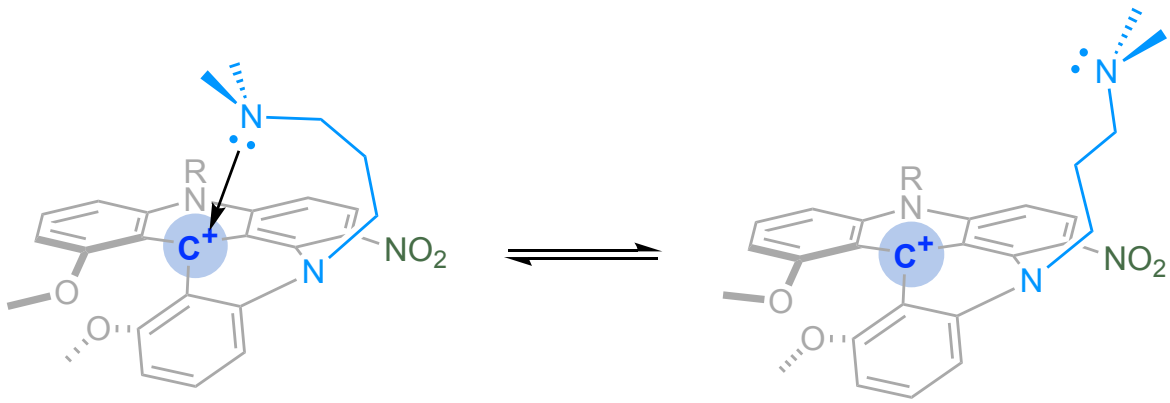

Scheme S1. NMe_2–C^+ interaction

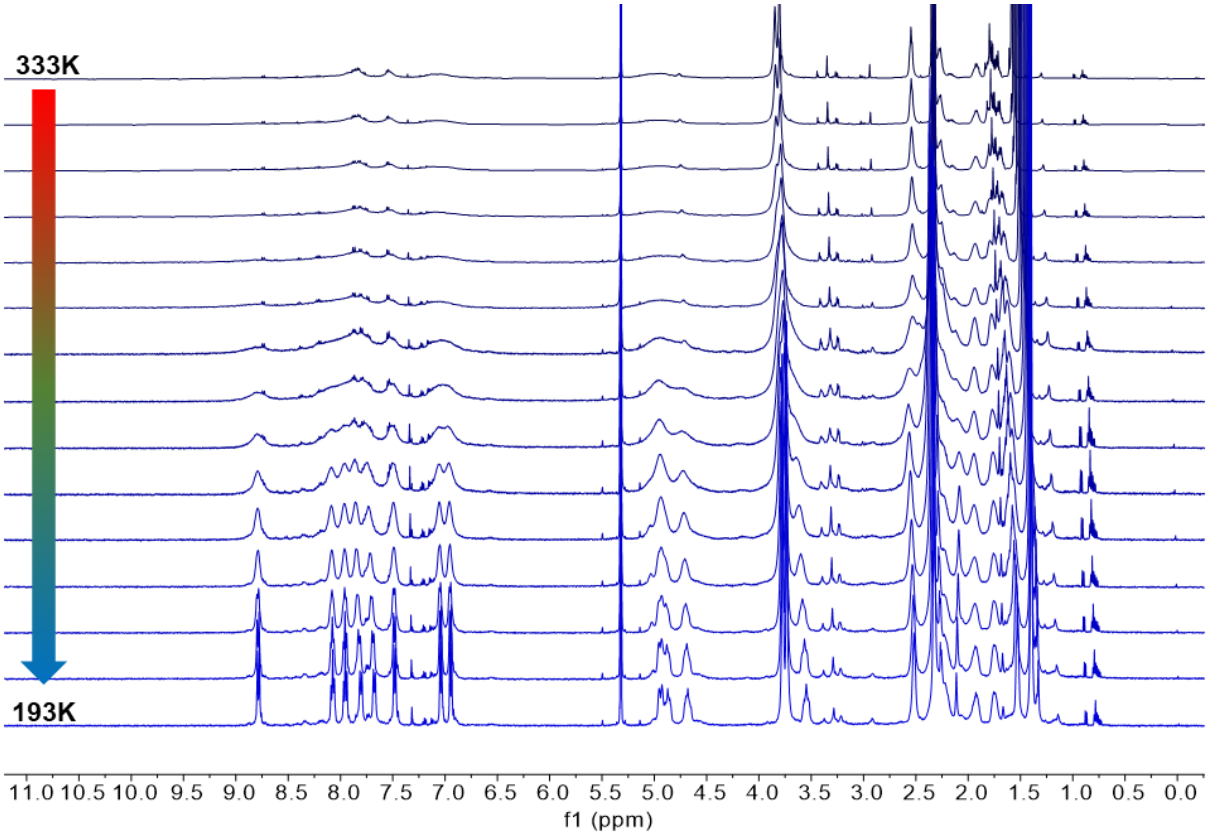

Figure S13 : ^{1}H NMR spectra of **2-NO$_2^+$** in CD_2Cl_2 between 333 K and 193 K with 10 K increments.

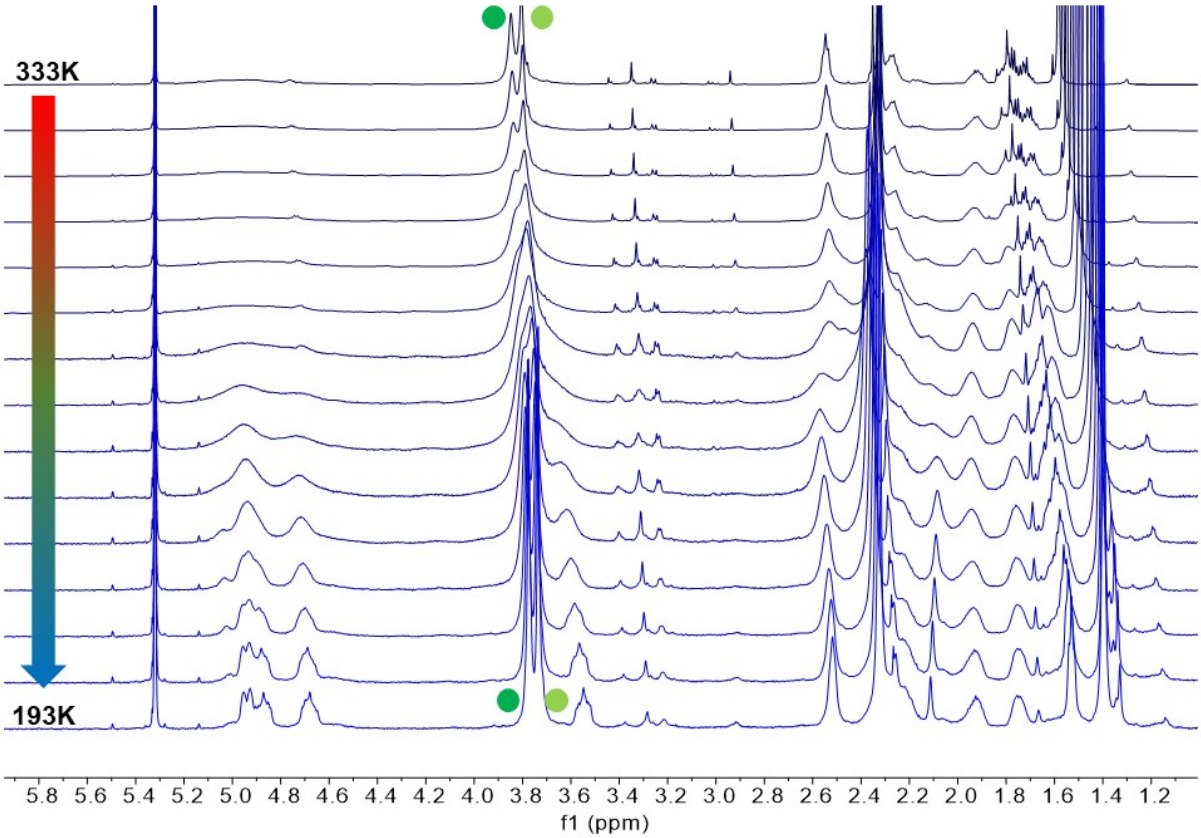

Figure S14 : ^{1}H NMR of **2-NO$_2^+$** in CD_2Cl_2 between 333 K and 193 K with 10 K increments.

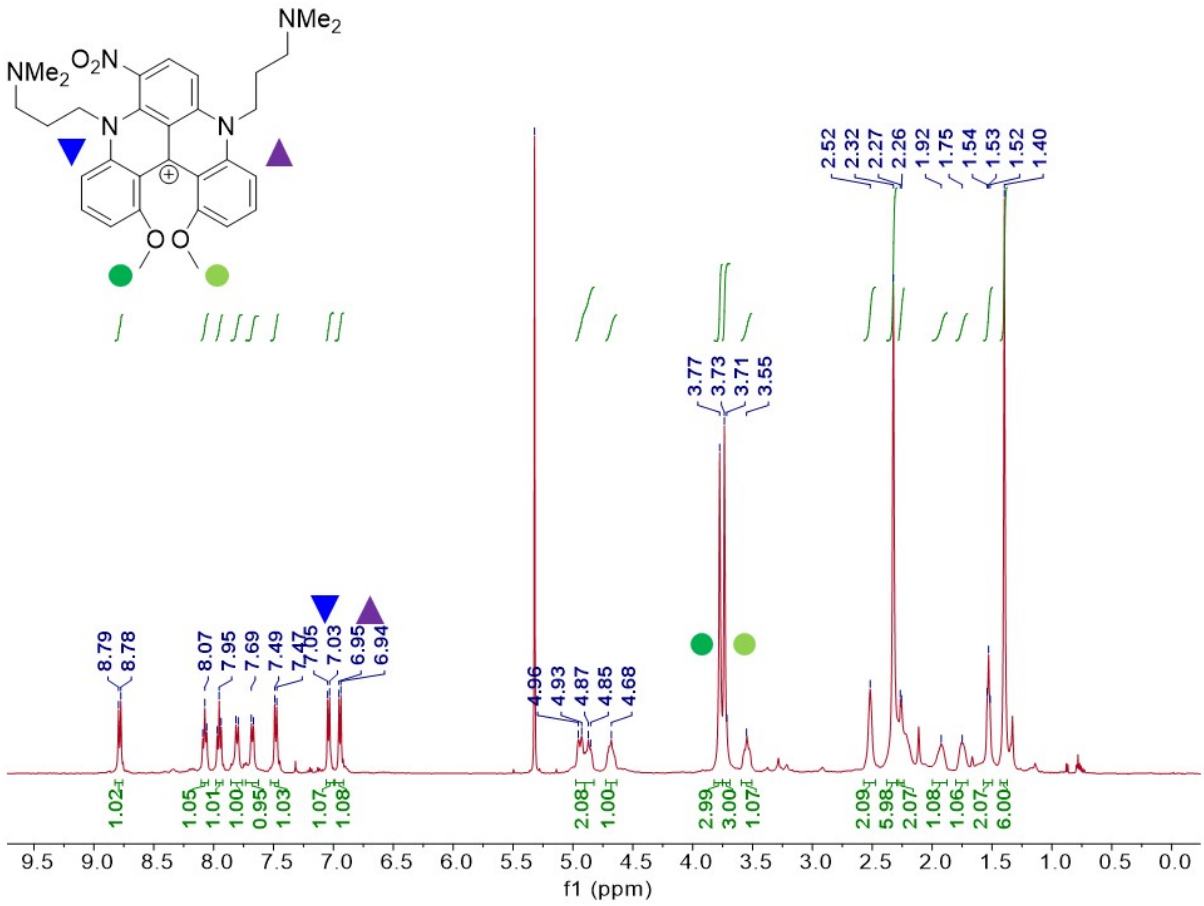

Figure S15: ^{1}H NMR of **2-NO$_2^+$** in CD_2Cl_2 at 193 K.

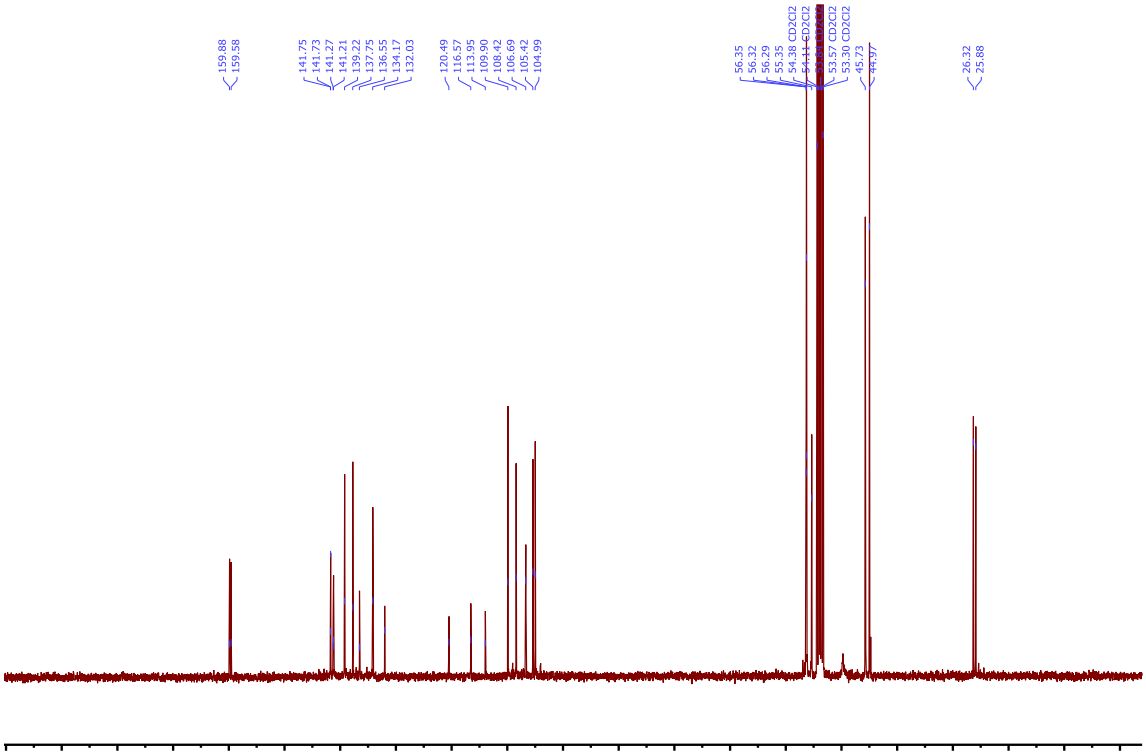

Figure S16. ^{13}C NMR spectrum of **2-NO$_2^+$** in CD_2Cl_2 at 193 K

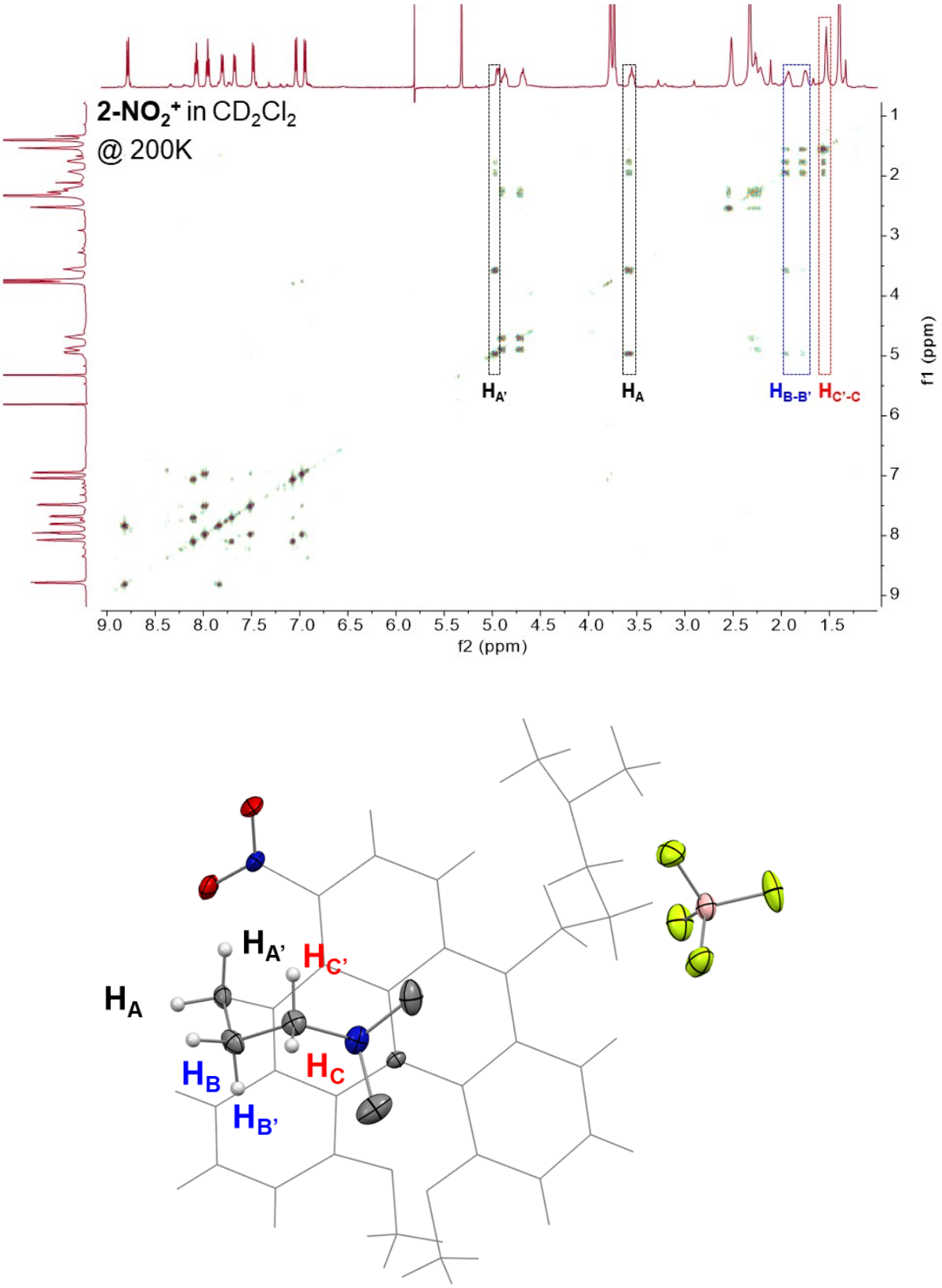

Figure S17: ^{1}H-^{1}HCOSY NMR spectrum of **2-NO$_2$**$^{+}$ in CD_2Cl_2 at 200K and XRD attribution.

III.3 NMR spectra of carbenium 3^+ - 5^+

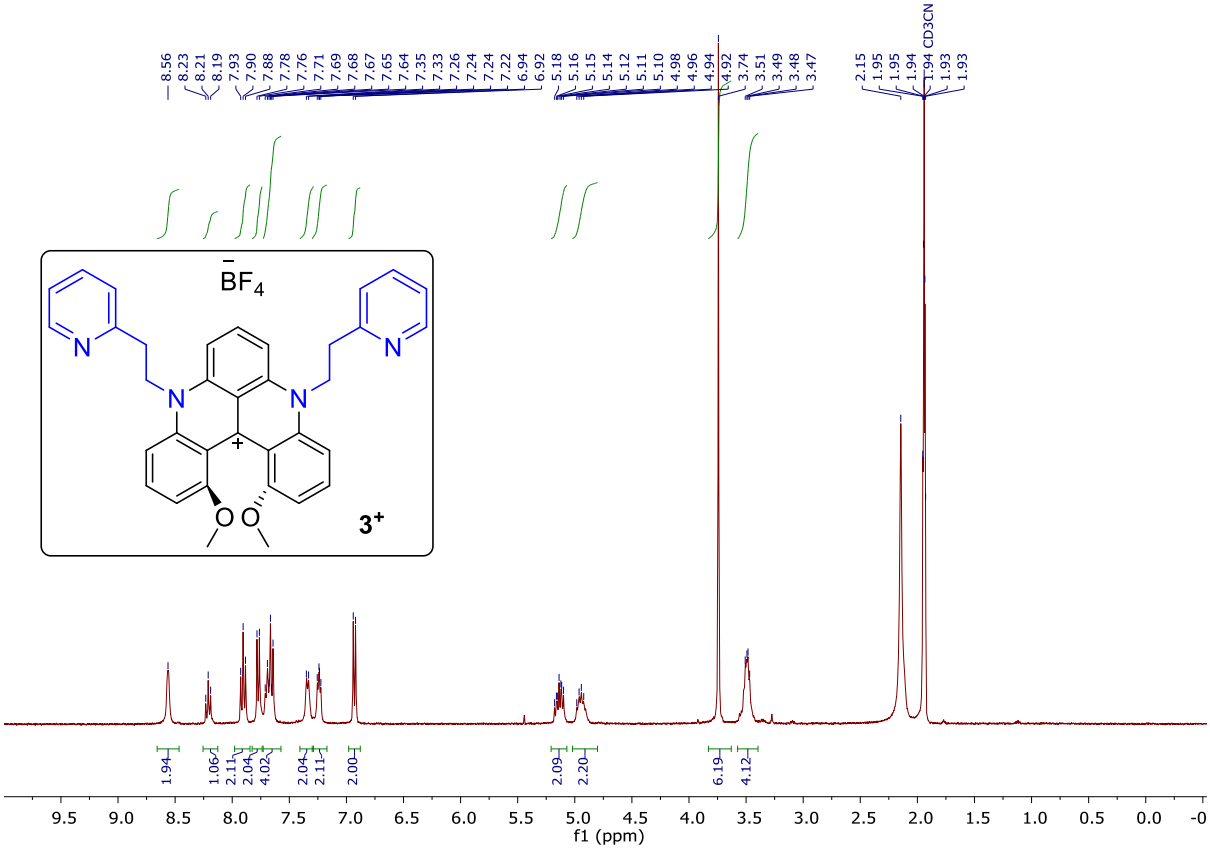

Figure S18. ^{1}H NMR spectrum of $\mathbf{3}^+$ in CD_3CN

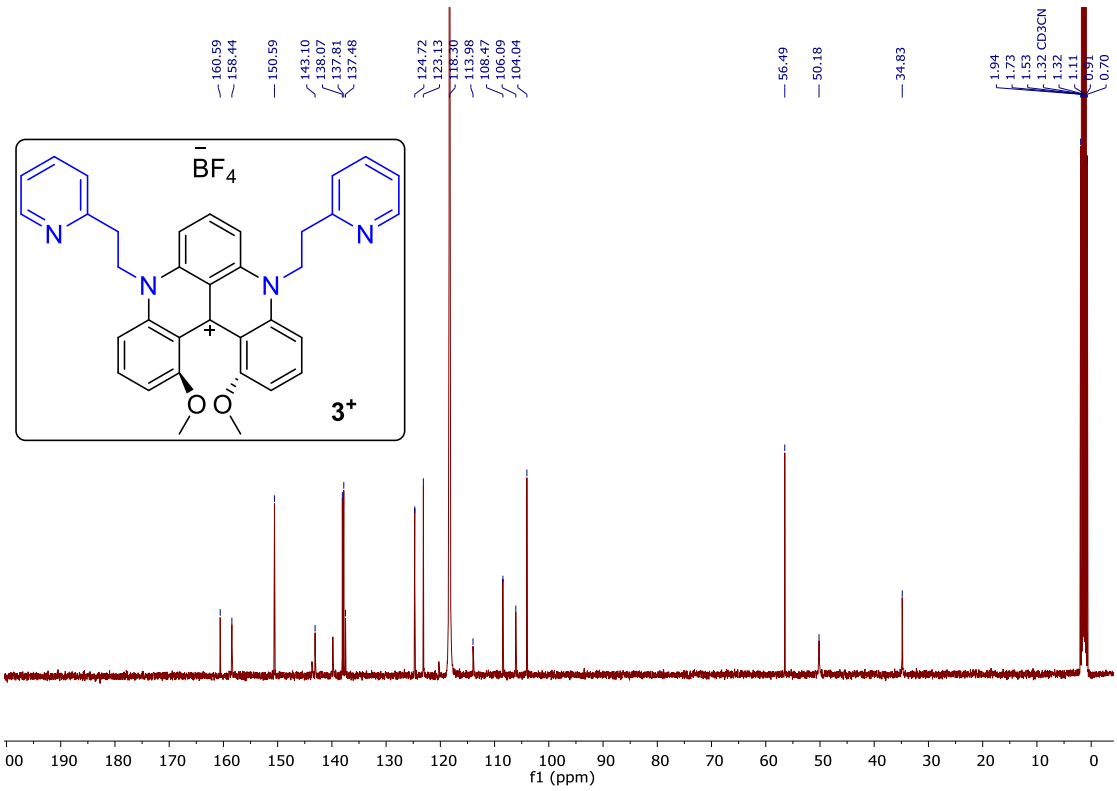

Figure S19. ^{13}C NMR spectrum of $\mathbf{3}^+$ in CD_3CN

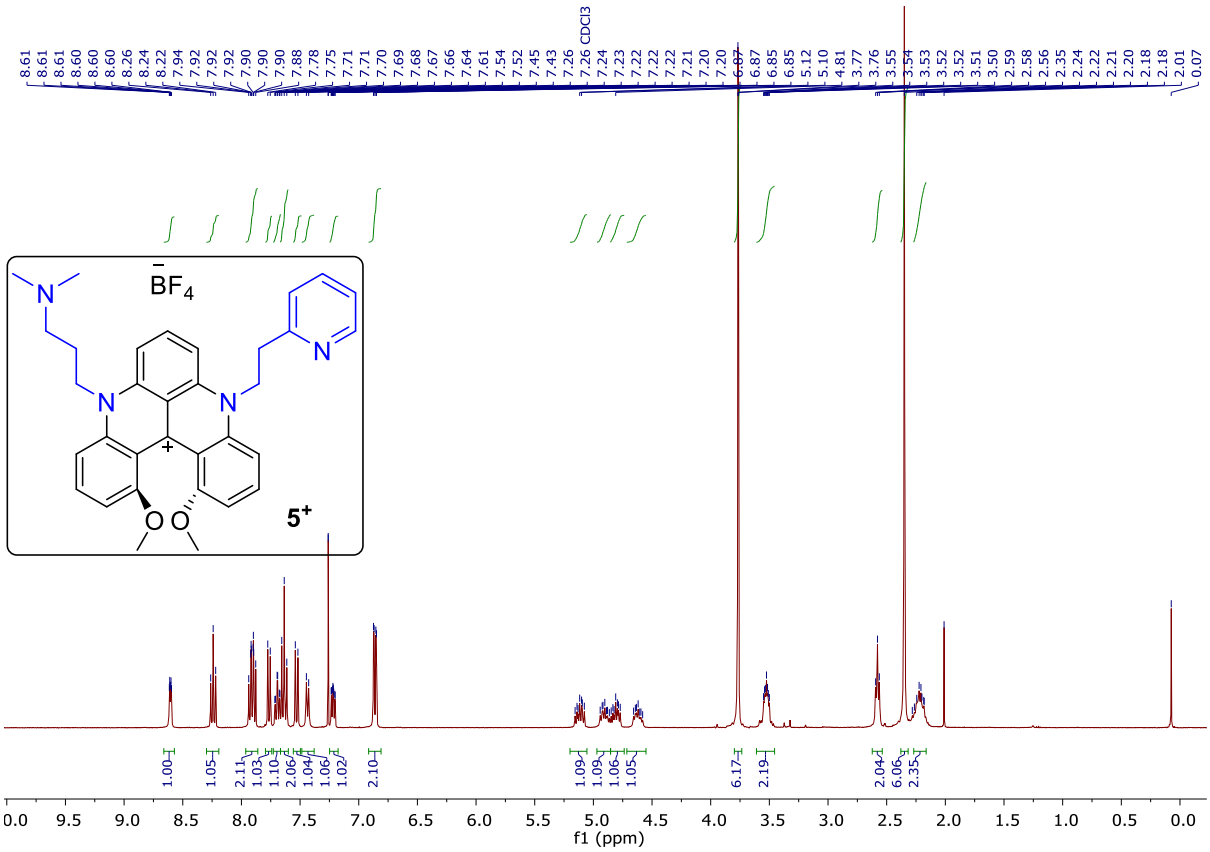

Figure S20. ^{1}H NMR spectrum of $\mathbf{5}^{+}$ in CD_3CN

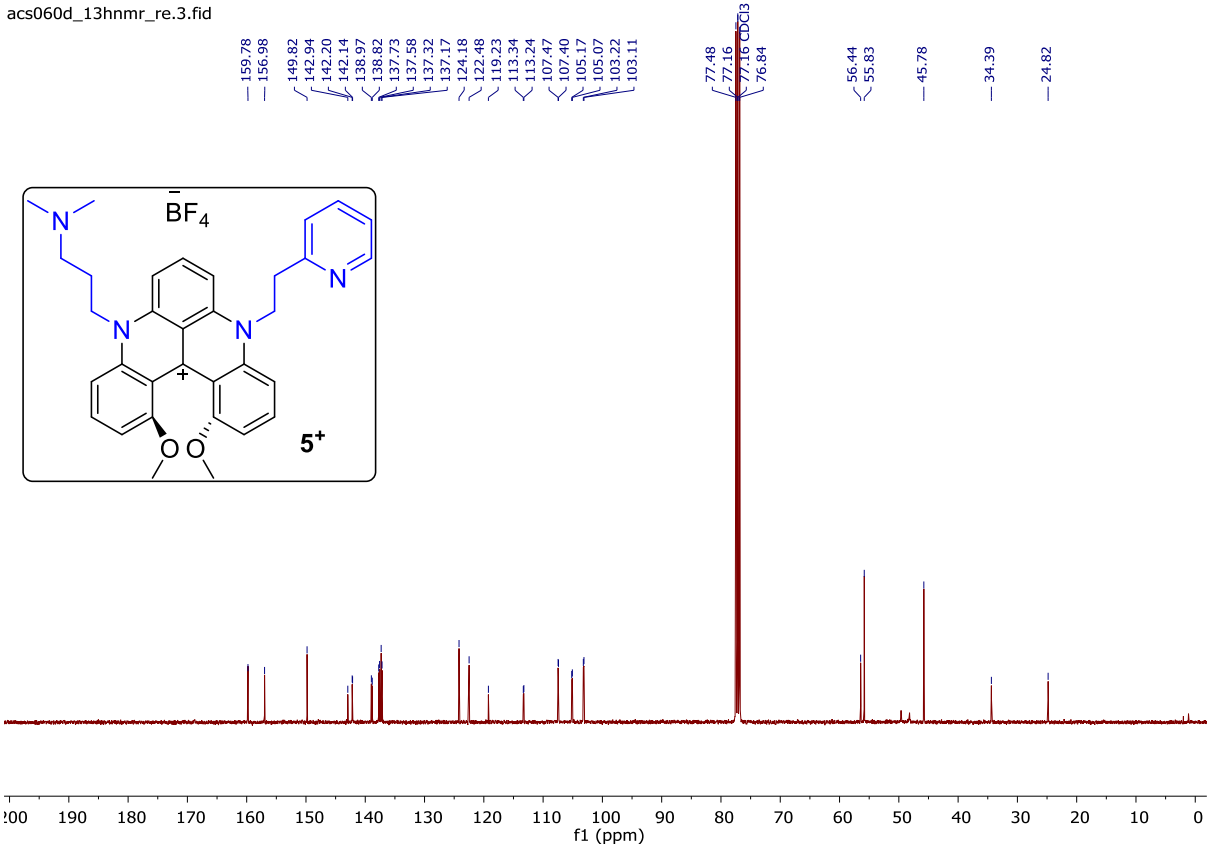

Figure S21. ^{13}C NMR spectrum of $\mathbf{5}^{+}$ in CD_3CN

III.3 NMR spectra of radical 2• - 5•

The molecules **2•-5•** were analyzed by paramagnetic ^{1}H NMR to determine if the pendant arms of the molecule have any effect or interaction with the radical system (see Figure S22-S23). The NMR sequence used to analyze these compounds had a window width of 100 ppm (SW = 100), a scan number of 256 (NS = 256) and a τ1 of 0.1 seconds (D1 = 0.1s).

Due to the pronounced radical nature of these compounds, the aromatic protons of the helicene radical scaffold are not observable However, the protons of the substituent arms *α* (N–***CH₂***–CH_2–R) and *β* (N–CH_2–***CH₂***–R) to the helicene core consistently appear broad and shifted at 17 and -7 ppm, respectively, for all radicals. The protons *γ* (N–CH_2–CH_2–***R***; R= C***H₃***, C***H₂***NMe_2, ***Py***) to the helicene core are less influenced by the radical, and while broad, resonate in the diamagnetic 10-0 ppm region. For **2-H•**, *γ*-protons as broad bands of 4 ppm wide centered around 5.71 ppm. The NO_2 electron-withdrawing group on **2-NO_2•** is speculated to have a widening effect on this band (from 9 to 2 ppm) still centered on around 5.71 ppm. The pyridinyl protons (*π*) for **3•** and **5•** are well-defined at 8.58, 7.38, 6.33 and 6.03 ppm respectively. In scaffold **5•**, the broad signature of *γ*-protons at 5.71 ppm is partially hidden by *π*-protons. The *γ*-protons on **4•** from the n-propyl groups are less affected by the radical system and appeared as a broad peak centered at 2.88 ppm. It thus appears that the nature of the chosen pendant arms has little influence on the radical character of the compounds **2•-5•**. Conversely, the substitution of a proton of the helicene core by an electron-withdrawing group induces a modification of the electronic structure of the resulting radical **2-NO_2•**.

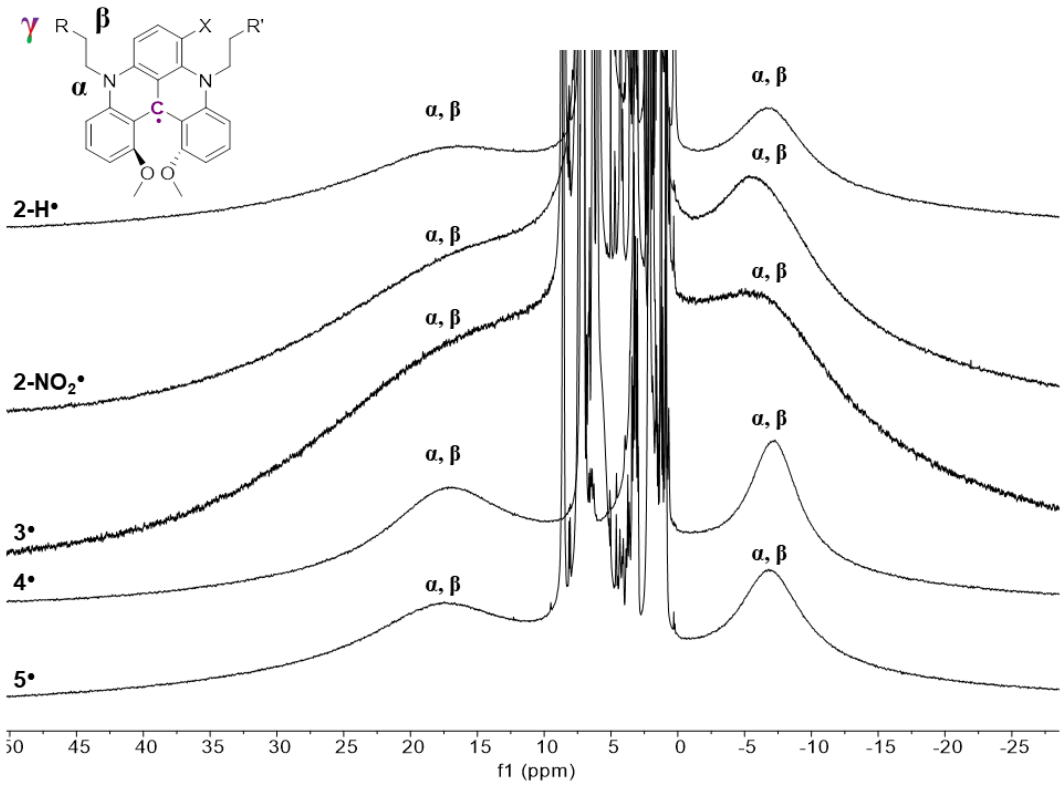

Figure S22 : ^{1}H NMR spectra of **2'-5'** in C_6D_6 at 298 K

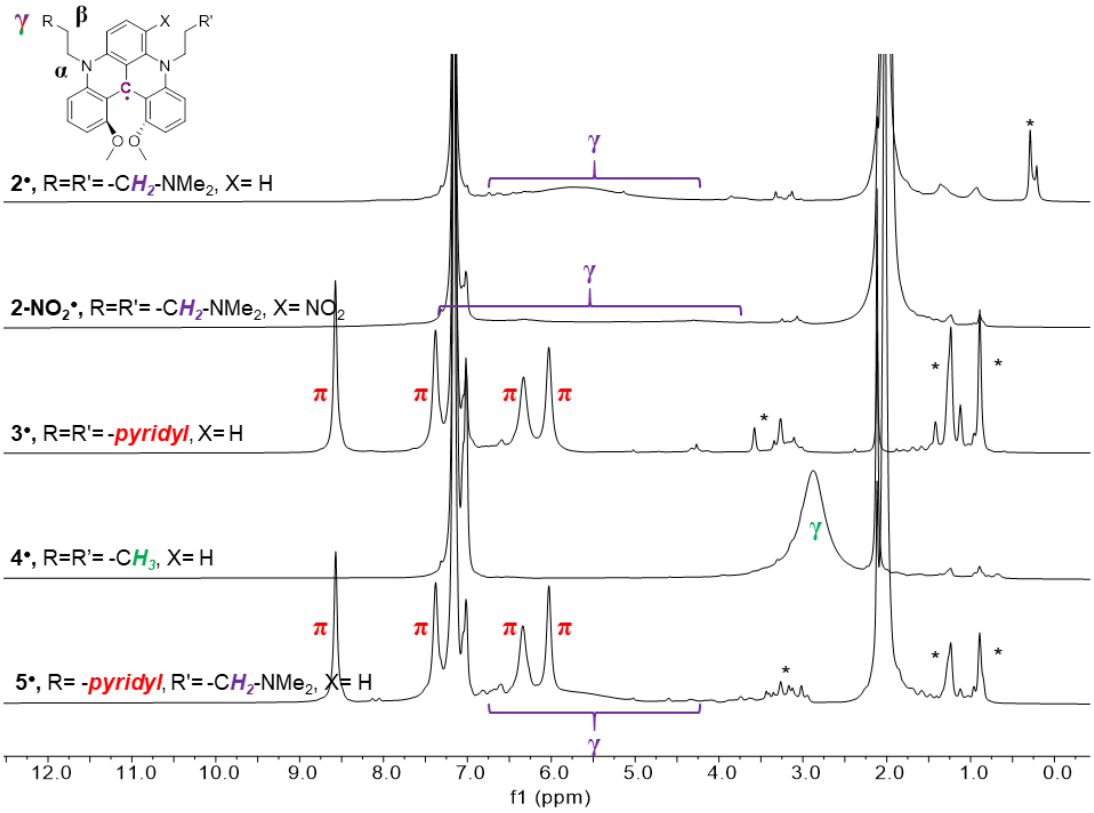

Figure S23 : ^{1}H NMR spectra of **2'-5'** in C_6D_6 at 298 K. Impurities are indicated by an asterisk (*)

IV. Single crystal X-ray Diffraction

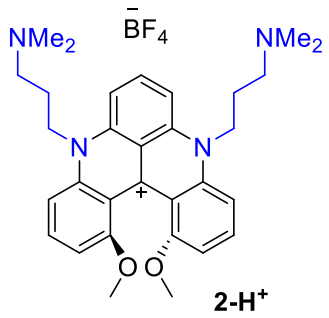

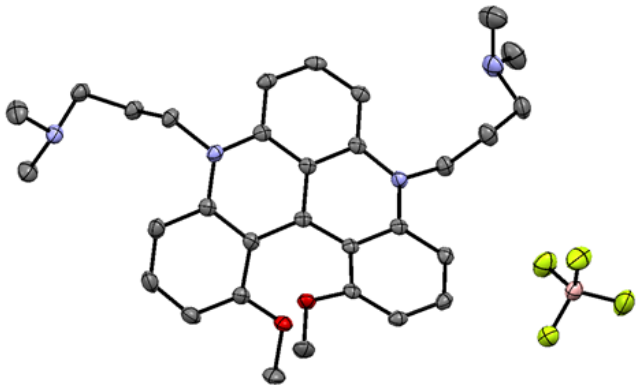

Table S1 Crystal data and structure refinement for 2-H$^+$

Identification code	2-H$^+$
CCDC	2004976
Empirical formula	$C_{32}H_{41}BCl_2F_4N_4O_2$
Formula weight	671.43
Temperature/K	100.0
Crystal system	triclinic
Space group	P-1
a/Å	11.5110(3)
b/Å	12.4254(3)
c/Å	13.1831(3)
α/°	85.1060(18)
β/°	78.778(2)
γ/°	64.945(3)
Volume/Å^3	1675.45(8)
Z	2
ρ_{calc}g/cm^3	1.3308
μ/mm^{-1}	0.251
F(000)	705.0
Crystal size/mm^3	0.3 × 0.25 × 0.2
Radiation	Mo Kα (λ = 0.71073)
2Θ range for data collection/°	6.3 to 52.74
Index ranges	-16 ≤ h ≤ 16, -17 ≤ k ≤ 17, -17 ≤ l ≤ 18
Reflections collected	35035
Independent reflections	6857 [R_{int} = 0.0227, R_{sigma} = 0.0230]
Data/restraints/parameters	6857/0/440
Goodness-of-fit on F^2	1.077
Final R indexes [I>=2σ (I)]	R_1 = 0.0460, wR_2 = 0.1040
Final R indexes [all data]	R_1 = 0.0508, wR_2 = 0.1066
Largest diff. peak/hole / e Å^{-3}	0.37/-0.25

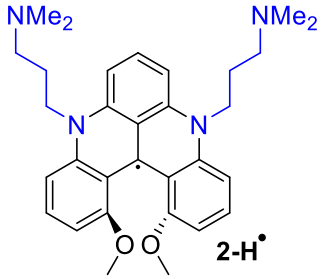

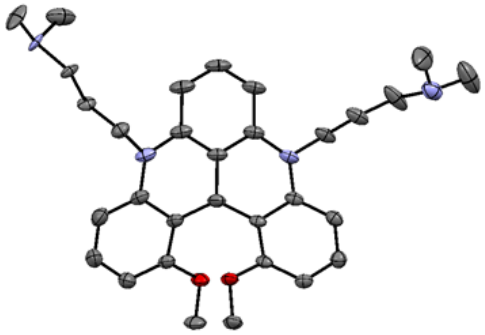

Table S2 Crystal data and structure refinement for 2-H•	
Identification code	2-H•
CCDC	2004977
Empirical formula	$C_{31}H_{39}N_4O_2$
Formula weight	500.53
Temperature/K	100.0
Crystal system	orthorhombic
Space group	Pbca
a/Å	20.1829(5)
b/Å	10.7314(3)
c/Å	25.5707(7)
α/°	90
β/°	90
γ/°	90
Volume/Å^3	5538.4(3)
Z	8
ρ_{calc}g/cm^3	1.201
μ/mm^{-1}	0.382
F(000)	2155.0
Crystal size/mm^3	0.12 × 0.1 × 0.05
Radiation	GaKα (λ = 1.34138)
2Θ range for data collection/°	7.12 to 146.538
Index ranges	-27 ≤ h ≤ 24, -13 ≤ k ≤ 14, -32 ≤ l ≤ 31
Reflections collected	45766
Independent reflections	7238 [R_{int} = 0.0549, R_{sigma} = 0.0405]
Data/restraints/parameters	7238/6/414
Goodness-of-fit on F^2	1.095
Final R indexes [I>=2σ (I)]	R_1 = 0.0669, wR_2 = 0.1402
Final R indexes [all data]	R_1 = 0.0906, wR_2 = 0.1506
Largest diff. peak/hole / e Å^{-3}	0.54/-0.25

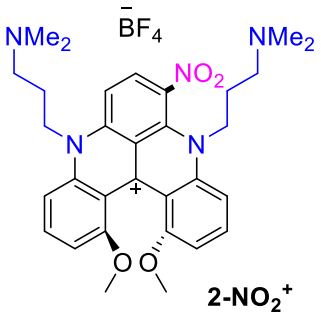

2-NO_2^+

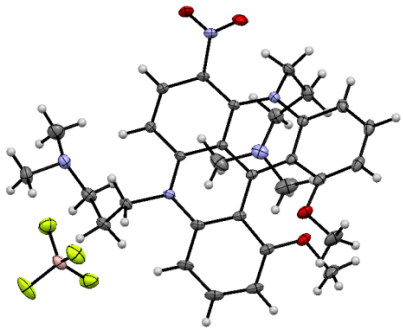

Table S3 Crystal data and structure refinement for 2-NO_2^+.

Identification code	**2-NO_2^+**
CCDC	2004974
Empirical formula	C31 H38 N5 O4
Formula weight	544.66
Temperature/K	100.0
Crystal system	triclinic
Space group	P-1
a/Å	10.834(7)
b/Å	11.010(7)
c/Å	13.357(9)
α/°	71.977(17)
β/°	84.217(17)
γ/°	64.762(17)
Volume/$Å^3$	1675.45(8)
Z	2
$\rho_{calc}g/cm^3$	1.3308
μ/mm^{-1}	0.251
F(000)	705.0
Crystal size/mm^3	0.3 × 0.25 × 0.2
Radiation	Mo Kα (λ = 0.71073)
2Θ range for data collection/°	6.3 to 52.74
Index ranges	$-16 \le h \le 16$, $-17 \le k \le 17$, $-17 \le l \le 18$
Reflections collected	35035
Independent reflections	6857 [R_{int} = 0.0227, R_{sigma} = 0.0230]
Data/restraints/parameters	6857/0/440
Goodness-of-fit on F^2	1.077
Final R indexes [I>=2σ (I)]	R_1 = 0.0460, wR_2 = 0.1040
Final R indexes [all data]	R_1 = 0.0508, wR_2 = 0.1066
Largest diff. peak/hole / e $Å^{-3}$	0.37/-0.25

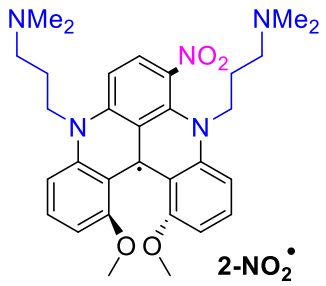

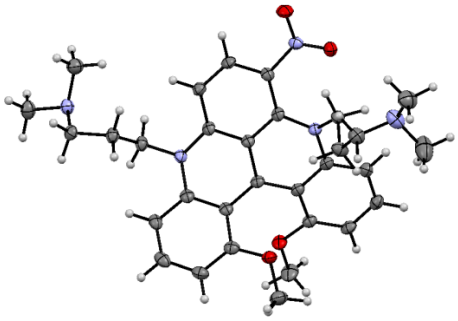

Table S4 Crystal data and structure refinement for 2-$NO_2^{\bullet}$

Identification code	**2-$NO_2^{\bullet}$**
CCDC	2004975
Empirical formula	C31 H38 N5 O4
Formula weight	544.66
Temperature/K	100.0
Crystal system	triclinic
Space group	P-1
a/Å	10.834(7)
b/Å	11.010(7)
c/Å	13.357(9)
α/°	71.977(17)
β/°	84.217(17)
γ/°	64.762(17)
Volume/$Å^3$	1369.6(16)
Z	2
$\rho_{calc}g/cm^3$	1.321
μ/mm^{-1}	0.089
F(000)	582.0
Crystal size/mm^3	0.12 × 0.1 × 0.05
Radiation	GaKα (λ = 1.34138)
2Θ range for data collection/°	7.12 to 146.538
Index ranges	-27 ≤ h ≤ 24, -13 ≤ k ≤ 14, -32 ≤ l ≤ 31
Reflections collected	45766
Independent reflections	7238 [R_{int} = 0.0549, R_{sigma} = 0.0405]
Data/restraints/parameters	7238/6/414
Goodness-of-fit on F^2	1.095
Final R indexes [I>=2σ (I)]	R_1 = 0.0669, wR_2 = 0.1402
Final R indexes [all data]	R_1 = 0.0906, wR_2 = 0.1506
Largest diff. peak/hole / e $Å^{-3}$	0.54/-0.25

Table S5. Characteristic Bond lengths and bond angles for **2-H$^+$**, **2-H$^\bullet$**, **2-NO$_2^+$** and **2-NO$_2^\bullet$**

	Bonds length (Å)			
Selected Bonds	**2-H$^+$**	**2-H$^\bullet$**	**2-NO$_2^+$**	**2-NO$_2^\bullet$**
C1–C2	1.406(2)	1.439(2)	1.431(1)	1.423(3)
C1–C3	1.435(3)	1.444(2)	1.413(1)	1.429(3)
C1–C4	1.431(3)	1.446(2)	1.440(1)	1.438(3)
O1–O2	2.743	2.772	2.659	2.773
C2–C5	-	-	1.435(1)	1.408(3)
C–NO$_2$	-	-	1.452(1)	1.444(3)
N2-O (NO$_2$)	-	-	1.233(1)/1.235(1)	1.226(2)/1.235(2)
	Angles (°)			
	2-H$^+$	**2-H$^\bullet$**	**2-NO$_2^+$**	**2-NO$_2^\bullet$**
o-(MeO)Ph ^ *o*-(MeO)Ph	41.93	45.92	38.37	52.05
NO$_2$-Ph ^ N-*n*Pr-NMe$_2$	-	-	37.69	45.60

V. DFT Computational Details

Density functional theory (DFT) calculations[1,2] were done on a full atom scale using the unrestricted long-range corrected version[3] of the hybrid 1993 Becke three-parameter exchange functional[4–6] and the Lee–Yang–Parr non-local correlation functional[7] (UCAM-B3LYP) implemented in Gaussian 09, revision D.01, software.[8] The internal triple-ζ quality basis set 6-311G(d,p) was applied on all atoms. The geometry optimized models were found to be minima in the potential energy surface by the lack of imaginary vibrations in the frequency calculations. Molecular orbitals (MO) and self-consistent field (SCF) spin density surfaces were obtained using the cubegen utility in Gaussian 09. All calculations were executed on the Ocelote cluster at the University of Arizona High Performance Computing center.

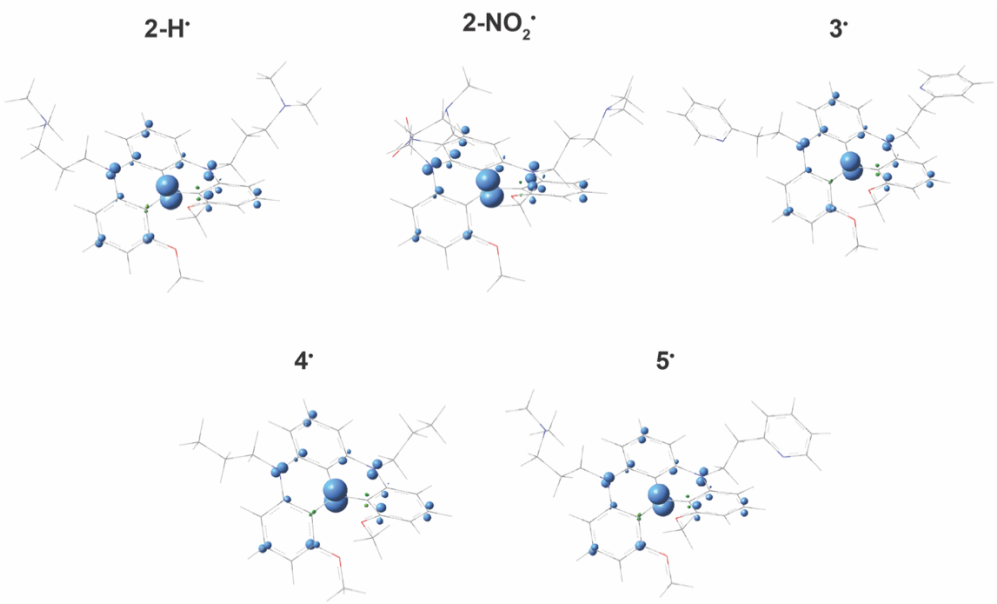

Figure S24. Spin density distribution for the calculated open-shell doublet models of **2–5**$^\bullet$. Surfaces were plotted at a 0.015 isovalue.

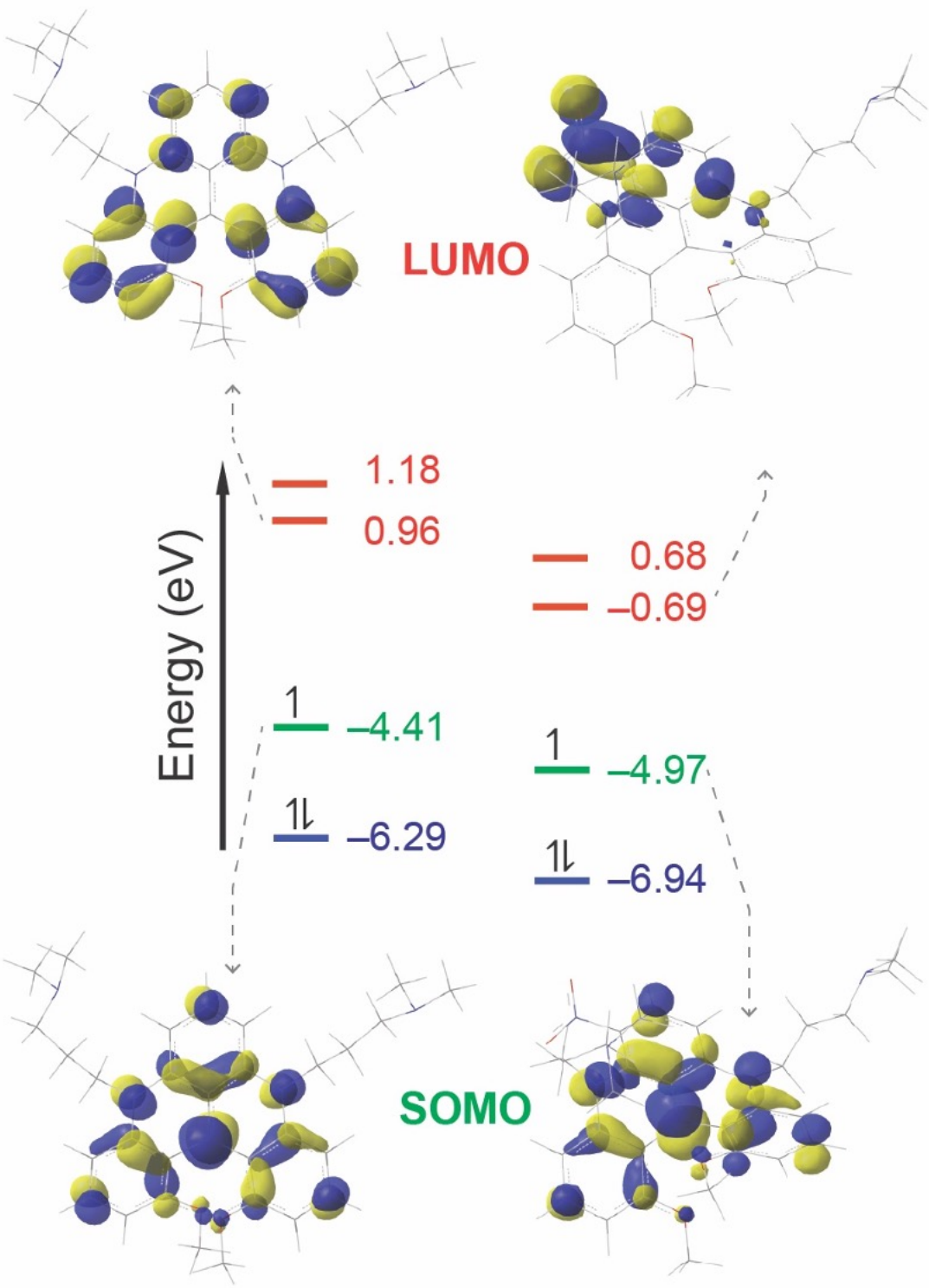

Figure 25. Frontier molecular orbital diagram of **2-H**$^{\bullet}$ (left) and **2-NO$_2$**$^{\bullet}$ (right) Percentage orbital contribution across the central carbon is also shown. Surfaces were plotted at a 0.04 isovalue.

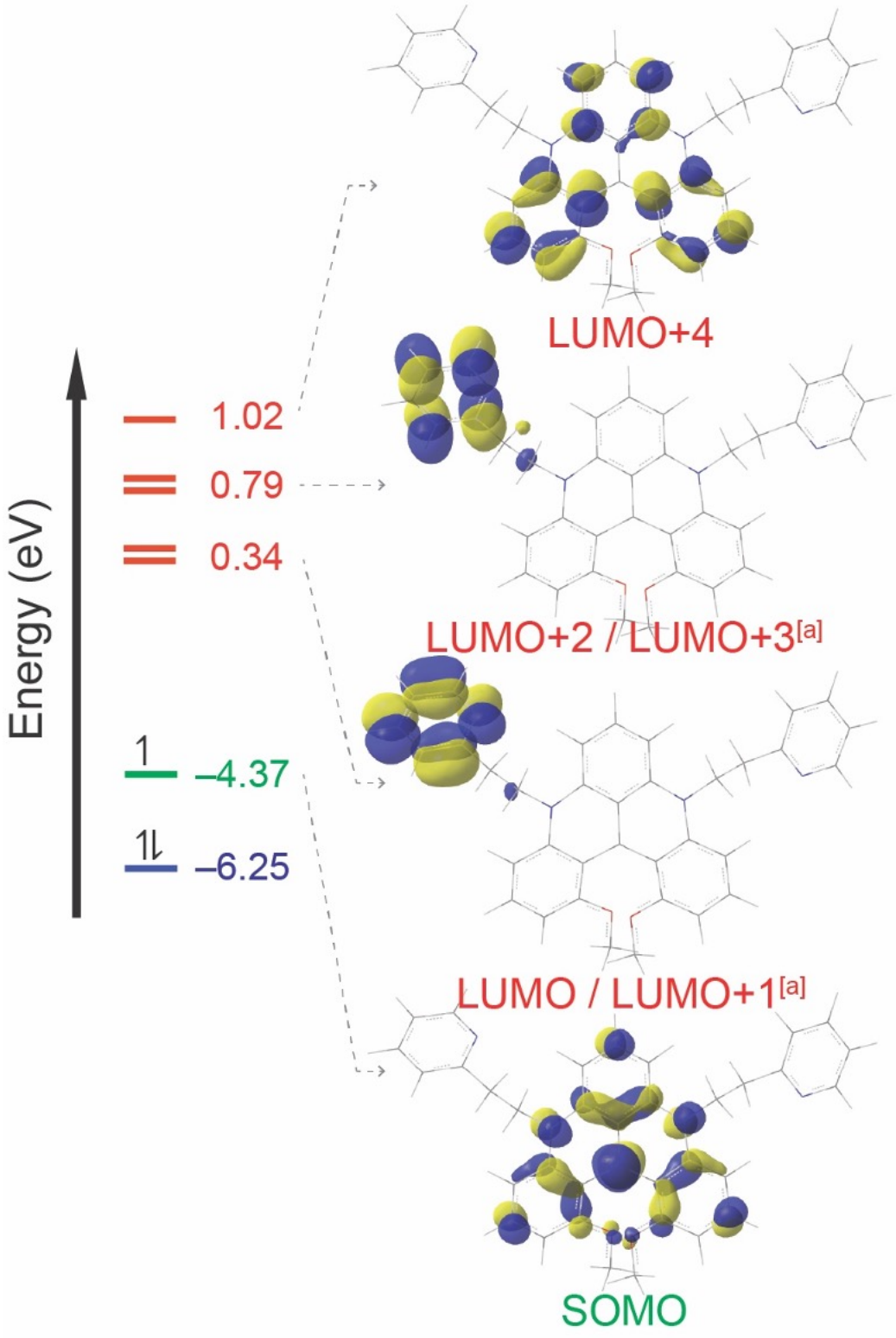

Figure S26. Frontier MO diagram for the calculated DFT model of **3**˙. Iso-surfaces corresponding to the alpha orbitals of the model are shown at a 0.04 value. [a] The set of degenerate MOs corresponds to the same π^* interaction located in the opposite pyridine moiety.

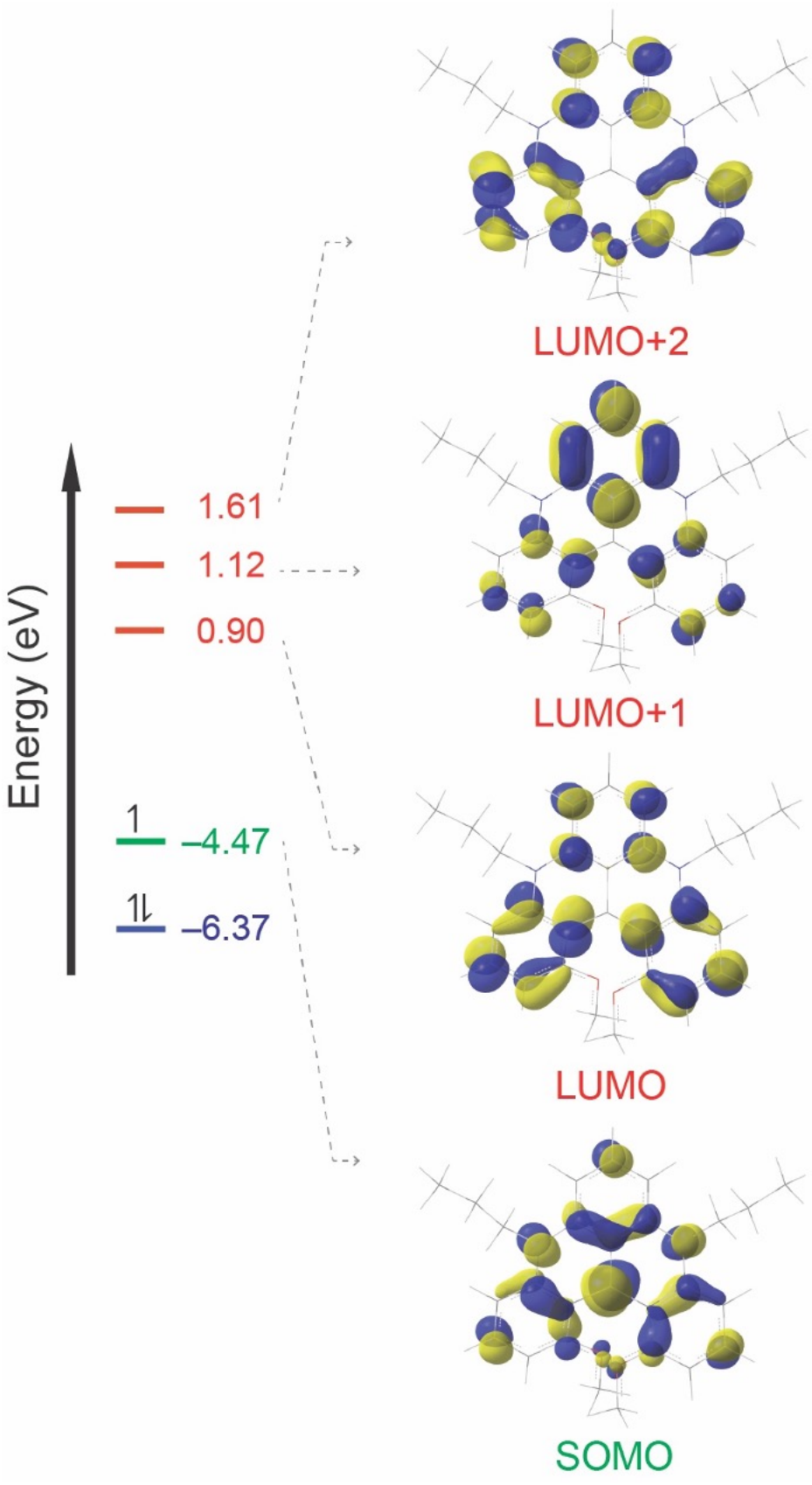

Figure S27. Frontier MO diagram for the calculated DFT model of **4˙**. Iso-surfaces corresponding to the alpha orbitals of the model are shown at a 0.04 value.

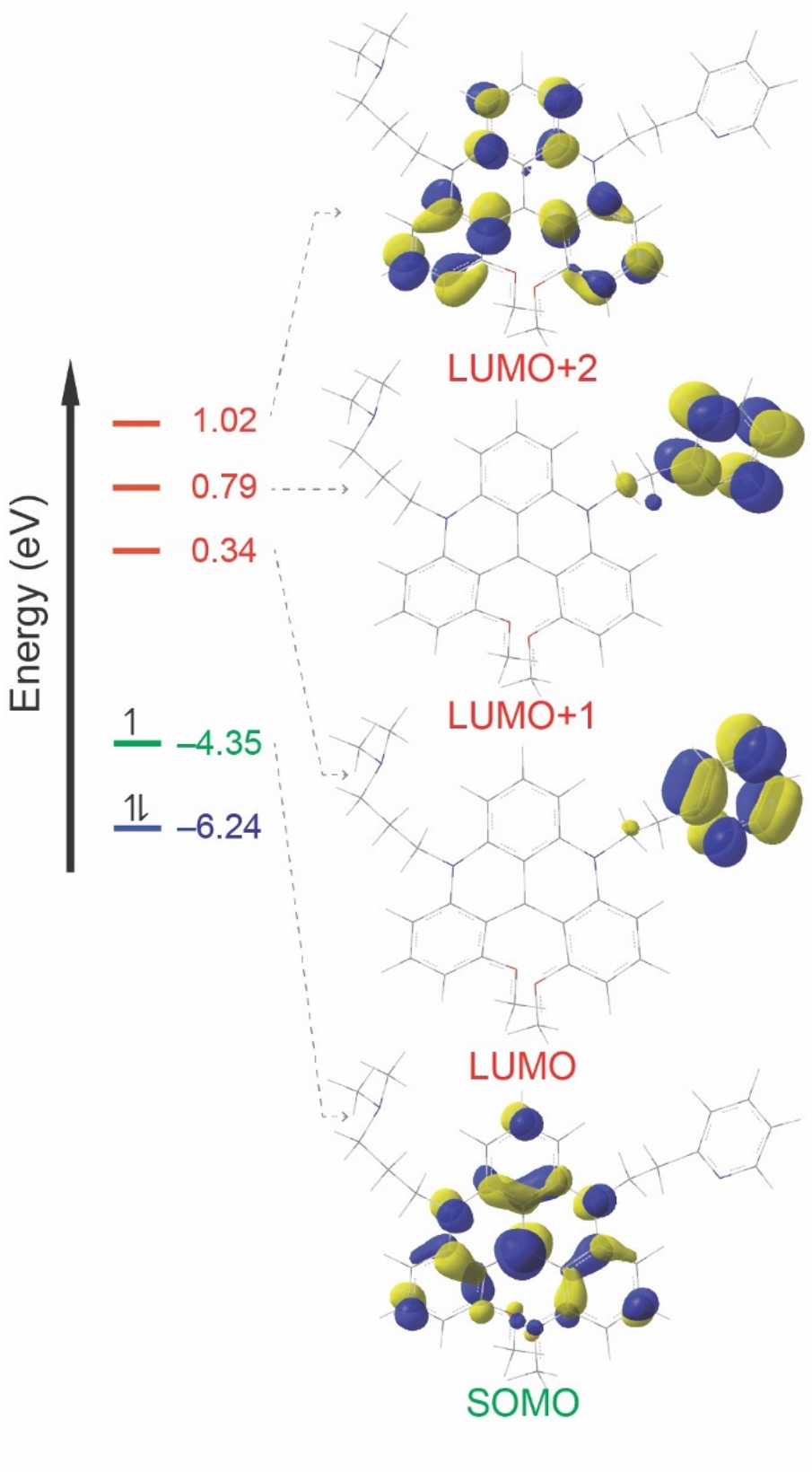

Figure S28. Frontier MO diagram for the calculated DFT model of **5**˙. Iso-surfaces corresponding to the alpha orbitals of the model are shown at a 0.04 value.

VI. EPR Spectroscopy

The continuous wave (CW) electron paramagnetic resonance (EPR) experiments were carried out at the University of Arizona EPR Facility, on the X-band EPR spectrometer Elexsys E500 (Bruker Biospin) equipped with the electron-nuclear double resonance (ENDOR) system and variable temperature nitrogen flow system.

The ^{1}H hfi constants determined by ENDOR (see Fig. 2 of the main text) were assigned to specific molecular positions by comparing them to the DFT calculations. Figure S29 shows the relevant part of the molecular structure of **2-H$^\bullet$** and **3$^\bullet$-5$^\bullet$** (i.e. one half of the structure is shown because the ring system has an approximate C_2 symmetry with respect to C-C bond shown by thick brown line in Fig. S29). The calculated spin populations for the ring carbons, nitrogen(s), and an oxygen are indicated in magenta. The ^{1}H *hfi* constants resulting from the calculated spin populations on the hydrogen atoms ($a_H = 1420\rho_H$ [MHz]) are shown in green, and the corresponding tentatively assigned experimental hfi constans are shown in light blue. The ENDOR line assignments are indicated in parentheses. The spin populations on the ring carbon atoms estimated from the experimental a_H values of the neighboring protons (α-protons) using the McConnell equation: $a_H = (-63\ \text{MHz})\rho_C$, are shown in Fig. S29 in dark blue.

For radical **2-NO$_2^\bullet$**, the hydrogen atom marked by an asterisk in Fig. S29 is substituted by the NO_2 group (on one side of the molecule only, see II-2). The spectroscopic result of this substitution is a ~ 30% decrease of the relative intensity of (*b*,*b'*) lines in the ENDOR spectrum and appearance of (*d*,*d'*) and (*e*,*e'*) lines corresponding to $a_H = 6.05$ and 5.37 MHz, respectively (see Fig. 2a of the main text). Such a significant decrease in the (*b*,*b'*) lines intensity can be explained by the fact that, according to our hfi assignments shown in Fig. S29, the H to NO_2 substitution removes one proton from the $a_H = 2.3$ MHz pool ((*b*,*b'*) lines). In addition, two more protons are "relocated" from the (*b*,*b'*) lines to the new (*d*,*d'*) and (*e*,*e'*) ENDOR lines. The three protons removed from the $a_H = 2.3$ MHz pool, which originally consisted of 10 protons, thus explain the 30% decrease of the (*b*,*b'*) lines intensity. The 6.05 and 5.37 MHz should most likely be assigned to the protons of the methylene group attached to the ring nitrogen neighbouring the NO_2 group in **2-NO$_2^\bullet$**, and the change of the a_H values for these protons from 2.3 MHz to 6.05 and 5.37 MHz is mostly caused by the conformational changes that result in their repositioning with respect to the spin-carrying electronic orbital.

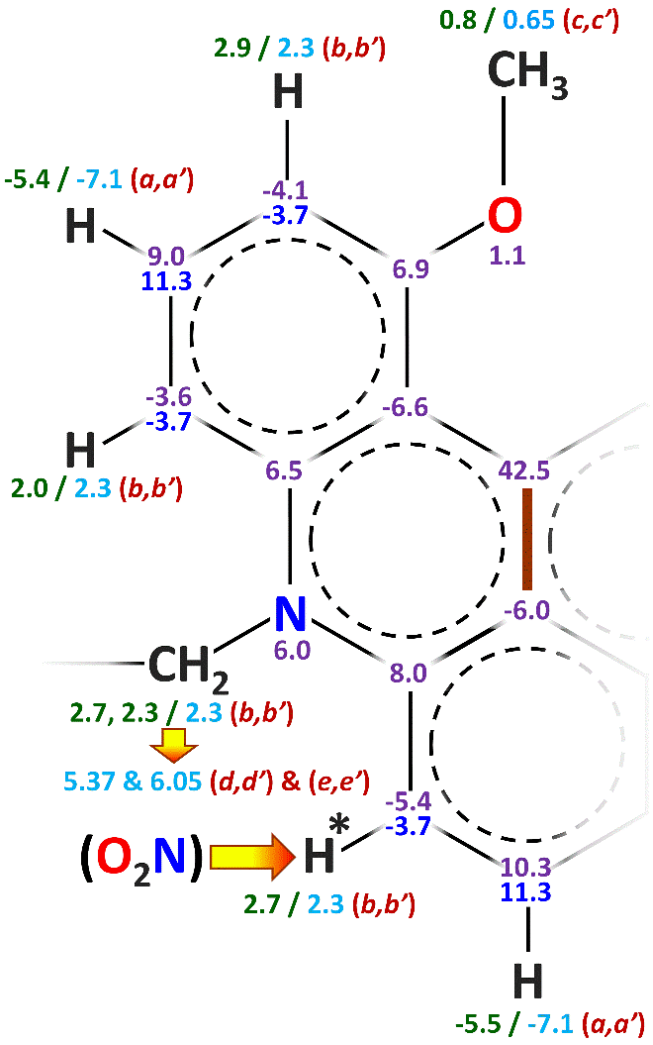

Figure S29. Spin populations and ^{1}H hfi constants in radicals **2**$^{\bullet}$-**5**$^{\bullet}$. Only one half of the ring system is shown. The other half is related by C_2 symmetry with respect to the C-C bond shown by the thick brown line. In radical **2-NO$_2$**$^{\bullet}$, the hydrogen marked by an asterisk is substituted by NO_2 group on one side of the molecule only. This substitution and the resulting change of the proton hfi constants are shown by the colored arrows. The calculated spin populations of the ring atoms are shown in magenta. The calculated ^{1}H hfi constants are shown in green, and those determined by ENDOR are in light blue. The ENDOR line assignments are in red color and in parentheses. The ring carbon spin populations estimated from the experimental hfi constants using the McConnell equation are shown in dark blue.

VII. Cyclic Voltammetry

Note: Cyclic voltammograms of $\mathbf{2}^{+}$-$\mathbf{5}^{+}$ (2 mM) in DCM ([TBA][PF_6] 0.1 M) solutions recorded at a platinum working electrode (n = 0.1 V/s) and Ag/Ag^{+} as internal reference electrode, Fc/Fc^{+} was used as secondary reference by setting its $E_{1/2} = 0$. The arrows indicate the direction of the scan. All the cyclic voltammograms were recorded at ambient temperature.

VII.1 CV data for $\mathbf{2\text{-}H}^{+}$

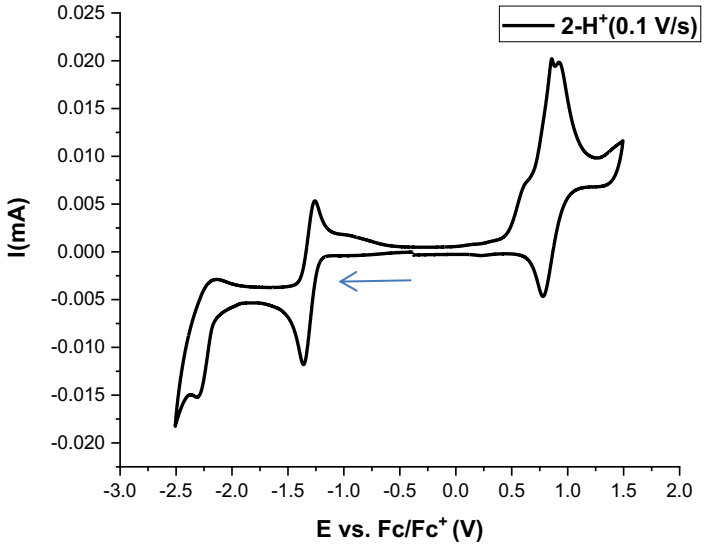

Figure 30. A cyclic voltammogram of $\mathbf{2\text{-}H}^{+}$ (2 mM) in CH_2Cl_2 ([TBA][PF_6] 0.1 M) solutions

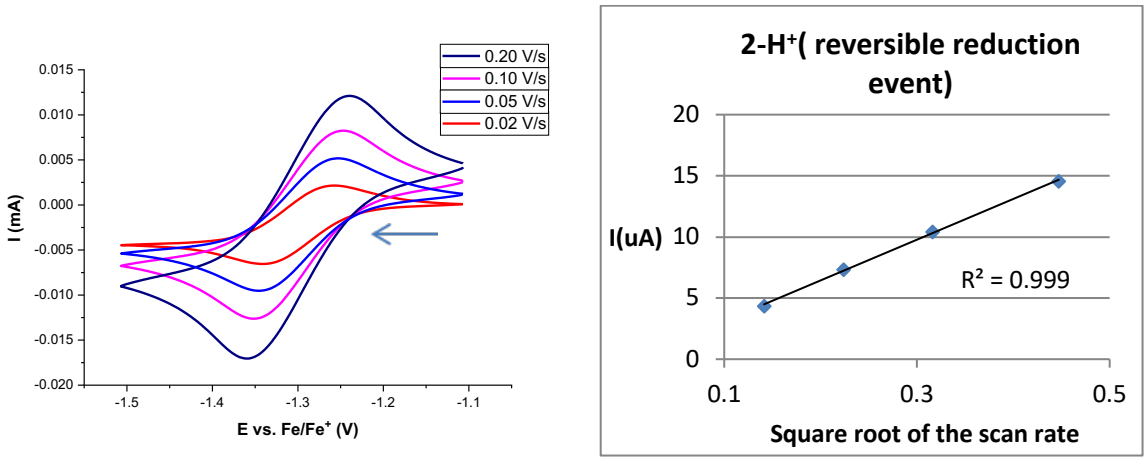

Figure S31. A reversible reduction cyclic voltammogram of $\mathbf{2\text{-}H}^{+}$ (2 mM) in CH_2Cl_2 ([TBA][PF_6] 0.1 M) solutions

VII.2 CV data for 2-NO_2^+

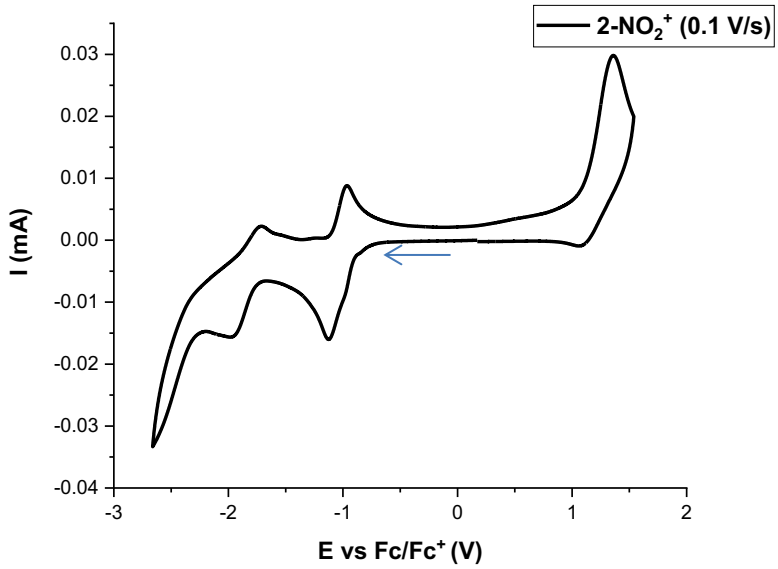

Figure 32. A cyclic voltammogram of **2-NO_2^+** (2 mM) in CH_2Cl_2 ([TBA][PF_6] 0.1 M) solutions

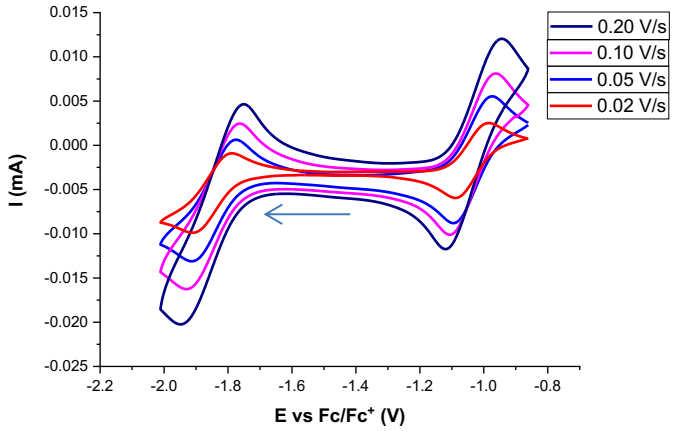

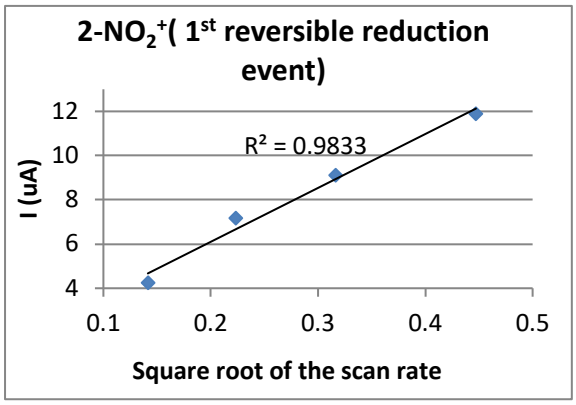

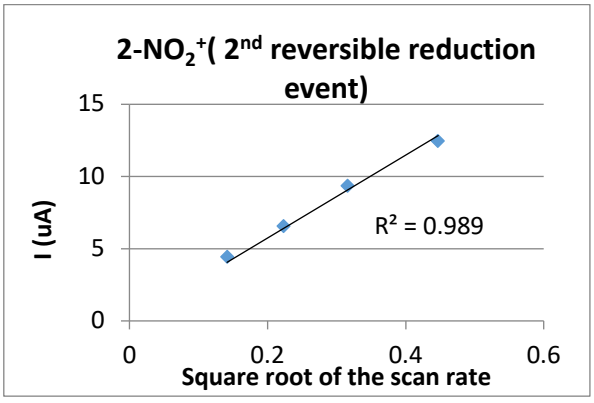

Figure S33. A reversible reduction cyclic voltammogram of **2-NO_2^+** (2 mM) in CH_2Cl_2 ([TBA][PF_6] 0.1 M) solutions

VII.3 CV data for 3^+

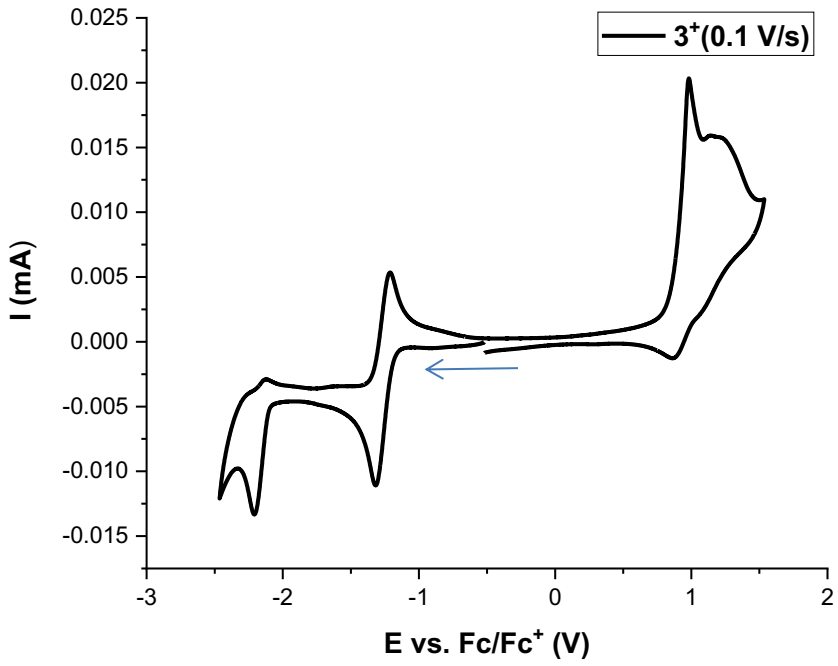

Figure 34. A cyclic voltammogram of $\mathbf{3}^+$ (2 mM) in CH_2Cl_2 ([TBA][PF_6] 0.1 M) solutions

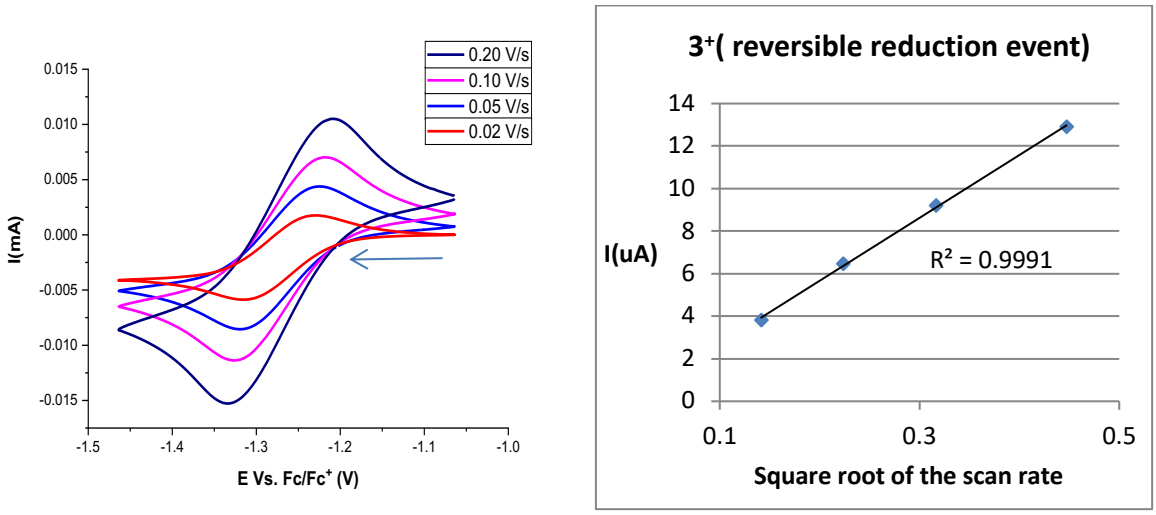

Figure S35. A reversible reduction cyclic voltammogram of $\mathbf{3}^+$ (2 mM) in CH_2Cl_2 ([TBA][PF_6] 0.1 M) solutions

VII.4 CV data for 4^+

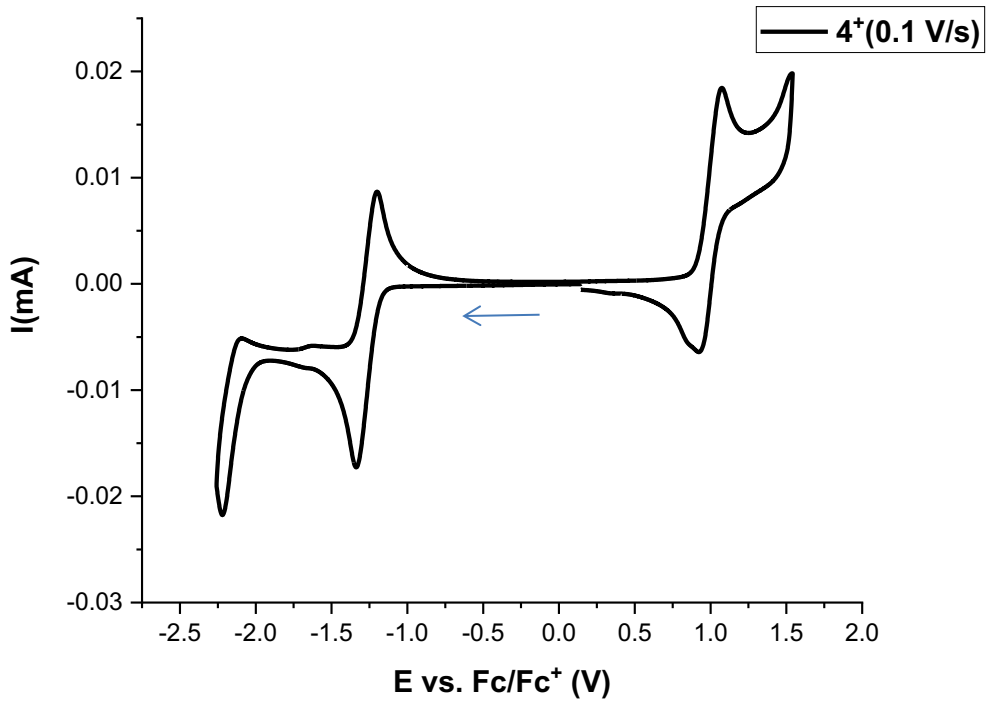

Figure 36. A cyclic voltammogram of $\mathbf{4}^+$ (2 mM) in CH_2Cl_2 ([TBA][PF_6] 0.1 M) solutions

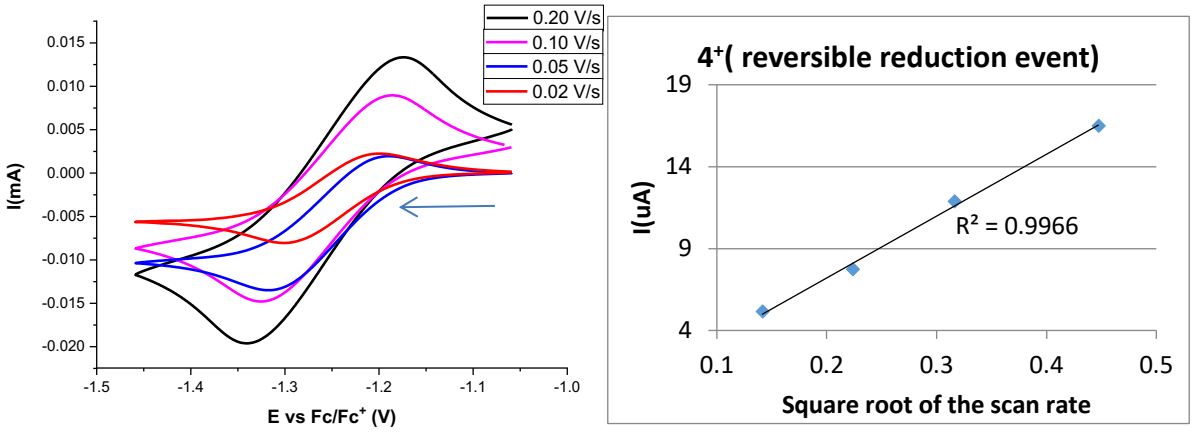

Figure S37. A first reversible reduction cyclic voltammogram of $\mathbf{4}^+$ (2 mM) in CH_2Cl_2 ([TBA][PF_6] 0.1 M) solutions

VII.5 CV data for 5^+

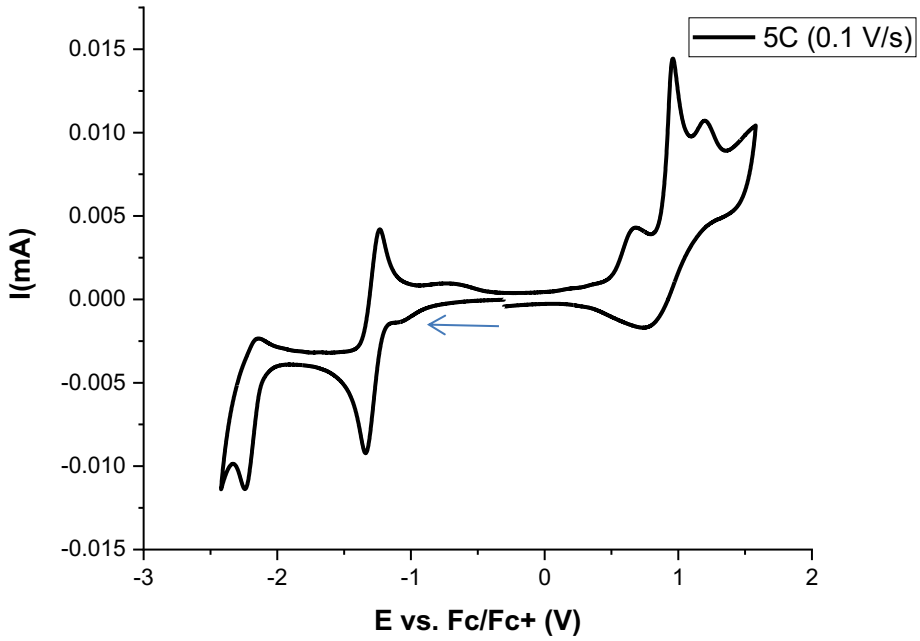

Figure 38. A cyclic voltammogram of $\mathbf{5}^+$ (2 mM) in CH_2Cl_2 ([TBA][PF_6] 0.1 M) solutions

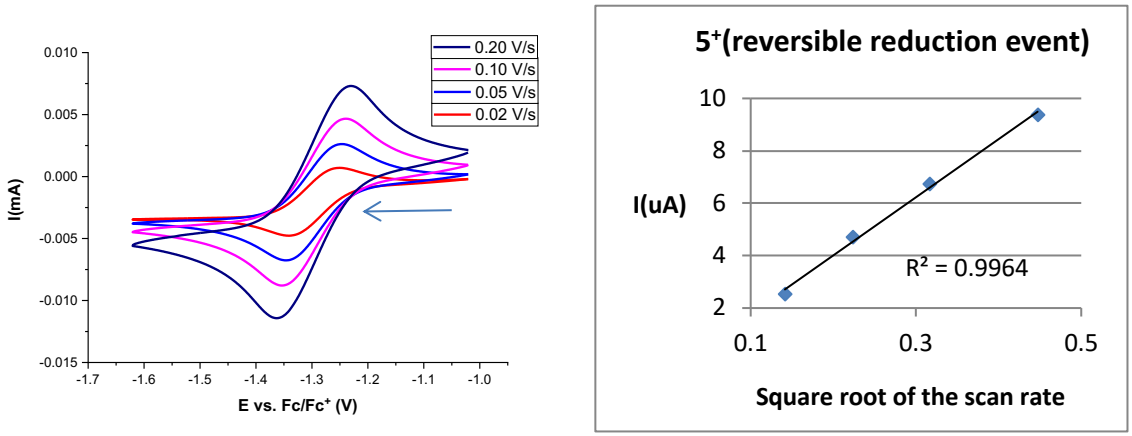

Figure S39. A second reversible reduction cyclic voltammogram of $\mathbf{5}^+$ (2 mM) in CH_2Cl_2 ([TBA][PF_6] 0.1 M) solutions

VIII. UV-vis Spectra Analysis

VIII.1 UV-vis Spectroscopy under anaerobic conditions

Absorption spectra were recorded on a ThermoScientific Evolution 220 UV-Visible spectrophotometer at 25 ˚C in analytical-grade solvents (con. 10-5 M). All UV samples for spectroscopy were prepared under an inert atmosphere in a Mbraun Labmaster glovebox maintained at less than 1 ppm O_2. A 3 mL gas-tight cuvette (Quartz Cuvette Self Masking Screw Cap) was used for anaerobic acquisition of spectra. All radicals decay kinetics were studied in the presence of oxygen, solutions of **2˙–5˙** in CF_3-toluene prepared in a N_2-filled glove box were exposed to air and monitored by UV−vis spectroscopy over time.

The compounds **2-H**$^+$, **3**$^+$-**5**$^+$ shows similar spectrum with three distinct absorption in the visible regions (l > 350nm), indicating that the nitrogen bridge substituents have a negligible effect on the transition energy (Figure S29, and Table S9). A sharp peak around 620 nm (ε > 1400), a shoulder at 570 nm (ε > 10000), and a broad absorption around 430 nm (ε > 6000).

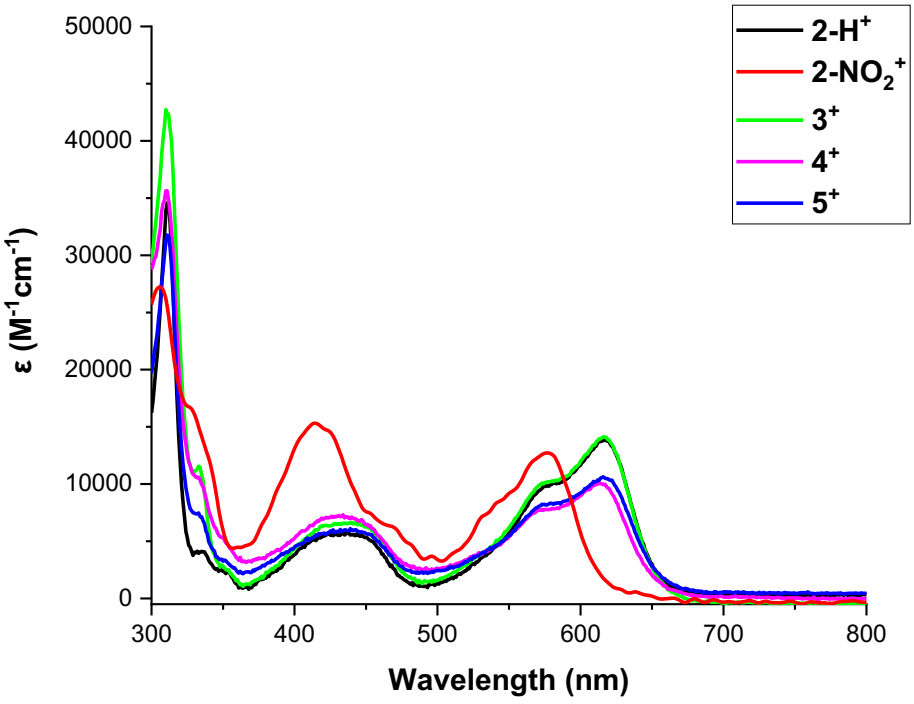

Figure S40. Combined UV-visible absorption spectra for **2**$^+$-**5**$^+$

All four radicals, **2-H$^{\bullet}$**, **3$^{\bullet}$-5$^{\bullet}$** have a sharp absorption band with the maximum absorbance around 390 nm ($\varepsilon > 15000$), a shoulder at around 450 nm ($\varepsilon > 5000$), and a broad absorption peak around 560 nm ($\varepsilon > 6000$) (Figure S40, and Table S9).The blue shift in absorption bands compared to their cationic analogs indicates the presence of radical character at the central atom and a reduction in the involvement of the heteroatoms in the molecular framework as well as a remarkably decreased conjugation.

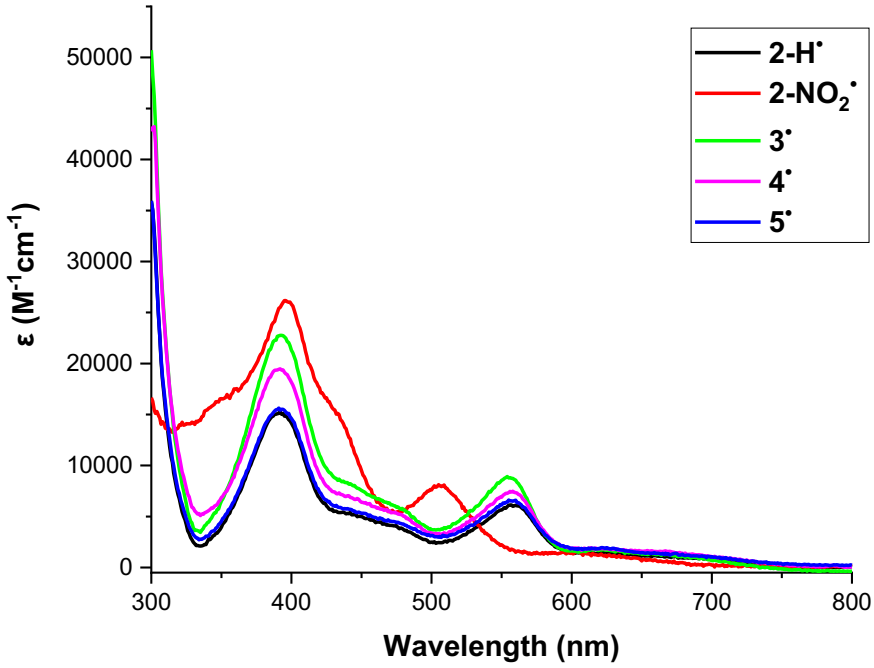

Figure S41. Combined UV-visible absorption spectra for **2$^{\bullet}$-5$^{\bullet}$**

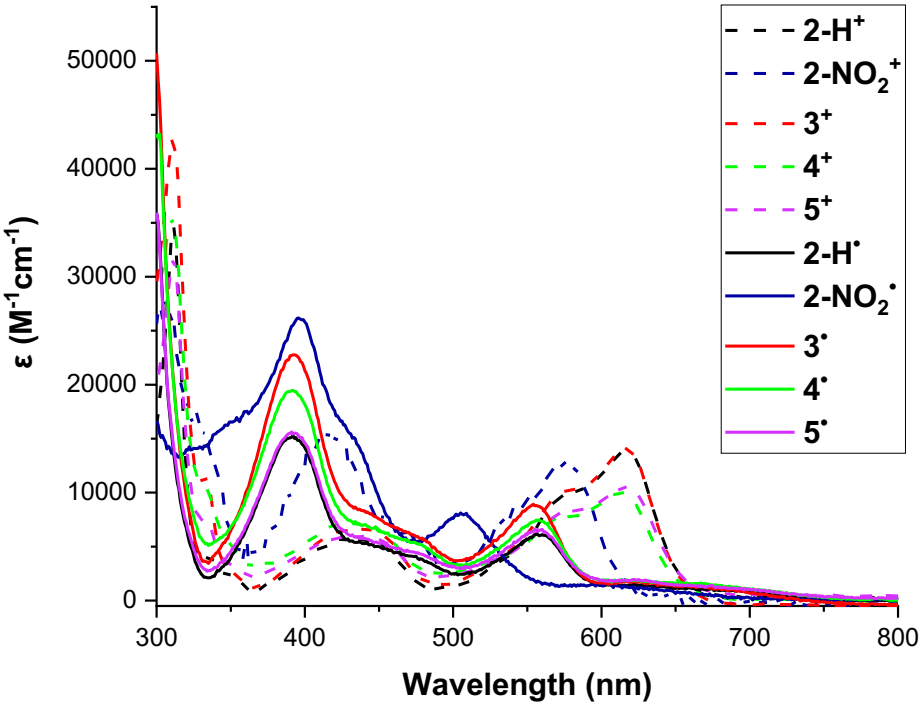

Figure S42 Combined UV-visible absorption spectra for **2**$^{+}$-**5**$^{+}$ and **2**$^{\bullet}$-**5**$^{\bullet}$

Table S6. Main features of UV-vis spectra of compounds of compounds **2-5** in *α,α,α*-Trifluorotoluene

Compound	λ_{max} absorption [nm] (ε [$M^{-1}.cm^{-1}$])
2-H^{+}	435 (6044), 577 (10526), 617 (14431)
2-H$^{\bullet}$	392 (15936), 445 (5093), 558 (6496)
2-NO$_2$ $^{+}$	417 (18320), 576 (12854)
2-NO$_2$ $^{\bullet}$	395 (26172), 505 (8116), 604 (1559)
3^{+}	433 (7501), 574 (10987), 612 (14925)
3$^{\bullet}$	392 (23422), 444 (8061), 554 (9555)
4^{+}	434 (7325), 570 (7706), 613 (10006)
4$^{\bullet}$	392 (19476), 476 (5245), 556 (7469)
5^{+}	440 (6368), 572 (8705), 615 (11032)
5$^{\bullet}$	391 (16222), 473 (5229), 557 (7160)

VIII.2 Monitoring of radical decay upon exposure to air by UV-vis Spectroscopy.

To quantify the stability of all radicals in the presence of oxygen, solutions of **2˙**–**5˙** in CF_3-toluene prepared in a N_2-filled glove box were exposed to air and monitored by UV−vis spectroscopy over time. The absorption spectrum of the cation and their radical analog under N2 atmosphere are shown in Figure S42, S44, S46, S48 and S50. The change in absorption spectroscopy for radical **2-H˙**, **2-NO_2˙**, and **3˙-5˙** after exposure to air are shown in Figure S43, S45, S47, S49 and S51 respectively, and show a slow decreased with time, reaching the lower absorption limit within hours.

The first order decay of the absorption of each radical, well as their $t_{1/2}$ is shown in Figure S41.

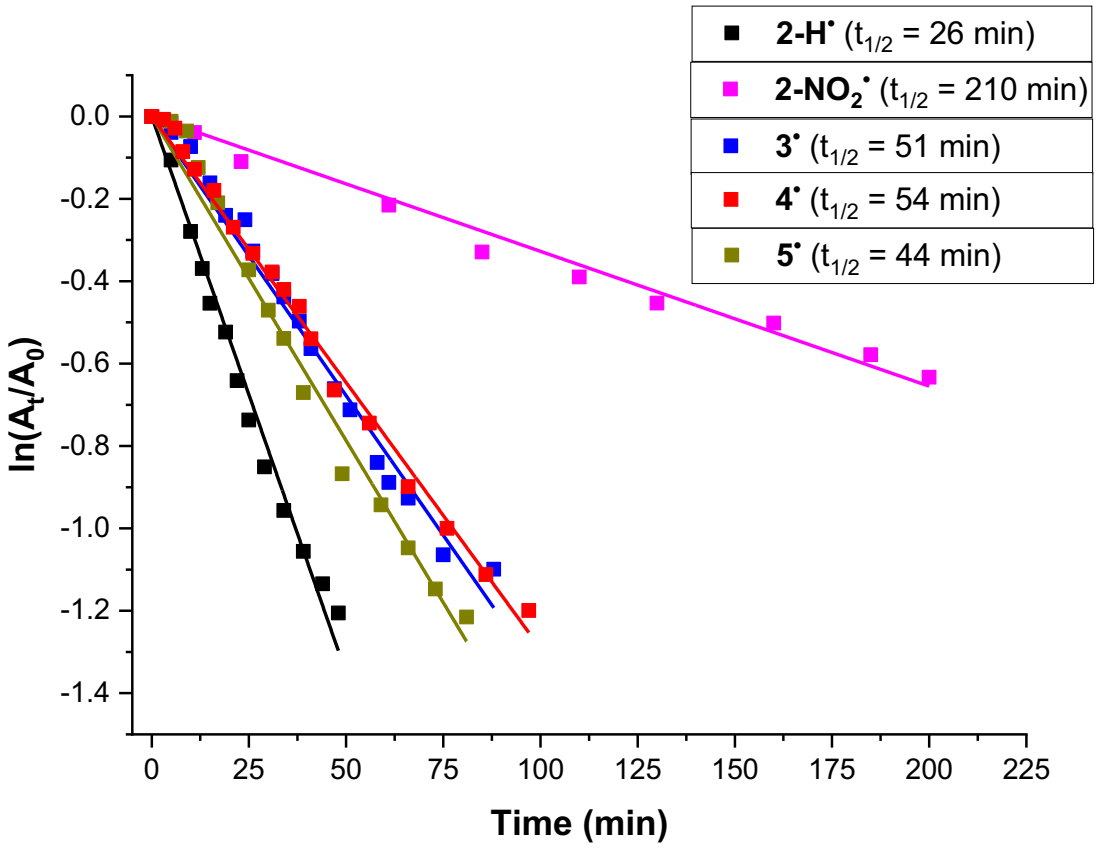

Figure S43. Plot of the first order decay of the absorbance for radical **2˙-5˙**

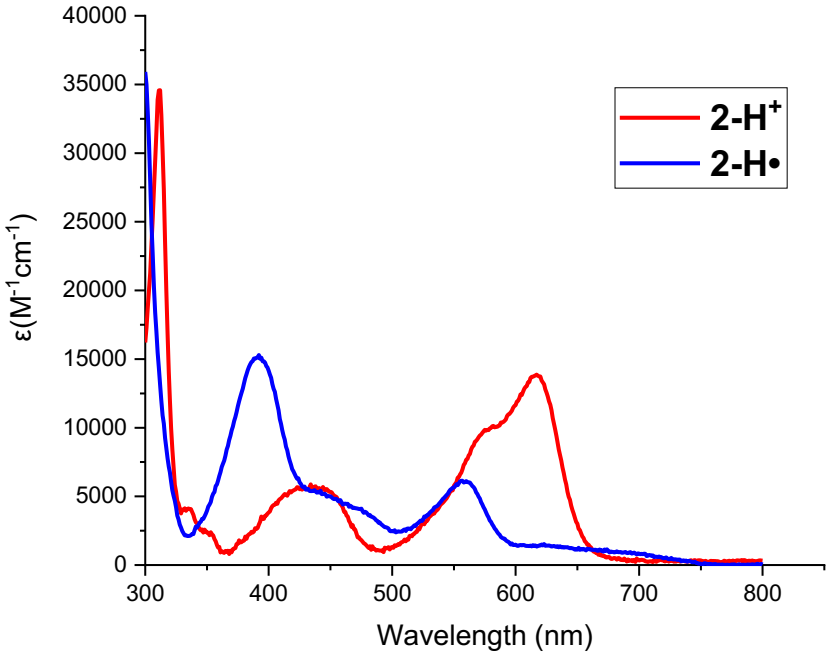

Figure S44: UV−vis spectra (6.8×10^{-5} M in CF_3-Toluene, room temperature) of **2-H**$^+$

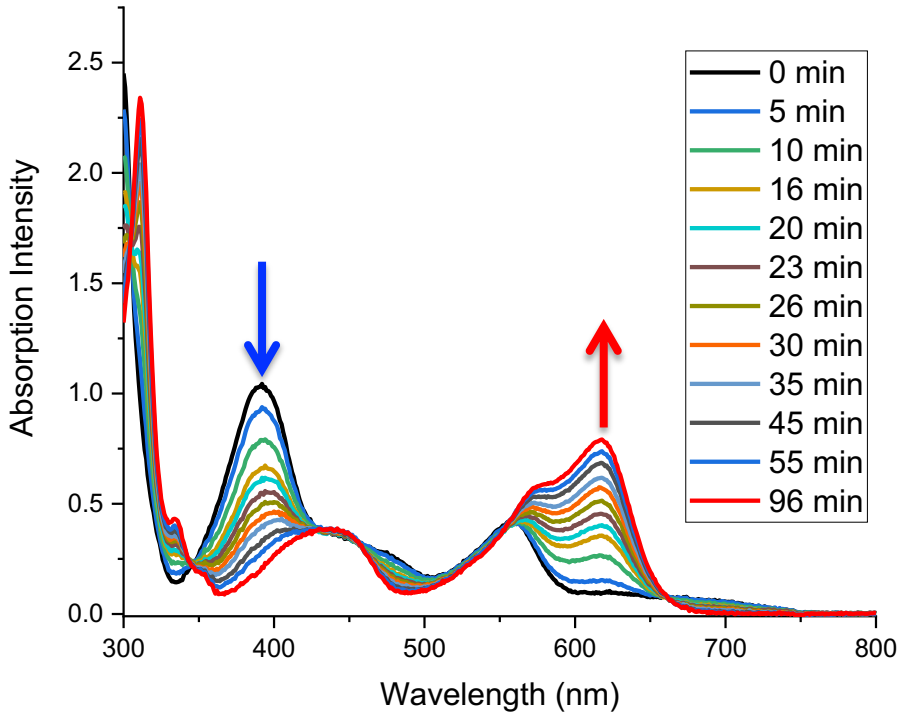

Figure S45. Change of UV-visible absorption spectra for **2-H**$^{\bullet}$ (6.8×10^{-5} M) with time after exposure to air

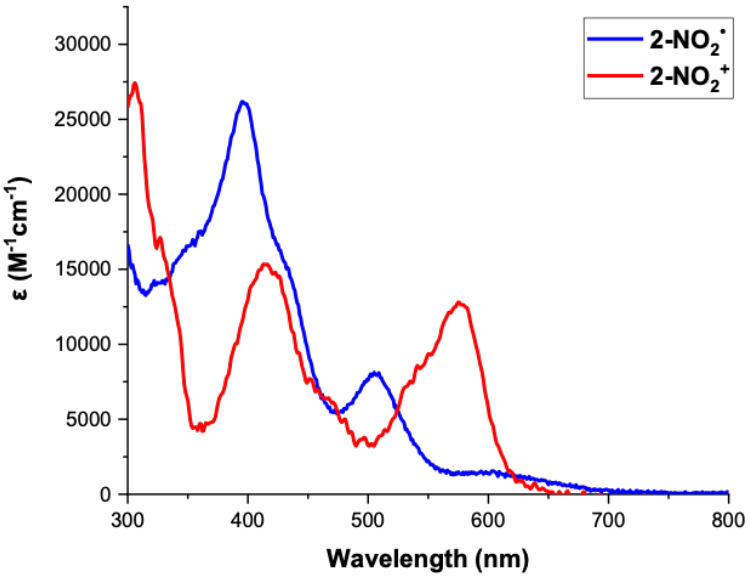

Figure S46: UV−vis spectra (5.9×10^{-5} M in CF_3-Toluene, room temperature) of **2-NO_2**

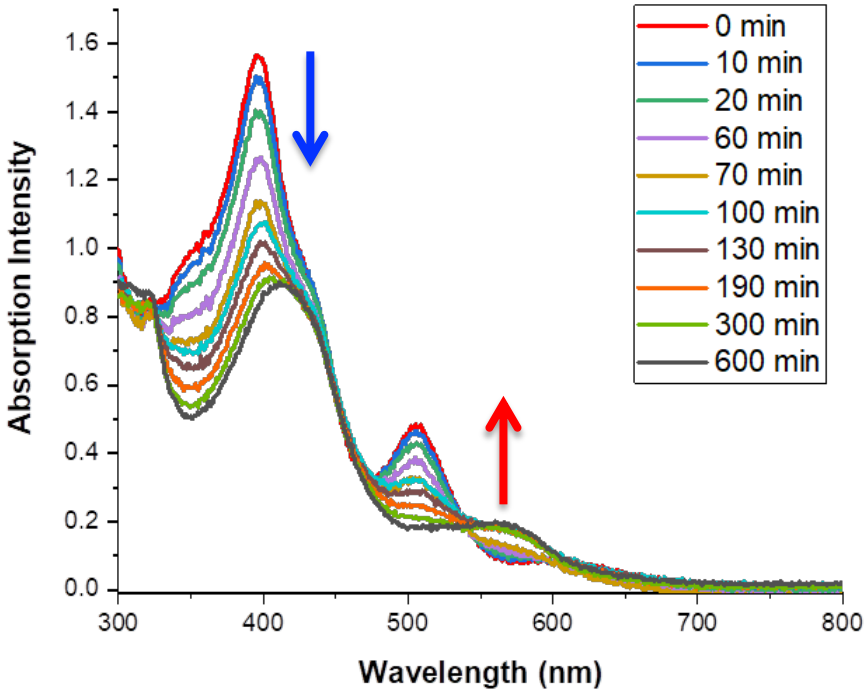

Figure S47. Change of UV-visible absorption spectra for **2-$NO_2^{\bullet}$** (5.9×10^{-5} M) with time after exposure to air

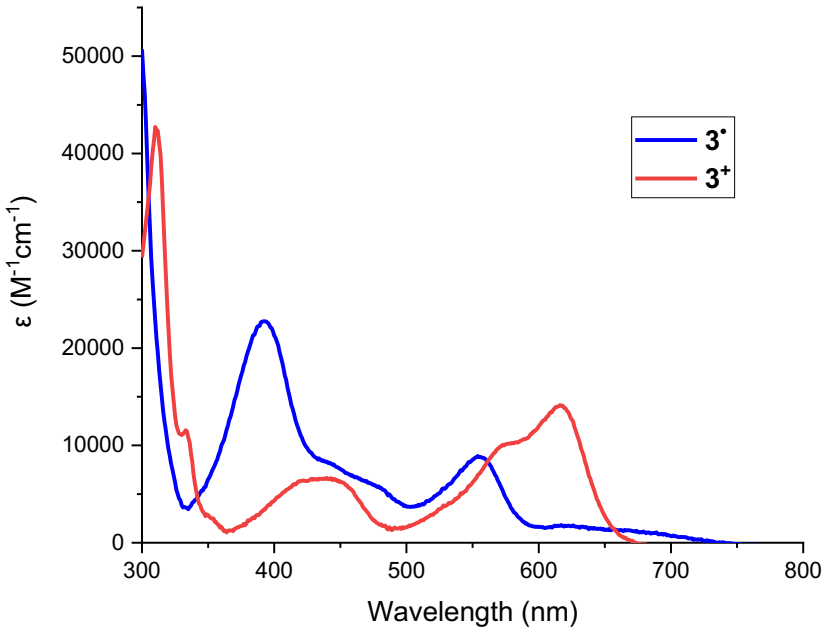

Figure S48: UV−vis spectra (6.5 x 10^{-5} M in CF_3-Toluene, room temperature) of **3**

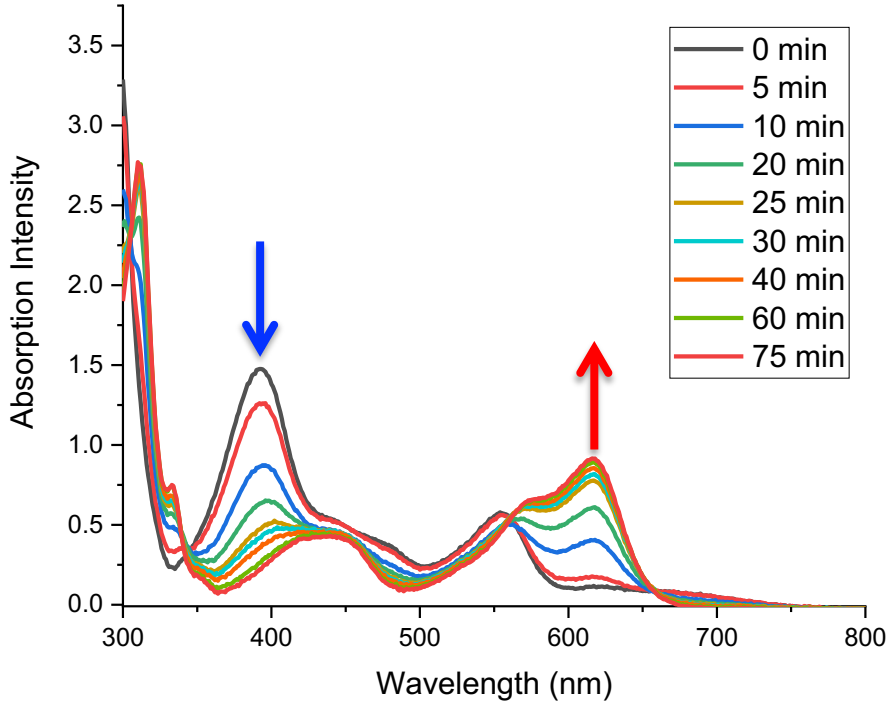

Figure S49. Change of UV-visible absorption spectra for **3•** (6.5 x 10^{-5} M) with time after exposure to air

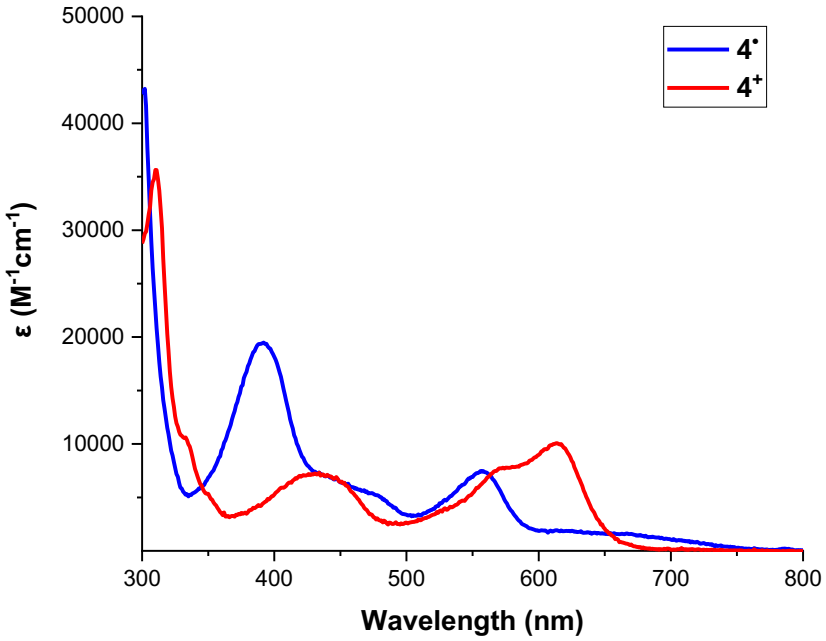

Figure S50: UV−vis spectra (8.7 × 10−5 M in CF_3-Toluene, room temperature) of **4**

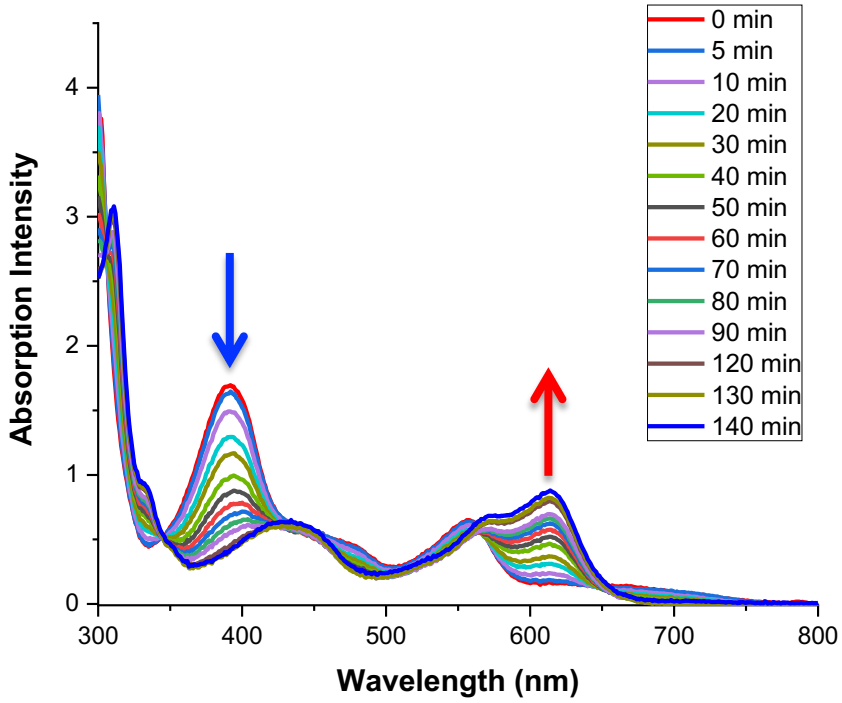

Figure S51. Change of UV-visible absorption spectra for **4•** (8.7 × 10−5 M) with time after exposure to air

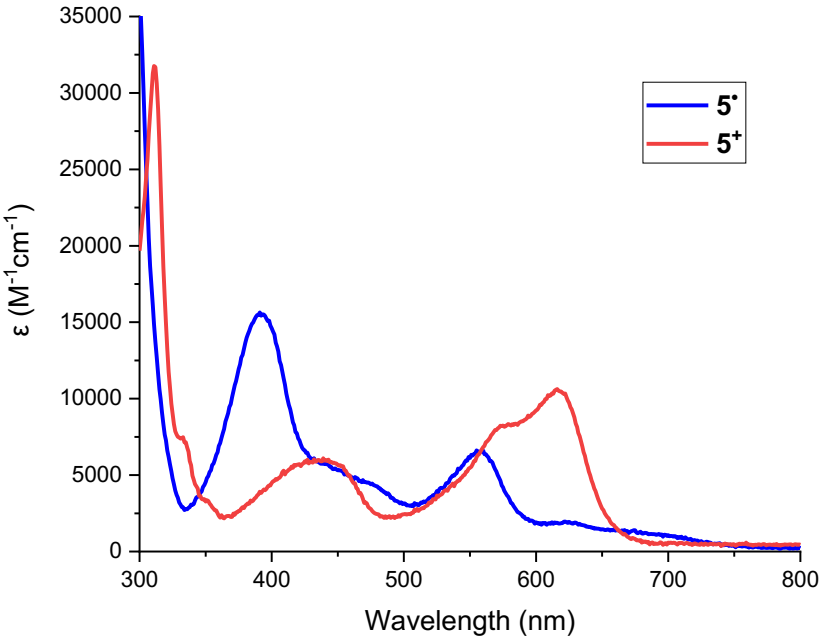

Figure S52: UV−vis spectra (6.3× 10^{-5} M in CF_3-Toluene, room temperature) of **5**

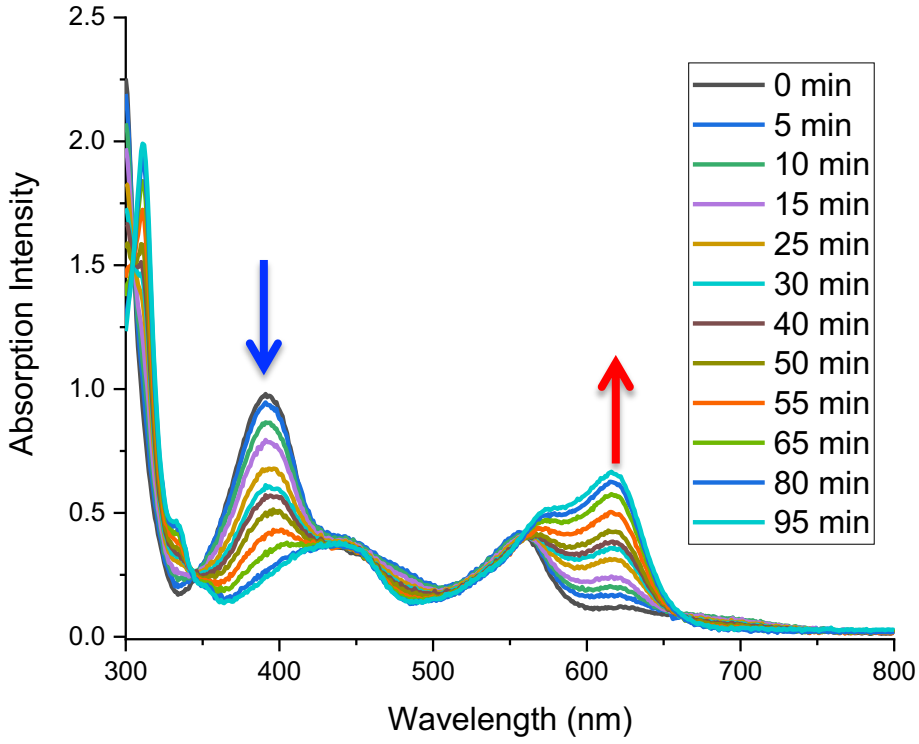

Figure S53. Change of UV-visible absorption spectra for **5•** (6.3× 10^{-5} M) with time after exposure to air

IX. Photocatalysis

Photophysical and electrochemical properties of 2-H$^{\bullet}$:

Samples for photophysical measurements were prepared in a nitrogen-filled glovebox using dry acetonitrile. Samples solution with 10^{-5}M concentration was prepared and transferred to a 4 mL quartz cell and sealed with a PTFE-lined screw cap. The solvent absorbance background was subtracted from the reported spectra. Fluorescence was record with Cary Eclipse Fluorescence Spectrophotometer. Emission spectra (1 nm step size, 5 nm bandwidth) are fully corrected for the spectral response of the instrument.

The radical **2-H$^{\bullet}$** shows two distinct absorption at 391nm and 561 nm, and an emission peak around 660 nm (excitation at 561 nm). The electrochemical behavior of its cationic species **2-H^{+}** has been well-studied by cyclic voltammetry (CV) in DCM (vide-supra). For consistency with our photocatalytic experiment, CV in CH_3CN was also performed (Figure S55) which featured a fully reversible reduction of C^{+} to $C^{\bullet}$ at $E^{red}_{1/2}$ = -0.79 V *versus* SCE.

Based on the reported literature,[9] excitation energy ($E_{0,0}$) is estimated by calculating the energy of the wavelength at which the compound's UV-Vis absorption and emission spectra overlap or of the wavelength at the midpoint between absorption and emission maxima. Then, excited state oxidation potential $E_{1/2}(C^{+}/C^{\bullet *})$ is calculated by $E_{1/2}(C^{+}/ C^{\bullet *+}) = E_{1/2}(C^{+}/C^{\bullet}) - E_{0,0}$. Thus, we can obtain the corresponding photophysical and redox potentials of **2-H$^{\bullet}$** :

Absorption λ_{max} = 561 nm

Emission λ_{max} = 660 nm

Intersect point of absorption and emission maxima λ = 620 nm

$E_{0,0}$ = 1240/620 eV = 2.00 eV

$E_{1/2}(C^{\bullet *}/C^{+}) = E_{ox} - E_{0,0}$ = - 0.79 – 2.00 V = -2.79 V

Table S7. Photophysical and electrochemical properties of **2-H$^{\bullet}$**

compound	$E_{0,0}$ (eV)[a]	$E_{1/2}$ ($C^{+}/C^{\bullet}$) (V)[b]	$E_{1/2}$ ($C^{\bullet *}/C^{+}$) (V)[c]	absorption λ_{max} (nm)	emission λ_{max} (nm)
2-H$^{\bullet}$	2.00	-0.79	-2.79	561	660

[a] Measured in CH_3CN (10^{-5} M). [b] Determined by cyclic voltammetry in CH_3CN versus SCE. [c] Excited state potentials were estimated from ground state redox potentials and the intersect point of the absorption and emission maxima.

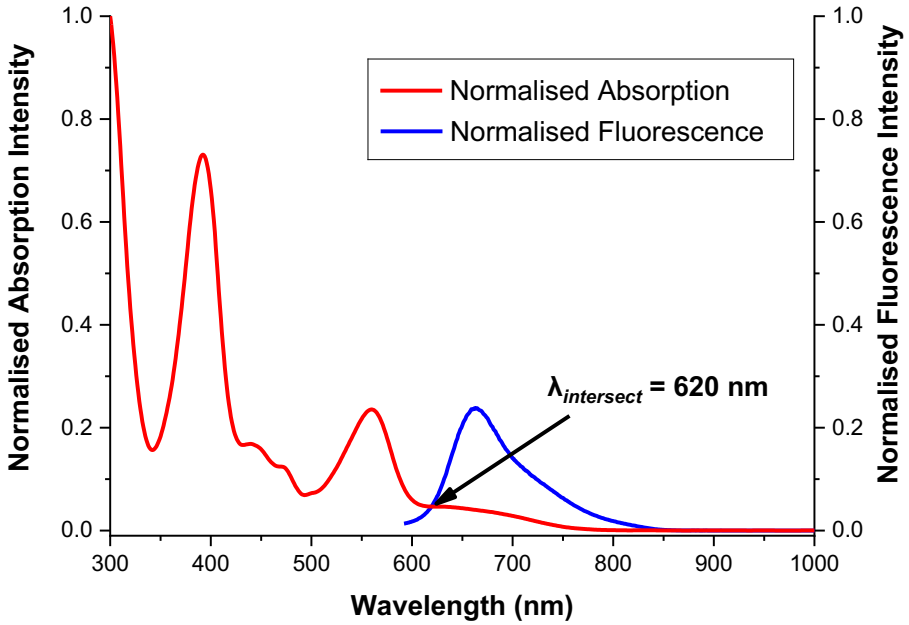

Figure S54. Solution steady-state normalized UV-visible absorption and emission spectra of **2-H$^{\bullet}$** in CH_3CN

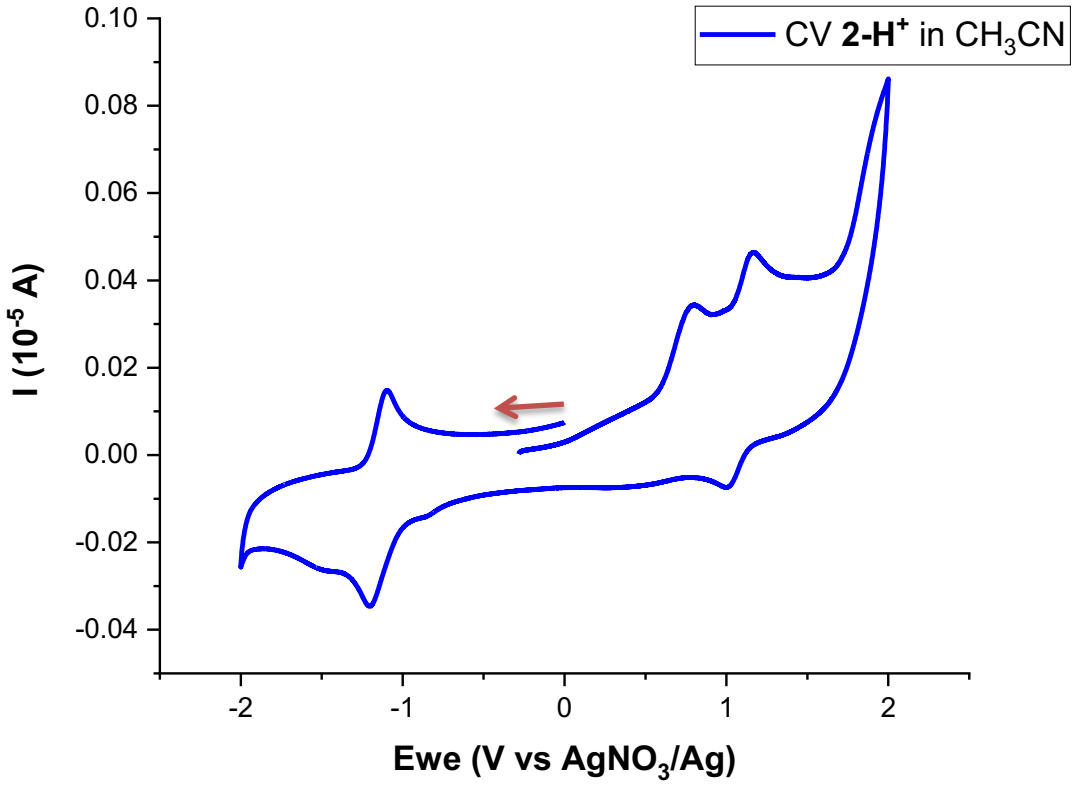

Figure S55. A cyclic voltammogram of **2-H**$^{+}$ (1 mM) in CH_3CN ([TBA][PF_6] 0.1 M) solutions at 298 K (scan rate: 0.1 V/s).

General Procedure for Photoreduction of Aryl Halides

In a nitrogen glove box, to a 10 ml Schlenk flask charged with a Teflon-coated stir bar was added aryl halide (0.1 mmol, 1.0 equiv.), 2H• (0.01 mmol, 0.1 equiv.), diisopropylethylamine (0.3 mmol, 3.0 equiv.) and 1.0 ml dry MeCN. The reaction mixture was sealed with a glass stopper and stirred under irradiation with 440 nm LED (Table S10) or 518 nm LED (table S11). After 16 h for reaction under blue light and 21 h for reaction under green light, the solvent was removed under vacuum and was dissolved with $CDCl_3$ followed with addition of 1,3,5-trimethoxybenzene (0.10 mmol, 1.0 equiv.) as the internal standard. Yields of the desired product were then calculated using crude ^{1}HNMR spectra.

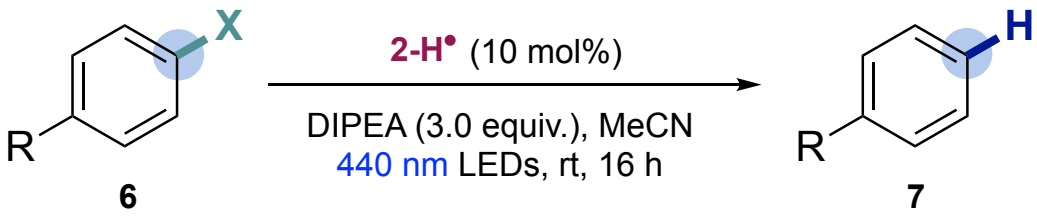

Table S8. Reaction scope using Blue LED

Entry	Substrate	Photocatalyst	DIPEA	LED	Yield
1	Ethyl-4-iodobenzoate, **6a**	**2-H•**	3.0 equiv.	440 nm	>99%
2	4-iodoaniline, **6b**	**2-H•**	3.0 equiv.	440 nm	83%
3	4-bromobenzonitrile, **6c**	**2-H•**	3.0 equiv.	440 nm	69%
4	4-bromoacetophenone, **6d**	**2-H•**	3.0 equiv.	440 nm	38%
5	4-bromoaniline, **6e**	**2-H•**	3.0 equiv.	440 nm	27%
6	4-chlorobenzonitrile, **6f**	**2-H•**	3.0 equiv.	440 nm	36%

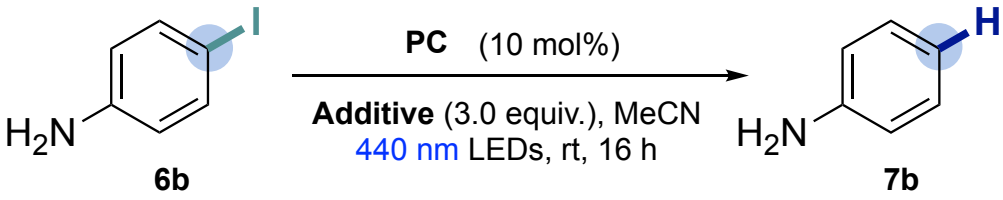

Table S9. Control Experiments with 4-iodoaniline, **6b**

Entry	Photocatalyst	Additive	LED	Yield
1	**2-H$^+$**	3 equiv. DIPEA	440 nm	42%†
2	**2-H$^\bullet$**	3 equiv. HE	440 nm	10%
3	**2-H$^\bullet$**	-	440 nm	0%†
4	**-**	3 equiv. DIPEA	440 nm	0%†

† = 14 h

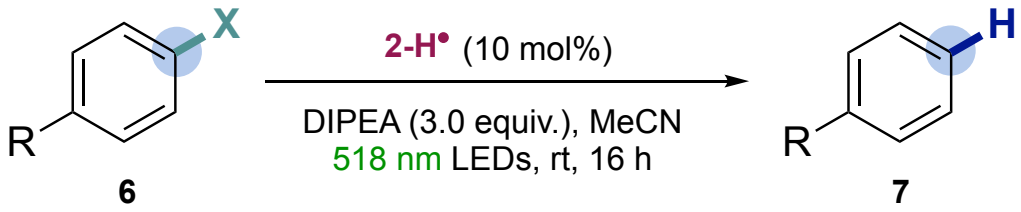

Table S10. Reaction scope using Green LED

Entry	Substrate	Photocatalyst	DIPEA	LED	Yield
1	Ethyl-4-iodobenzoate, **6a**	**2-H$^\bullet$**	3.0 equiv.	518 nm	45%
2	4-iodoaniline, **6b**	**2-H$^\bullet$**	3.0 equiv.	518 nm	15%
3	4-bromobenzonitrile, **6c**	**2-H$^\bullet$**	3.0 equiv.	518 nm	45%
4	4-bromoacetophenone, **6d**	**2-H$^\bullet$**	3.0 equiv.	518 nm	18%
5	4-bromoaniline, **6e**	**2-H$^\bullet$**	3.0 equiv.	518 nm	5%
6	4-chlorobenzonitrile, **6f**	**2-H$^\bullet$**	3.0 equiv.	518 nm	trace

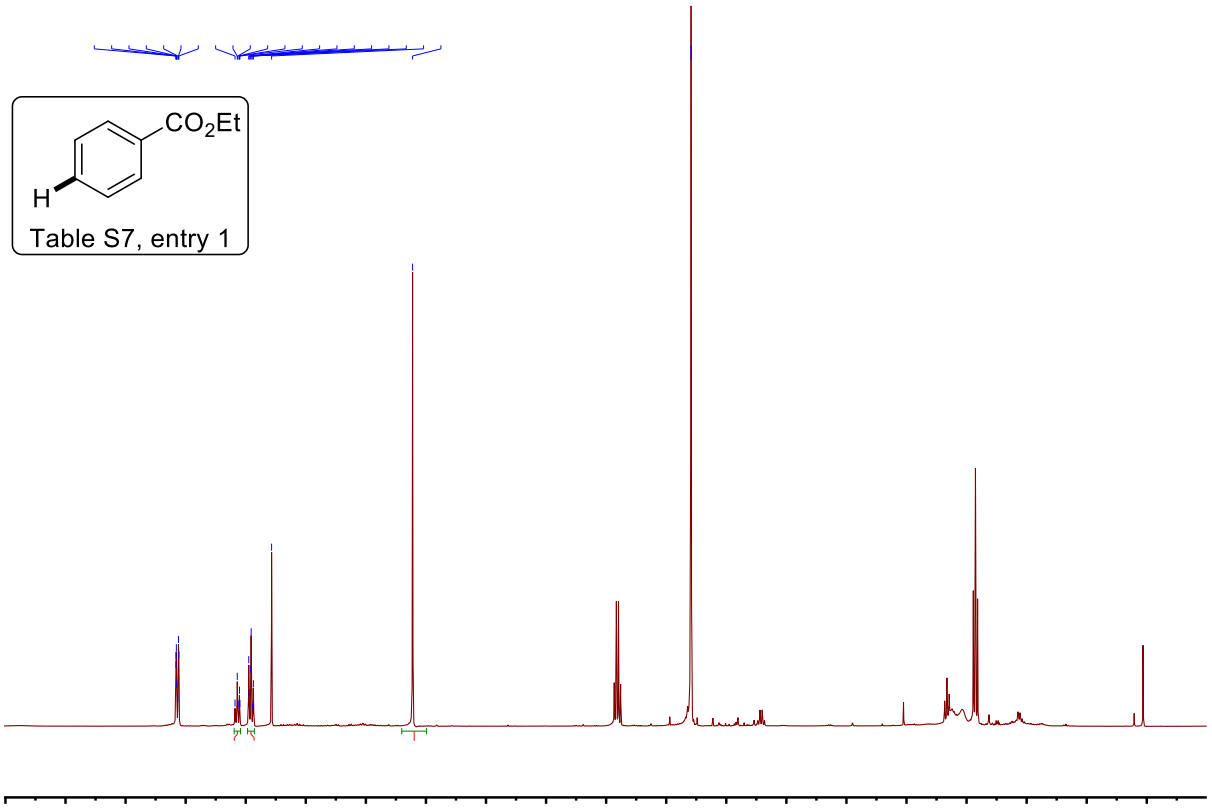
CO2Et
H
Table S7, entry 1

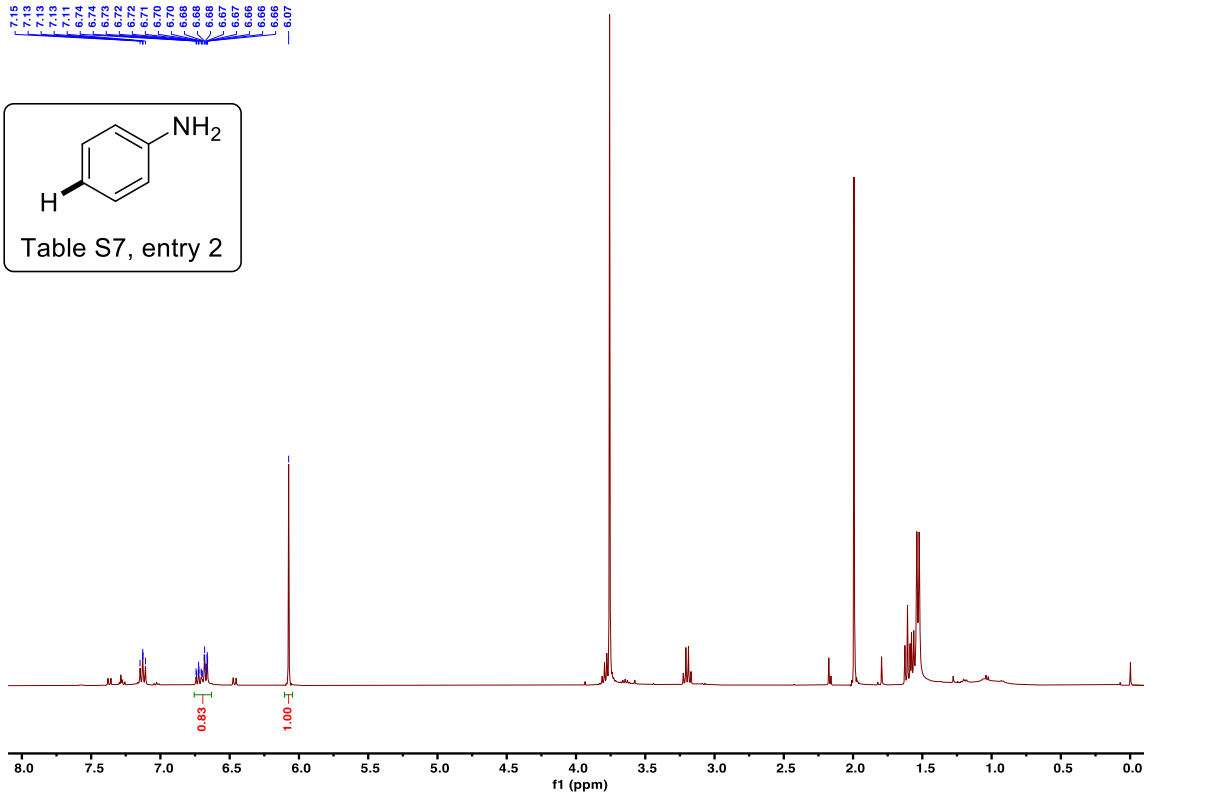
7.15
7.13
7.13
7.13
7.11
6.74
6.74
6.73
6.72
6.72
6.71
6.70
6.70
6.68
6.68
6.68
6.67
6.67
6.66
6.66
6.66
6.07
NH2
H
Table S7, entry 2
0.83
1.00
8.0
7.5
7.0
6.5
6.0
5.5
5.0
4.5
4.0
3.5
3.0
2.5
2.0
1.5
1.0
0.5
0.0
f1 (ppm)

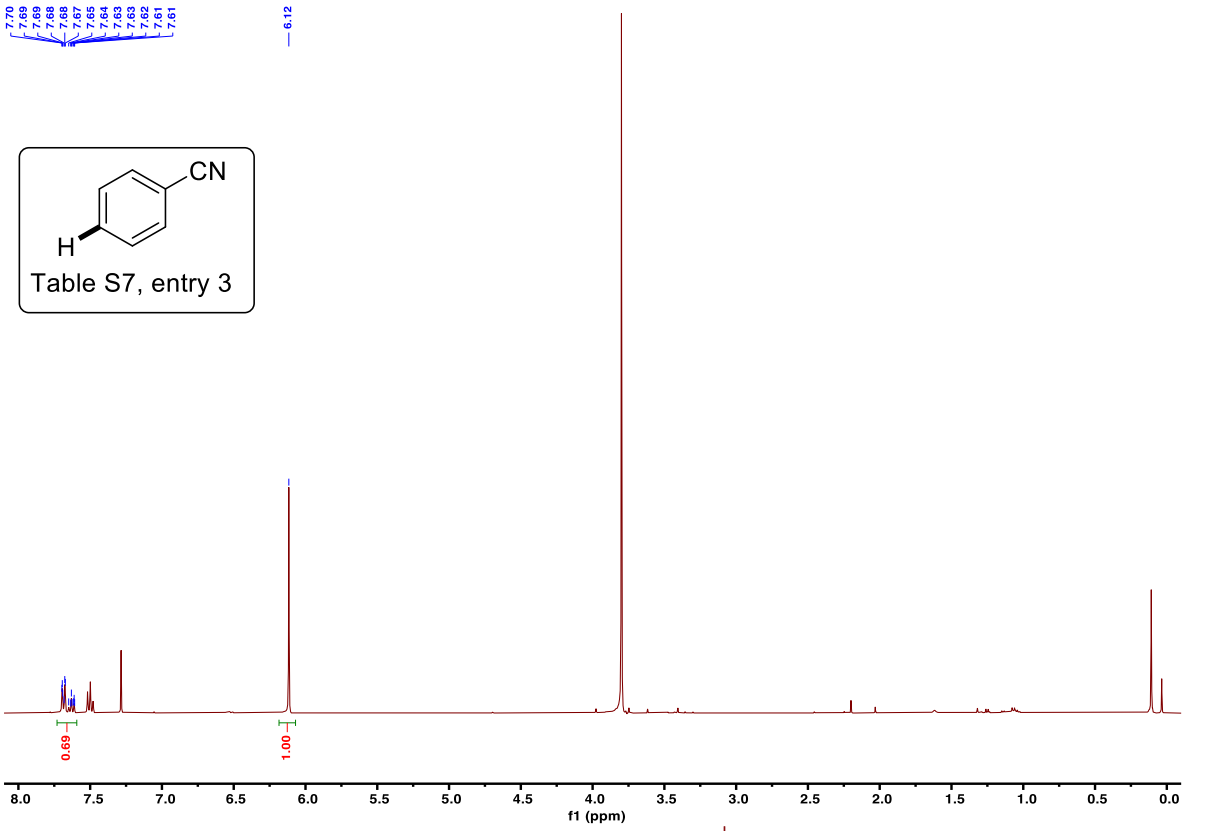
7.70
7.69
7.69
7.68
7.68
7.67
7.65
7.64
7.63
7.63
7.62
7.61
7.61
6.12
CN
H
Table S7, entry 3
0.69
1.00
8.0
7.5
7.0
6.5
6.0
5.5
5.0
4.5
4.0
3.5
3.0
2.5
2.0
1.5
1.0
0.5
0.0
f1 (ppm)

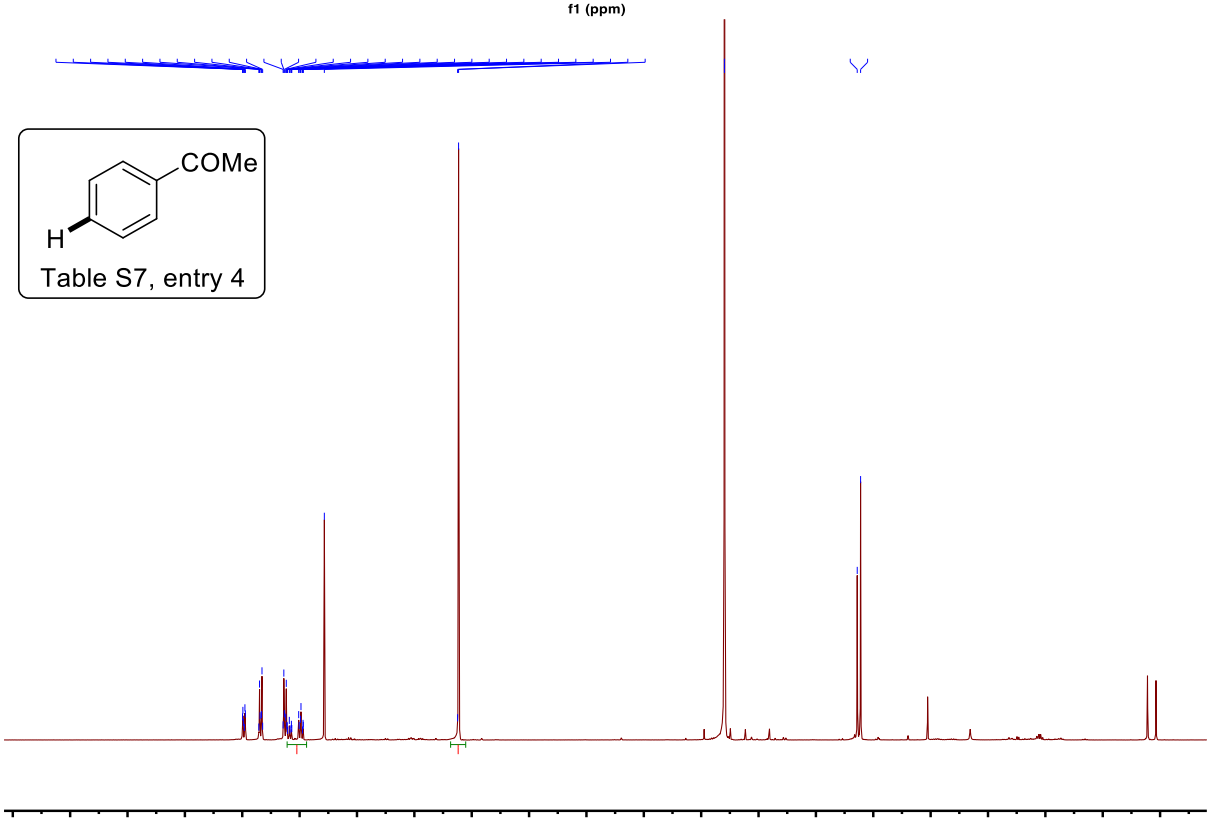
COMe
H
Table S7, entry 4

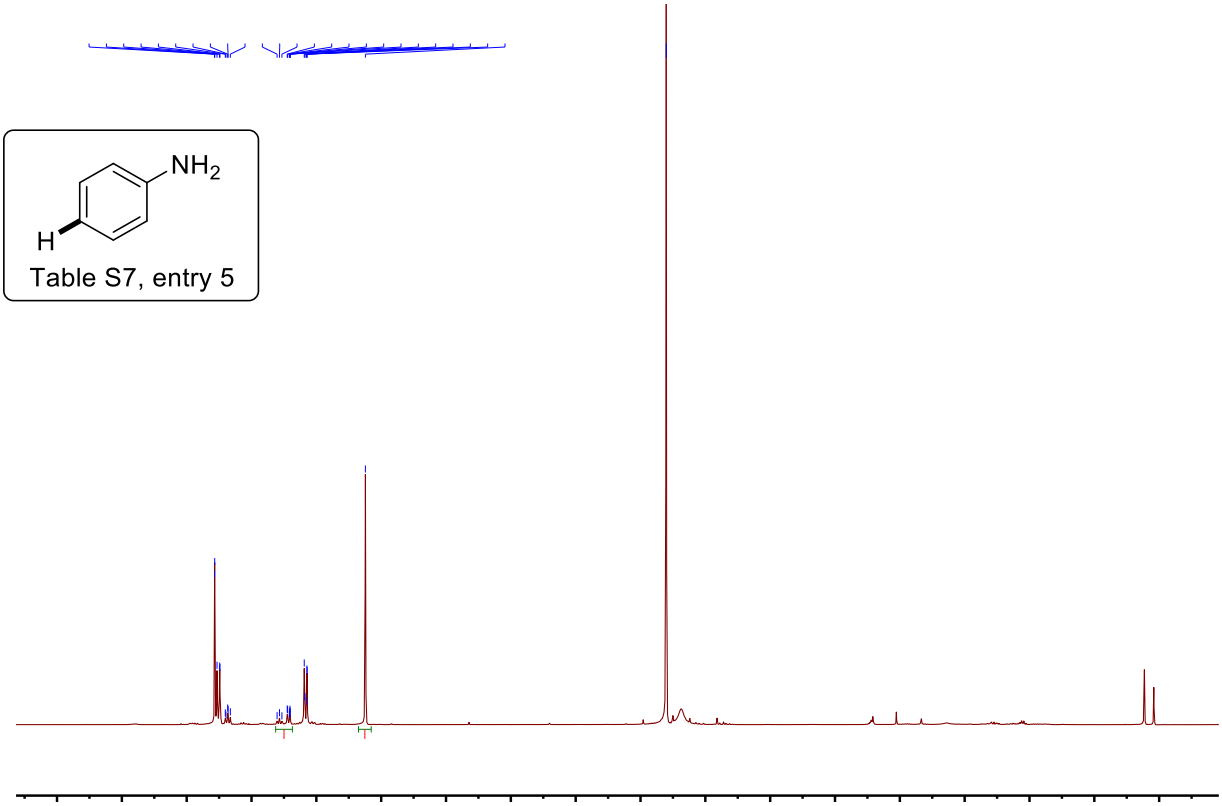
NH2
H
Table S7, entry 5

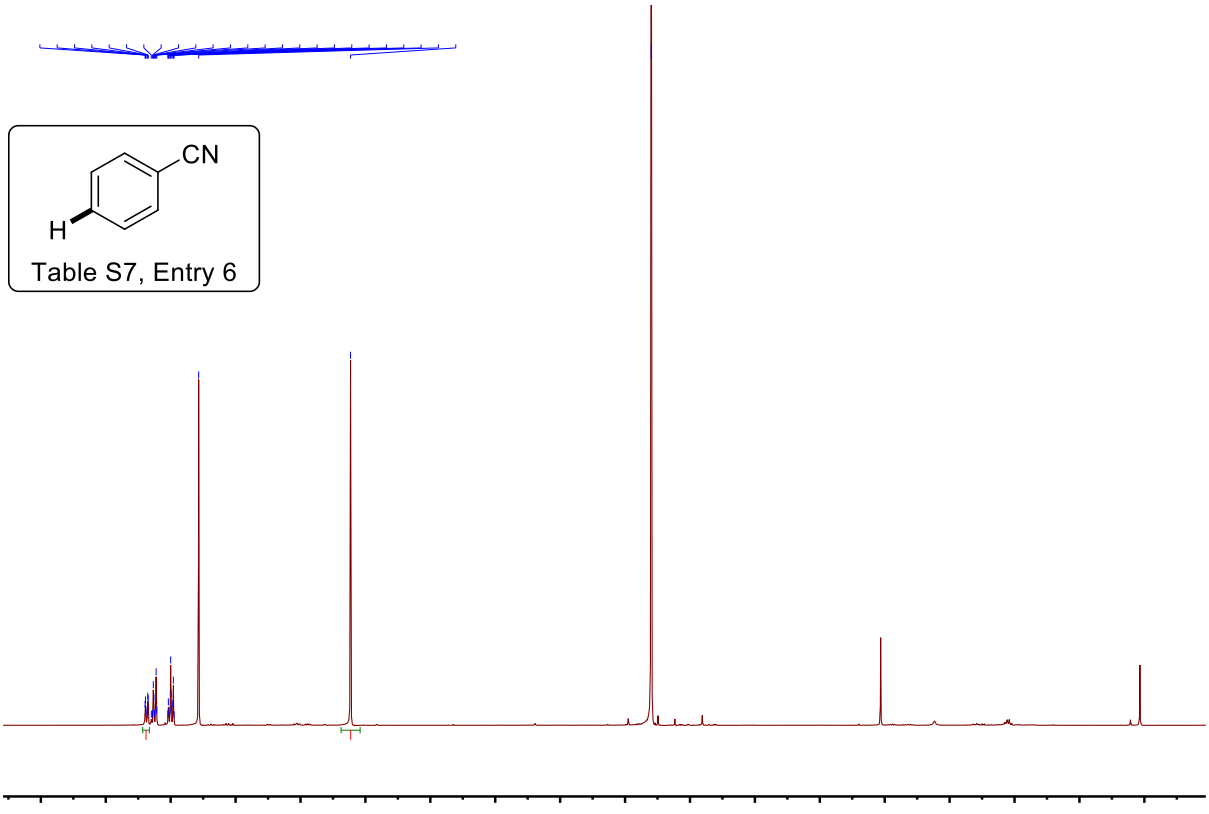
CN
H
Table S7, Entry 6

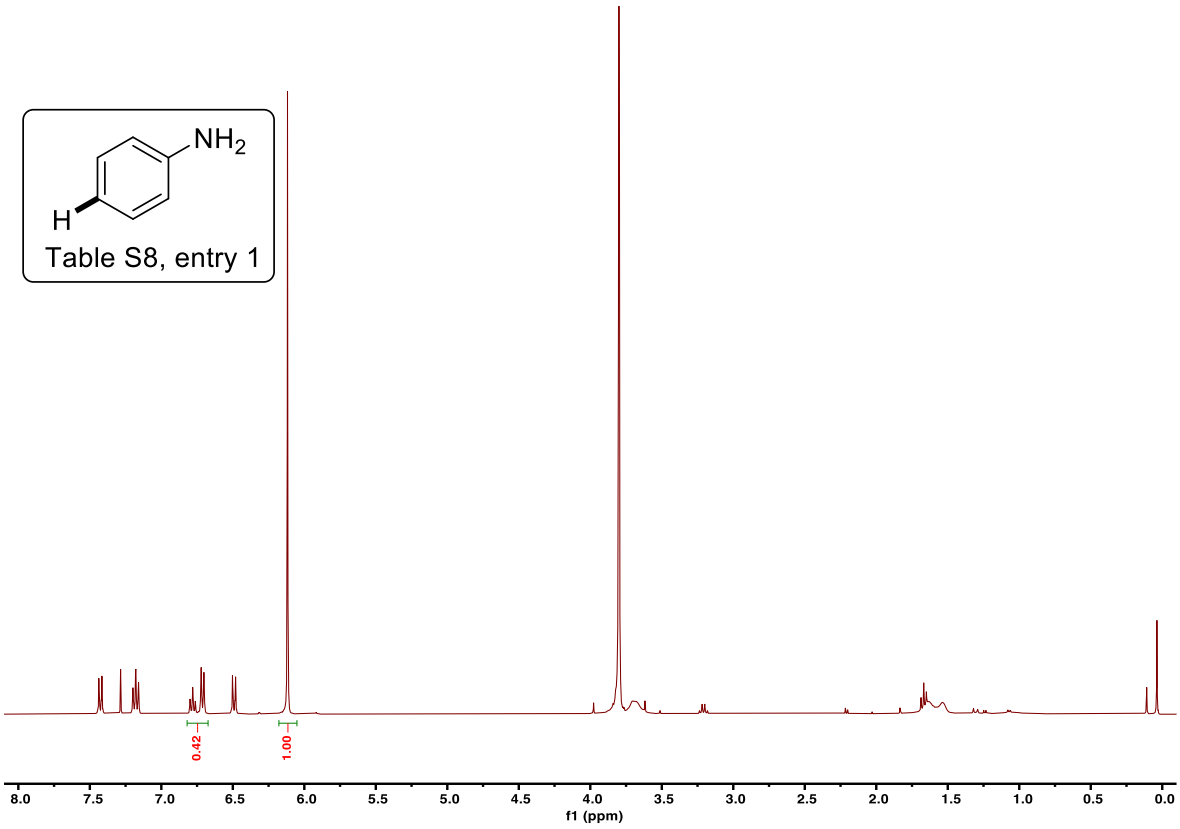

References

(1) Patterson, J. D. *Density-Functional Theory of Atoms and Molecules*; Oxford University Press: Oxford, 1989.

(2) Hohenberg, P.; Kohn, W. "Inhomogeneous Electron Gas". *Phys. Rev.* **1964**, *136*, B864–B871. [DOI:10.1103/PhysRev.136.B864].

(3) Yanai, T.; Tew, D. P.; Handy, N. C. "A New Hybrid Exchange–Correlation Functional Using the Coulomb-Attenuating Method (CAM-B3LYP)". *Chem. Phys. Lett.* **2004**, *393*, 51–57.

(4) Becke, A. D. "A New Mixing of Hartree–Fock and Local Density-functional Theories". *J. Chem. Phys.* **1993**, *98*, 1372–1377. [DOI:10.1063/1.464304].

(5) Becke, A. D. "Density-functional Thermochemistry. III. The Role of Exact Exchange". *J. Chem. Phys.* **1993**, *98*, 5648–5652. [DOI:10.1063/1.464913].

(6) Becke, A. D. "Density-Functional Exchange-Energy Approximation with Correct Asymptotic Behavior". *Phys. Rev. A* **1988**, *38*, 3098–3100. [DOI:10.1103/PhysRevA.38.3098].

(7) Lee, C.; Yang, W.; Parr, R. G. "Development of the Colle-Salvetti Correlation-Energy Formula into a Functional of the Electron Density". *Phys. Rev. B* **1988**, *37*, 785–789. [DOI:10.1103/PhysRevB.37.785].

(8) Frisch, M. J.; Trucks, G. W.; Schlegel, H. B.; Scuseria, G. E.; Robb, M. A.; Cheeseman, J. R.; Scalmani, G.; Barone, V.; Mennucci, B.; Petersson, G. A.; et al. "Gaussian 09". Gaussian Inc.: Wallingford, CT 2016.

(9) Christensen, J. A.; Phelan, B. T.; Chaudhuri, S.; Acharya, A.; Batista, V. S.; Wasielewski, M. R. "Phenothiazine Radical Cation Excited States as Super-Oxidants for Energy-Demanding Reactions". *J. Am. Chem. Soc.* **2018**, *140*, 5290–5299. [DOI:10.1021/jacs.8b01778].